Defining Recurrent Laryngeal Nerve Injury in a Mouse Model for Regenerative Therapeutic Investigations

---

A Dissertation

Presented to the

Faculty of the Graduate School

at the University of Missouri-Columbia

In Partial Fulfillment

of the Requirements for the Degree

Doctor of Philosophy

By

Megan M. Haney

Dr. Teresa E. Lever, Dissertation Supervisor

July 2019

The undersigned, appointed by the dean of the Graduate School, have examined the dissertation entitled

DEFINING RECURRENT LARYNGEAL NERVE INJURY IN A MOUSE MODEL FOR REGENERATIVE THERAPEUTIC INVESTIGATIONS

Presented by Megan M. Haney,

A candidate for the degree of doctor of philosophy,

And hereby certify that, in their opinion, it is worthy of acceptance.

_____
Teresa Lever, PhD

_____
Chris Lorson, PhD

_____
Mahesh Thakkar, PhD

_____
James Amos-Landgraf, PhD

_____
Kevin Cummings, PhD

Dedication

This dissertation is dedicated to my newborn daughter, Austen. I hope that she one day grows up to be an empowered woman with the determination, grit, and enthusiasm to conquer whatever quest she may aspire to.

Acknowledgements

First, I would like to thank Dr. Teresa Lever for her guidance and support throughout my dissertation work. She has been an amazing mentor, and her passion for research and positive attitude are infectious. Performing research in her lab has been extremely rewarding and one of the best experiences of my life.

I would also like to thank all of my other committee members, Dr. Chris Lorson, Dr. Mahesh Thakkar, Dr. Jim Amos-Landgraf, and Dr. Kevin Cummings for all of their insightful comments and questions during committee meetings. Our discussions enabled me to grow as a researcher and helped strengthen my work. In addition to my committee members, there are many other faculty members, including Dr. Nicole Nichols and Dr. Filiz Bunyak, who have guided me along the way and I would not have been able to finish my research without them. I also could not have survived without the help and support of Kate Osman and the many students in Dr. Lever's lab.

I sincerely thank all of the comparative medicine faculty and my fellow residents. You have all taught me something in some shape or form and have made this program a fun and fulfilling experience. I also could not have done all of the animal work without the help of the animal care staff. For your excellent animal care, I thank you!

Lastly, I would like to thank my family. I would not be where I am without my parents. They were always there to help me learn and supported me in all of my endeavors. I do not think I would be where I am today if my dad had not taught me

that pi equals 3.14 and Avogadro's constant is 6.022×10^{23} when I was three years old. He also let me in on the secret that I get my good looks from DNA. Last, but not least, I would like to thank my husband, Ryan Madison, for his continued support and patience with me during this time. Thank you for putting up with some of my long hours and for always bringing me food on long surgery days. Thank you for enduring long science conversations and my occasionally high stress levels. I look forward to our next adventures both professionally and personally, especially with the addition of our new baby girl.

To all of you who have supported me on this journey, I sincerely thank you.

Table of Contents

List of Figures

List of Tables

Abstract

Injury of the recurrent laryngeal nerve (RLN), a branch of the vagus nerve, results in ipsilateral vocal fold (VF) paralysis that contributes to dysphagia, dysphonia, and dyspnea (i.e., swallow, vocal, and respiratory dysfunction, respectively). Unfortunately, there is no clinical intervention that will reliably restore physiologic movement to the VF after an RLN injury. Throughout this work, the effects of RLN injury on murine VF motion, swallowing behavior, vocalization production, and respiratory function are examined. Furthermore, methods for refining the functional assays used to assess these behaviors are developed, allowing for the production of more reliable and translatable results. Therefore, in Chapter 2, the effects of RLN injury are explored to confirm the fidelity of the laryngeal innervation pattern and functional outcomes (for vocal fold motion and swallowing) between mice and humans. In Chapter 3, an automated VF tracking and quantification software is developed to objectively measure dynamic VF motion, which is further refined in Chapter 4. Also in Chapter 4, we expand our translational mouse model to characterize swallow, vocal, and respiratory function in mice with unilateral VF paralysis following RLN injury. Lastly, VNS and its role as a therapeutic intervention for RLN injury is studied (Chapter 2), as well as the potential off-target effects this therapy may have on the many other organ systems provided innervation by the vagus nerve (Chapter 5). In conclusion, this work aims to provide a refined and reproducible animal model for researchers to use to investigate RLN pathophysiology and treatment options.

Chapter One

INTRODUCTION

1.1 Recurrent Laryngeal Nerve Injury

Injury of the recurrent laryngeal nerve (RLN), a branch of the vagus nerve, results in ipsilateral vocal fold (VF) paralysis that contributes to dysphagia, dysphonia, and dyspnea (i.e., swallow, vocal, and respiratory dysfunction, respectively).[1-5] RLN injury may occur as a result of idiopathic disease, infection, inflammation, neck trauma, or malignancy, but the nerve is particularly prone to iatrogenic injury during surgical procedures that target the anterior neck and upper thoracic cavity, such as thyroidectomies and anterior cervical discectomy and fusion.[3,6-9] During surgery, the nerve may be injured through a variety of mechanisms, including traction, compression, thermal, electrical, and transection injuries.[6,10] The increased incidence of RLN injury during these procedures is attributed to the RLN's location, long length, and variable topographical patterns.[11,12] As a result, dysphagia, dysphonia, and dyspnea are common upper airway complications following cervical and thoracic surgeries.[13] These conditions, especially if chronically persistent, are associated with poor quality of life, major depression, increased financial burden, and decreased general health for the patient.[1,5,7,14]

Though the peripheral nervous system initiates a robust regenerative response after an RLN injury, functional recovery is often inadequate.[2] The RLN innervates the majority of intrinsic laryngeal adductor muscles, as well as the only abductor muscle, the posterior cricoarytenoid.[4] Poor specificity during reinnervation of these antagonist muscles after an injury can lead to weak, uncoordinated, and sometimes paradoxical muscle contraction of the VFs (i.e., synkinesis).[6,10] In addition to reduced specificity of reinnervation, poor clinical recovery can be attributed to slow and staggered rates of axonal regeneration and death of neuronal cell bodies in the brainstem motor nucleus, the nucleus ambiguus, the extent of which depends on the severity and location of the injury.[10,15,16] Therefore, while the RLN may attempt to regenerate after damage, return to absolute normal function is not guaranteed.

Unfortunately, there is no clinical intervention that will reliably restore physiologic movement to the VF after an RLN injury.[3,17-19] Many of the current therapeutic interventions for VF paralysis focus on behavioral exercises and modifications (e.g., altering respiration while speaking or adjusting swallow behavior to prevent aspiration of food material) to improve laryngeal function.[20] Alternative therapeutic strategies include medialization of the impaired VF, which provides structural support for more favorable glottic closure, but does little to address VF mobility or muscle denervation atrophy. Invasive secondary surgeries, such as RLN anastomosis or nerve graft procedures, may also be attempted to reinnervate RLN target organs in order to improve tone to VF musculature.[10,14,21]

However, these techniques, even if successful, also fail to restore true physiologic movement to the VFs.

Thus, it is imperative to continue research for potential treatments for RLN injury that will overcome the deficiencies in the nerve regenerative process and will restore full functionality to inadvertently impaired VFs following surgical procedures. To do so, animal models are required, as RLN injury and its associated sequelae are often impossible and unethical to scientifically investigate in human patients. Moreover, it is necessary that animal models consistently replicate the many symptoms and complications associated with RLN damage to increase translatability to human patients. In addition to the animals themselves, reliable functional assays to quantify these symptoms are fundamental to systematically and consistently evaluate the pathophysiology, recovery, and potential treatments for this complicated injury.

1.2 Functional Assays to Investigate RLN Injury in Animal Models

1.2.1 Vocal Fold Motion Analysis

The most common method to confirm ipsilateral VF paralysis and evaluate functional recovery after RLN injury is through the use of endoscopy to visualize and record the movement of the VFs.[9,16,22,23] This technique provides immediate and robust information concerning the movement of the VF, but does not directly evaluate the other functional aspects of RLN injury, such as swallow, vocal, and respiratory function. However, as endoscopy is the most widely used procedure for assessing RLN injury and recovery, there are various approaches used by

research groups to evaluate and quantify VF motion with this technique. A common method utilizes subjective rating scales to categorize VF motion.[9,13,16,24-26] For example, the VF may be scored as zero if immobile, one if partially immobile, and two if fully mobile. Though subjective scoring of VF motion is relatively simple and time efficient, scores may vary between observers and small changes in VF movement over time are not measureable and are likely missed. Thus, objective measures are available to better quantify VF motion.

Most approaches for objectively determining VF function rely on using still-frame image analysis while the VFs are in a state of maximum abduction and maximum adduction. In each of these states, one can calculate angles[9,16,23] and/or the glottal area[18,22,27] between the VFs to determine the degree of movement of the injured VF between maximum opening and maximum closing. However, these objective methods also have their own inherent limitations, which are discussed in depth in Chapter 3. One significant weakness of these types of objective measures is that they rely on static images from only two time points during the respiratory cycle. Thus, no information is provided about the dynamics of VF motion as a whole.

To overcome this problem, one group performed frame-by-frame analysis to measure the displacement of each VF from midline throughout a video clip.[28] Through this technique, they were able to detect residual VF motion during or after an RLN injury. However, this method required the manual analysis of over 100 individual video frames, rendering this method extremely time consuming and labor intensive, limiting its usefulness. While manual frame-by-frame analysis may

not be a practical tool, especially in a clinical setting, an automated approach may produce similar results and would increase efficiency. Furthermore, automated analysis could provide valuable, novel, and reproducible outcome metrics of VF motion throughout an entire video clip of a clinically meaningful duration (i.e., several seconds to minutes). The development of this technology would likely allow high throughput, reliable analysis of dynamic VF motion, potentially benefitting researchers and clinicians alike.

1.2.2 Swallow Function Analysis

Swallowing is a vital human function to move nutritional material from the oral cavity through the oropharynx and into the esophagus.[29] For a normal swallow, proper laryngeal kinematics are critical to move the bolus in the appropriate direction and to protect the airways from foreign material. The VFs, specifically, play an essential role in protecting the airway during this complex process. This protective mechanism is mediated, in part, by the RLN. Similarly, the laryngeal adductor reflex (LAR), another protective mechanism to prevent aspiration of foreign material into the airways, also relies on the RLN. The entire reflex is initiated when mechanoreceptors and chemoreceptors in the laryngopharyngeal mucosa are stimulated. The superior laryngeal nerve (SLN) transmits sensory information from these receptors to the brainstem. Motor information is then projected along the RLN, which in an intact nerve will stimulate a brief bilateral contraction of the VF adductor muscles, causing medialization of the VFs and protection of the airway from penetration of foreign material.[30,31] Therefore, RLN

injury may compromise VF closure during swallowing and/or the LAR, resulting in a less responsive and unprotected airway that can contribute to dysphagia with laryngeal penetration and/or aspiration.[1] These conditions may in turn lead to aspiration pneumonia, asphyxiation, malnutrition, and dehydration, further decreasing the general health of the patient.[29]

The RLN also provides innervation to the esophagus, particularly the upper esophagus and the cricopharyngeus muscle, a major component of the upper esophageal sphincter.[32,33] As such, patients with RLN injury may experience symptoms related to esophageal dysphagia, rather than or in addition to oropharyngeal dysfunction. In fact, studies using manometry in rat and rabbit models have shown that RLN transection significantly decreases the negative pressure of the upper esophageal sphincter during swallowing.[29,34] Thus, swallow dysfunction after RLN injury is likely due to a combination of incomplete opening of the upper esophageal sphincter and incomplete closure of the glottis.[34] In addition, RLN injury may initiate a cascade of events that impact interneural connections in the central nervous system, which in turn may influence the muscles and structures involved in swallowing beyond those solely innervated by the RLN.[35,36]

In clinical settings, dysphagia is most commonly assessed using videofluoroscopic and videoendoscopic techniques.[37-40] During a video-fluoroscopic swallow study, the gold standard diagnostic test for dysphagia, a human patient is positioned in a fluoroscopy machine to assess the real time movement of food or liquid traveling from the mouth to the stomach. Video

recordings of multiple swallows can then be analyzed for various physiologic outcome metrics for each patient.[41] This technique has been limited in animal models due to unique challenges, such as reliance on sedation and nonphysiologic feeding positions, motion artifact, and opposition to ingestion of oral contrast material.[42,43]

Fortunately, these challenges have been largely overcome by recent research groups. In fact, videofluoroscopy has been adapted for use to assess normal and abnormal swallowing in freely-behaving (i.e., unanesthetized) non-human primates[44], cats[45], dogs[43], infant pigs[35,36,46-50], rats[51], and mice[41,52,53]. Yet, dysphagia, specifically after RLN injury, has only been extensively investigated in the infant pig model. Through this model, it has been shown that RLN injury results in dysphagia with compromised airway protection and esophageal dysfunction.[49] Furthermore, a unilateral RLN injury in this model likely affects central brainstem integration and the complex interneuron connections within the brain; thus, it influences the activity of other muscles involved with swallowing, such as muscles responsible for bolus aggregation and movement (e.g., geniohyoid and genioglossus muscles) that are not directly innervated by the RLN.[35] Despite the many impressive and novel findings obtained from the infant pig model, the results are better translational to neonatal patients whose nervous system is in similar stages of development. However, as many anterior neck surgical procedures are performed in older patients (greater than 50 years of age),[1,54] an aged RLN injury model with a fully developed nervous system is necessary to investigate the pathophysiology and treatment of this injury in this target population.

1.2.3 Vocal Function Analysis

Up to 80%-100% of patients with unilateral VF paralysis are affected by dysphonia (i.e., vocal dysfunction).[1,5,22] Though dysphonia itself is not life threatening, it is perhaps the most life-altering complication of RLN injury. Dysphonia can greatly interfere with one's social life and employment, potentially even necessitating a career change.[1] Though animals obviously "speak" and articulate information differently than humans, vocalization in animals is extremely important for intraspecies communication and expressing emotion.[55-59] Therefore, vocalizations in animal models are often recorded and analyzed for the frequency (pitch), duration, and amplitude of their vocalizations, as well as for various call types, which differ between species. Rodents are unique in that they express both audible and ultrasonic (i.e., tones above 20 kHz) vocalizations. Despite different frequencies and functions of these calls, the larynx is likely the source of each.[60]

Early laryngeal nerve transection studies have shown that unilateral RLN injury severely disrupts ultrasonic vocalizations in rodents, which begin to recover one week following the injury.[60-63] These studies have noted that there is a decrease in the proportion of rodents that vocalize, as well as a reduction in the number of calls in this early timeframe after surgery. Thus, unilateral RLN transection has become a method to acutely "devocalize" rodents for other investigations examining the role of ultrasonic production in mating behavior or to ensure vocalizations are collected from a specific test subject when two mice are paired together.[64,65] However, the analyses in these early studies is limited to audible calls and ultrasonic calls with a specific frequency, 70 kHz for mice.[63] Also,

only the number of calls were quantified. Without a more extensive and thorough analysis, it is difficult to translate the vocal impairment in rodent models after RLN injury to the complex, vocal dysfunction seen in human patients.

Fortunately, with new technology, analysis software, and methods, ultrasonic calls can be detected in a wide frequency range and can be characterized by the type of call and the complexity of the call, along with various other parameters, such as frequency, bandwidth, duration, rate, and relative intensity of the calls.[59,65] With the advent of better analysis techniques, more recent studies have used ultrasonic vocalizations to behaviorally phenotype certain neurologic disorders in rodent models, such as Down syndrome and Parkinson's disease models.[66-69] Thus, improved ultrasonic vocalization analysis is now possible in rodent models of RLN injury to better characterize the impairment and subsequent recovery of vocalization that has been noted in the past after RLN transection.

Though detailed analyses of rodent *ultrasonic* vocalizations following RLN injury have yet to be performed, one group has utilized *audible* vocalizations in rats to determine functional impairment and recovery after RLN transection injury.[9,10] These audible vocalizations are evoked by restraining the rat and firmly pressing on the hindlimb with forceps. Subjectively, it was noted the vocalizations of denervated rats sounded hoarse and deep compared to an uninjured control group. Spectral analysis revealed shorter vocalizations with low amplitudes in RLN transected rats at three weeks post injury that gradually increased over time, with the amplitude reaching control levels by a 16 week time period.[9,10] As such, both

audible and ultrasonic vocalizations are potentially useful tools for examining vocal function after RLN injury, as they can be easily recorded and quantified using a variety of outcome metrics. However, as most audible vocalizations in rodents are a result of stressful or painful stimuli[59], it may be more humane and translational to systematically assess ultrasonic vocalizations rather than audible calls in rodent species.

1.2.4 Respiratory Function Analysis

Dyspnea, respiratory dysfunction, is a complex condition, occurring in a variety of cardiopulmonary and functional disorders. One such mechanism of dyspnea is increased work of breathing due to increases of mechanical loading when the VFs are adducted during inspiration, when they should be fully abducted.[70] In patients with VF paralysis, the affected VF is often maintained in a paramedian position, but can vary between individuals, and may be maintained in a lateral to fully adducted location.[71] As such, any adduction of the VF during inspiration may cause obstruction of the airway and inhibit airflow, creating difficulty in breathing for patients with VF paralysis after RLN injury.[72] Another likely source of dyspnea in patients with unilateral VF paralysis may be due to an air leak from incomplete closure of the glottis, as opposed to a true obstruction.[73,74] This can lead to the use of compensatory mechanisms, contributing to vocal fatigue and the feeling of having shortness in breath.

Though respiratory distress is immediate and severe following *bilateral* VF paralysis[1] due to airway obstruction, this severe distress is usually not detected in

patients with *unilateral* paralysis. However, despite the fact that patients with unilateral VF immobility may have normal or near normal working respiratory capacity, many of these patients (up to 76%) complain of respiratory impairment in clinical settings, particularly with problems pertaining to breathing during phonation and physical effort.[1,5,71,75-77] Although breathing impairment is a common complaint from patients with unilateral VF paralysis, little work has been done in human populations or animal models to investigate this phenomenon. In fact, no nonpulmonary dyspnea scales have been published that allow for systematic assessment of the laryngeal portion of breathing in patients with unilateral VF paralysis.[76] However, of the few publications available, most have noted impaired inspiratory flow rates in patients with unilateral VF paralysis, which may or may not be worsened with a VF medialization procedure.[72,77-80]

While no animal model has been utilized to directly investigate the effect of RLN injury on respiration, work has been done in the aforementioned infant pig model to examine the coordination between breathing and swallowing with this injury.[48] This study noted a greater magnitude of coordination changes (e.g., a greater delay between swallow time and onset of inspiration) from neonatal to pre-weanling pigs after an RLN injury, perhaps providing a protective effect during swallowing. However, as discussed above, these findings were discovered in pigs with developing nervous systems and cannot be extrapolated well to humans or animals with a well-developed and potentially aged nervous system.

As a large majority of the previous RLN injury work has been performed in rodent models, it would be logical for future studies to examine respiration in these

species either through invasive or noninvasive methods. Invasive techniques for assessing respiratory function in rodents include invasive plethysmography and forced oscillation.[81] However, the invasive nature and often necessity of anesthesia in these methods can interfere with results and limit longitudinal analysis. For non-invasive, longitudinal assessment of respiration, unrestrained whole-body plethysmography (WBP) is often utilized.[81] Not only is WBP useful for collecting respiratory parameters including tidal volume, respiration rate, inspiratory and expiratory times, and flow rates, it is valuable for detecting changes in breathing associated with sighs and apneic episodes. Thus, any future work with rodent models of RLN injury should include one or more of these tests to begin to better understand the dyspnea reported by human patients with unilateral VF paralysis.

1.3 The RLN as a Branch of the Vagus Nerve

The RLN is a branch of the 10th and longest cranial nerve, the vagus nerve. The vagus is composed of thousands of axons, both afferent and efferent, and provides a vast majority of the autonomic innervation in the body.[82] Consisting of three different fiber types, A, B, and C, the vagus carries sensory, sympathetic, parasympathetic, and somatic information to various parts of the body.[82] The vagus nerve not only innervates the larynx, pharynx, and lungs, but also the heart and gastrointestinal tract, regulating homeostasis in a multitude of organs. Given the vagus nerve's wide-ranging anatomic targets and functions within the body, it

is critical to consider this nerve as a whole when investigating pathologic outcomes and preventative and therapeutic interventions for RLN injury.

1.3.1 Vagus Nerve Stimulation to Detect RLN Injury

Exogenous stimulation of the vagus nerve results in contraction of the VFs, and has proven to be a useful “tool” for detecting and preventing RLN injury during surgery. With the use of continuous intraoperative nerve monitoring (CIONM), the surgeon can be alerted to RLN damage in real time, and potentially reduce the extent of the damage.[83,84] CIONM involves atraumatically placing a stimulating electrode on the vagus nerve during anterior neck surgical procedures. Vagal nerve stimulation (VNS) is then applied as an automatic repeated pulse throughout the surgical procedure to evoke serial contraction of the VFs.[84] VF movement is subsequently detected by EMG electrodes positioned on a specialized endotracheal tube. If RLN injury occurs during the surgery, action potentials from the vagus nerve to the VFs are interrupted, resulting in lack of EMG activity and a loss of signal. An alert will sound, and the surgeon can consequently change his or her surgical technique or make necessary modifications.

Though CIONM has the potential to decrease the incidence of RLN injury and post-operative upper airway complications, it is not 100% preventative.[85] If the loss of signal is due to a more gradual and milder RLN injury, such as a traction injury, it is easier for the surgeon to adjust and release disturbed nerves to prevent long-term injury and post-operative complications. However, if the loss of signal is due to a rapid or severe RLN injury, such as transection or thermal injury from

electrocautery, the damage cannot be easily reversed by the surgeon. Unfortunately, these situations often yield slower recovery rates of VF function,[85] resulting in poor quality of life for the patient following surgery. In the case of rapid onset RLN injury, an effective intraoperative therapeutic strategy to increase the efficiency of nerve healing post-operatively would be beneficial to shorten recovery time and improve quality of life in the patient, while avoiding medical litigation against the surgeon.

1.3.2 Potential Therapeutic Role of Vagal Nerve Stimulation after RLN Injury

VNS has been shown as an effective therapeutic strategy for a multitude of disorders, and various forms of VNS are currently FDA-approved for treating refractory epilepsy, depression, migraines, cluster headaches, and obesity.[82,86-89] However, VNS, especially chronic implantable VNS for epileptic patients, has been known to have adverse effects on VF function and voice. This is likely due to the stimulation parameters, such as stimulus intensity, that are required to produce a positive effect in epileptic patients.[90] Even at low stimulus intensities, VNS can produce a profound effect on the VFs, such as VF contraction and subsequent hoarseness in the patient.[91] However, with the right stimulation settings, this relative ease of VF contraction elicited with VNS may prove beneficial for promoting nerve regeneration in the case of RLN injury. Though further work is necessary to determine the optimal stimulation parameters for this purpose.

In fact, electrical nerve stimulation is a continually evolving treatment modality for peripheral nerve damage. When applied proximal to a nerve injury

site, electrical stimulation has been beneficial in promoting functional recovery in rodent models of multiple different nerve injuries[26,92-94], as well as in humans with carpal tunnel syndrome.[92] The enhanced functional recovery observed after nerve stimulation is largely attributed to upregulation of neurotrophic factors and regeneration-associated genes in the nerve cell bodies that may function to accelerate axonal regeneration across the injury site and improve the specificity of target reinnervation[94-96]. Interestingly, electrical stimulation is most effective in early stages after injury, as its effects on gene expression occur acutely, despite long-term daily treatment.[95,97] Thus, a treatment of one hour or less immediately after the injury may be therapeutic to promote RLN regeneration and functional recovery.

Therefore, intraoperative VNS may prove to be a useful tool in preventing or alleviating post-operative complications. If the optimal stimulation settings were discovered, VNS could be applied immediately after an RLN injury is detected during surgery to promote nerve regeneration. In this case, vagal nerve monitoring equipment could be modified to allow adjustments for therapeutic settings, removing the need for further RLN or vagal nerve manipulation to apply an electrical stimulus. However, before employing VNS as a treatment in clinical settings, work must be done to evaluate the optimal settings and safety of VNS for this purpose, including any “off-target” effects VNS may have on other organ systems such as the cardiorespiratory or gastrointestinal systems that are also innervated by the vagus nerve.

1.4 Conclusions

Despite nerve identification and intraoperative monitoring techniques, iatrogenic RLN injury remains a genuine concern for patients undergoing cervical or thoracic surgical procedures. A thorough understanding of RLN reinnervation and an effective treatment to restore physiologic function after injury is critical, as these procedures carry significant risk to reduce quality of life in patients and potential litigation against the medical professionals performing them. Therefore, work in animal models is essential to further our understanding of this injury. However, the translational potential in current studies is lacking, as many fail to investigate all functional aspects associated with VF paralysis.

The majority of animal work has utilized laryngoscopy and histological techniques to examine VF motion and RLN reinnervation, respectively. However, other translatable outcome measures such as voice, respiration, and swallow function have yet to be comprehensively investigated in a single model. It is critical to examine these behaviors to obtain a complete understanding of the dysfunction caused by an RLN injury. Therefore, one of the overarching goals of this research is to characterize and refine a mouse model of RLN injury for use in future therapeutic investigations.

Throughout this work, the effects of RLN injury on murine VF motion, swallowing behavior, ultrasonic vocalization production, and respiratory function are examined. Furthermore, methods for refining the functional assays used to assess these behaviors are developed, allowing for the production of more reliable and translatable results. Therefore, in Chapter 2, we explore the effects of SLN vs

RLN injury to confirm the fidelity of the laryngeal innervation pattern and functional outcomes (for vocal fold motion and swallowing) between mice and humans. In Chapter 3, we develop an automated VF tracking and quantification software to objectively measure dynamic VF motion, which is further refined in Chapter 4. Also in Chapter 4, we expand our translational mouse model to characterize swallow, vocal, and respiratory function in mice with unilateral VF paralysis following RLN injury. Lastly, VNS and its role as a therapeutic intervention for RLN injury is studied (Chapter 2), as well as the potential off-target effects this therapy may have on the many other organ systems provided innervation by the vagus nerve (Chapter 5). In conclusion, this work aims to provide a refined and reproducible animal model for researchers to use to investigate RLN pathophysiology, with the hope that one day there may be effective treatment options to fully restore physiologic function to patients with RLN injury and VF paralysis.

1.5 References

1. Chandrasekhar SS, Randolph GW, Seidman MD, et al. Clinical practice guideline: improving voice outcomes after thyroid surgery. *Otolaryngol Head Neck Surg.* 2013;148(6 Suppl):S1-37.

2. Mattsson P, Hydman J, Svensson M. Recovery of laryngeal function after intraoperative injury to the recurrent laryngeal nerve. *Gland Surg.* 2015;4(1):27-35.

3. Rosko AJ, Kupfer RA, Oh SS, Haring CT, Feldman EL, Hogikyan ND. Immunohistologic analysis of spontaneous recurrent laryngeal nerve reinnervation in a rat model. *Laryngoscope.* 2018;128(3):E117-e122.

4. Behkam R, Roberts KE, Bierhals AJ, et al. Aortic arch compliance and idiopathic unilateral vocal fold paralysis. *Journal of applied physiology (Bethesda, Md : 1985).* 2017;123(2):303-309.

5. Francis DO, Sherman AE, Hovis KL, et al. Life Experience of Patients With Unilateral Vocal Fold Paralysis. *JAMA Otolaryngol Head Neck Surg.* 2018;144(5):433-439.

6. Lynch J, Parameswaran R. Management of unilateral recurrent laryngeal nerve injury after thyroid surgery: A review. *Head Neck.* 2017;39(7):1470-1478.

7. Ta JH, Liu YF, Krishna P. Medicolegal Aspects of Iatrogenic Dysphonia and Recurrent Laryngeal Nerve Injury. *Otolaryngol Head Neck Surg.* 2016;154(1):80-86.

8. Erwood MS, Walters BC, Connolly TM, et al. Voice and swallowing outcomes following reoperative anterior cervical discectomy and fusion with a 2-team surgical approach. *J Neurosurg Spine.* 2018;28(2):140-148.

9. Wang B, Yuan J, Chen X, Xu J, Li Y, Dong P. Functional regeneration of the transected recurrent laryngeal nerve using a collagen scaffold loaded with laminin and laminin-binding BDNF and GDNF. *Scientific reports.* 2016;6:32292.

10. Wang B, Yuan J, Xu J, Xie J, Wang G, Dong P. Neurotrophin expression and laryngeal muscle pathophysiology following recurrent laryngeal nerve transection. *Mol Med Rep.* 2016;13(2):1234-1242.

11. Erman AB, Kejner AE, Hogikyan ND, Feldman EL. Disorders of Cranial Nerves IX and X. *Seminars in neurology.* 2009;29(1):85-92.

12. Kandil E, Anwar MA, Bamford J, Aslam R, Randolph GW. Electrophysiological identification of nonrecurrent laryngeal nerves. *Laryngoscope.* 2017;127(9):2189-2193.

13. Chambers KJ, Raol N, Song PC, Randolph GW, Hartnick CJ. Laryngeal Reinnervation Using a Split-Hypoglossal Nerve Graft in a Canine Model. *JAMA Otolaryngol Head Neck Surg.* 2015;141(7):620-627.

14. Wang W, Chen D, Chen S, et al. Laryngeal Reinnervation Using Ansa Cervicalis for Thyroid Surgery-Related Unilateral Vocal Fold Paralysis: A Long-Term Outcome Analysis of 237 Cases. *PLoS ONE.* 2011;6(4):e19128.

15. Navarro X, Vivo M, Valero-Cabre A. Neural plasticity after peripheral nerve injury and regeneration. *Progress in neurobiology.* 2007;82(4):163-201.

16. Hernandez-Morato I, Valderrama-Canales FJ, Berdugo G, et al. Reorganization of laryngeal motoneurons after crush injury in the recurrent laryngeal nerve of the rat. *J Anat.* 2013;222(4):451-461.

17. Kupfer RA, Old MO, Oh SS, Feldman EL, Hogikyan ND. Spontaneous laryngeal reinnervation following chronic recurrent laryngeal nerve injury. *Laryngoscope.* 2013;123(9):2216-2227.

18. Nishimoto K, Kumai Y, Yumoto E. Paradoxical movement of rat vocal folds following recurrent laryngeal nerve injury. *Acta oto-laryngologica.* 2014;134(11):1164-1171.

19. Old MO, Oh SS, Feldman E, Hogikyan ND. Novel model to assess laryngeal function, innervation, and reinnervation. *The Annals of otology, rhinology, and laryngology.* 2011;120(5):331-338.

20. Neel HB, Harner SG, Benninger MS, et al. Evaluation and Treatment of the Unilateral Paralyzed Vocal Fold. *Otolaryngology -- Head and Neck Surgery.* 1994;111(4):497-508.

21. Aynehchi BB, McCoul ED, Sundaram K. Systematic review of laryngeal reinnervation techniques. *Otolaryngol Head Neck Surg.* 2010;143(6):749-759.

22. Choi JS, Oh SH, An HY, Kim YM, Lee JH, Lim JY. Functional regeneration of recurrent laryngeal nerve injury during thyroid surgery using an asymmetrically porous nerve guide conduit in an animal model. *Thyroid.* 2014;24(1):52-59.

23. Hernandez-Morato I, Sharma S, Pitman MJ. Changes in neurotrophic factors of adult rat laryngeal muscles during nerve regeneration. *Neuroscience.* 2016;333:44-53.

24. Tessema B, Pitman MJ, Roark RM, Berzofsky C, Sharma S, Schaefer SD. Evaluation of functional recovery of recurrent laryngeal nerve using transoral laryngeal bipolar electromyography: a rat model. *The Annals of otology, rhinology, and laryngology.* 2008;117(8):604-608.

25. Tessema B, Roark RM, Pitman MJ, Weissbrod P, Sharma S, Schaefer SD. Observations of recurrent laryngeal nerve injury and recovery using a rat model. *Laryngoscope.* 2009;119(8):1644-1651.

26. Monaco GN, Brown TJ, Burgette RC, et al. Electrical stimulation and testosterone enhance recovery from recurrent laryngeal nerve crush. *Restor Neurol Neurosci.* 2015;33(4):571-578.

27. Motoyoshi K, Hyodo M, Yamagata T, Gyo K. Restoring vocal fold movement after transection and immediate suturing of the recurrent laryngeal nerve with local application of basic fibroblast growth factor: an experimental study in the rat. *Laryngoscope.* 2004;114(7):1247-1252.

28. Mor N, Naggar I, Das O, et al. Quantitative video laryngoscopy to monitor recovery from recurrent laryngeal nerve injury in the rat. *Otolaryngol Head Neck Surg.* 2014;150(5):824-826.

29. Tsujimura T, Suzuki T, Yoshihara M, et al. Involvement of hypoglossal and recurrent laryngeal nerves on swallowing pressure. *Journal of applied physiology (Bethesda, Md : 1985).* 2018;124(5):1148-1154.

30. Domer AS, Kuhn MA, Belafsky PC. Neurophysiology and Clinical Implications of the Laryngeal Adductor Reflex. *Current otorhinolaryngology reports.* 2013;1(3):178-182.

31. Shock LA, Gallemore BC, Hinkel CJ, et al. Improving the Utility of Laryngeal Adductor Reflex Testing: A Translational Tale of Mice and Men. *Otolaryngol Head Neck Surg.* 2015;153(1):94-101.

32. Mu L, Sanders I. The innervation of the human upper esophageal sphincter. *Dysphagia.* 1996;11(4):234-238.

33. Wilson JA, Pryde A, White A, Maher L, Maran AG. Swallowing performance in patients with vocal fold motion impairment. *Dysphagia.* 1995;10(3):149-154.

34. Fukushima S, Shingai T, Takahashi Y, Taguchi Y, Noda T, Yamada Y. Genesis of the decrement of intraluminal pressure in the UES during swallowing in rabbits. *Brain Res.* 2005;1044(1):122-126.

35. DeLozier KR, Gould FDH, Ohlemacher J, Thexton AJ, German RZ. Impact of recurrent laryngeal nerve lesion on oropharyngeal muscle activity and sensorimotor integration in an infant pig model. *Journal of applied physiology (Bethesda, Md : 1985).* 2018;125(1):159-166.

36. Gould FD, Ohlemacher J, Lammers AR, et al. Central nervous system integration of sensorimotor signals in oral and pharyngeal structures: oropharyngeal kinematics response to recurrent laryngeal nerve lesion. *Journal of applied physiology (Bethesda, Md : 1985).* 2016;120(5):495-502.

37. Rugiu MG. Role of videofluoroscopy in evaluation of neurologic dysphagia. *Acta otorhinolaryngologica Italica : organo ufficiale della Societa italiana di otorinolaringologia e chirurgia cervico-facciale.* 2007;27(6):306-316.

38. Martin-Harris B, Jones B. The videofluorographic swallowing study. *Phys Med Rehabil Clin N Am.* 2008;19(4):769-785, viii.

39. Langmore SE, Schatz K, Olson N. Endoscopic and videofluoroscopic evaluations of swallowing and aspiration. *The Annals of otology, rhinology, and laryngology.* 1991;100(8):678-681.

40. Madden C, Fenton J, Hughes J, Timon C. Comparison between videofluoroscopy and milk-swallow endoscopy in the assessment of swallowing function. *Clinical otolaryngology and allied sciences.* 2000;25(6):504-506.

41. Lever TE, Braun SM, Brooks RT, et al. Adapting human videofluoroscopic swallow study methods to detect and characterize dysphagia in murine disease models. *J Vis Exp.* 2015(97).

42. Levine JS, Pollard RE, Marks SL. Contrast videofluoroscopic assessment of dysphagic cats. *Veterinary radiology & ultrasound : the official journal of the American College of Veterinary Radiology and the International Veterinary Radiology Association.* 2014;55(5):465-471.

43. Harris RA, Grobman ME, Allen MJ, et al. Standardization of a Videofluoroscopic Swallow Study Protocol to Investigate Dysphagia in Dogs. *Journal of veterinary internal medicine.* 2017;31(2):383-393.

44. Best MD, Nakamura Y, Kijak NA, et al. Semiautomatic marker tracking of tongue positions captured by videofluoroscopy during primate feeding. *Conf Proc IEEE Eng Med Biol Soc.* 2015;2015:5347-5350.

45. Kobara-Mates M, Logemann JA, Larson C, Kahrilas PJ. Physiology of oropharyngeal swallow in the cat: a videofluoroscopic and electromyographic study. *The American journal of physiology.* 1995;268(2 Pt 1):G232-241.

46. Gould FDH, Yglesias B, Ohlemacher J, German RZ. Pre-pharyngeal Swallow Effects of Recurrent Laryngeal Nerve Lesion on Bolus Shape and Airway Protection in an Infant Pig Model. *Dysphagia.* 2017;32(3):362-373.

47. Gross A, Ohlemacher J, German R, Gould F. LVC Timing in Infant Pig Swallowing and the Effect of Safe Swallowing. *Dysphagia.* 2018;33(1):51-62.

48. Ballester A, Gould F, Bond L, et al. Maturation of the Coordination Between Respiration and Deglutition with and Without Recurrent Laryngeal Nerve Lesion in an Animal Model. *Dysphagia.* 2018.

49. Gould FDH, Lammers AR, Ohlemacher J, et al. The physiologic impact of unilateral recurrent laryngeal nerve (RLN) lesion on infant oropharyngeal and esophageal performance. *Dysphagia.* 2015;30(6):714-722.

50. German RZ, Crompton AW, Owerkowicz T, Thexton AJ. Volume and rate of milk delivery as determinants of swallowing in an infant model animal (Sus scrofia). *Dysphagia.* 2004;19(3):147-154.

51. Russell JA, Ciucci MR, Hammer MJ, Connor NP. Videofluorographic assessment of deglutitive behaviors in a rat model of aging and Parkinson disease. *Dysphagia.* 2013;28(1):95-104.

52. Lever TE, Brooks RT, Thombs LA, et al. Videofluoroscopic Validation of a Translational Murine Model of Presbyphagia. *Dysphagia.* 2015;30(3):328-342.

53. Hinkel CJ, Sharma R, Thakkar MM, Takahashi K, Hopewell BL, Lever TE. Neural Mechanisms Contributing to Dysphagia in Mouse Models. *Otolaryngol Head Neck Surg.* 2016;155(2):303-306.

54. Marawar S, Girardi FP, Sama AA, et al. National trends in anterior cervical fusion procedures. *Spine (Phila Pa 1976).* 2010;35(15):1454-1459.

55. Subramanian HH, Arun M, Silburn PA, Holstege G. Motor organization of positive and negative emotional vocalization in the cat midbrain periaqueductal gray. *The Journal of comparative neurology.* 2016;524(8):1540-1557.

56. Burgdorf J, Panksepp J. Tickling induces reward in adolescent rats. *Physiol Behav.* 2001;72(1-2):167-173.

57. Burgdorf J, Kroes RA, Moskal JR, Pfaus JG, Brudzynski SM, Panksepp J. Ultrasonic vocalizations of rats (Rattus norvegicus) during mating, play, and aggression: Behavioral concomitants, relationship to reward, and self-administration of playback. *Journal of comparative psychology (Washington, DC : 1983).* 2008;122(4):357-367.

58. Heckman J, McGuinness B, Celikel T, Englitz B. Determinants of the mouse ultrasonic vocal structure and repertoire. *Neurosci Biobehav Rev.* 2016;65:313-325.

59. Lahvis GP, Alleva E, Scattoni ML. Translating Mouse Vocalizations: Prosody and Frequency Modulation. *Genes, brain, and behavior.* 2011;10(1):4-16.

60. Roberts LH. Evidence for the laryngeal source of ultrasonic and audible cries of rodents. *Journal of Zoology.* 1975;175(2):243-257.

61. Thomas DA, Talalas L, Barfield RJ. Effect of devocalization of the male on mating behavior in rats. *Journal of Comparative and Physiological Psychology.* 1981;95(4):630-637.

62. Thiessen DD, Kittrell EM, Graham JM. Biomechanics of ultrasound emissions in the Mongolian gerbil, Meriones unguiculatus. *Behavioral and neural biology.* 1980;29(4):415-429.

63. Nunez AA, Pomerantz SM, Bean NJ, Youngstrom TG. Effects of laryngeal denervation on ultrasound production and male sexual behavior in rodents. *Physiol Behav.* 1985;34(6):901-905.

64. Pomerantz SM, Nunez AA, Jay Bean N. Female behavior is affected by male ultrasonic vocalizations in house mice. *Physiology & Behavior.* 1983;31(1):91-96.

65. White NR, Prasad M, Barfield RJ, Nyby JG. 40- and 70-kHz vocalizations of mice (Mus musculus) during copulation. *Physiol Behav.* 1998;63(4):467-473.

66. Scattoni ML, Crawley J, Ricceri L. Ultrasonic vocalizations: a tool for behavioural phenotyping of mouse models of neurodevelopmental disorders. *Neuroscience and biobehavioral reviews.* 2009;33(4):508-515.

67. Fischer J, Hammerschmidt K. Ultrasonic vocalizations in mouse models for speech and socio-cognitive disorders: insights into the evolution of vocal communication. *Genes, brain, and behavior.* 2011;10(1):17-27.

68. Grant LM, Richter F, Miller JE, et al. Vocalization deficits in mice over-expressing alpha-synuclein, a model of pre-manifest Parkinson's disease. *Behavioral neuroscience.* 2014;128(2):110-121.

69. Grant LM, Kelm-Nelson CA, Hilby BL, et al. Evidence for early and progressive ultrasonic vocalization and oromotor deficits in a PINK1 gene knockout rat model of Parkinson's disease. *J Neurosci Res.* 2015;93(11):1713-1727.

70. Weinberger M, Doshi D. Vocal cord dysfunction: a functional cause of respiratory distress. *Breathe (Sheffield, England).* 2017;13(1):15-21.

71. Brunner E, Friedrich G, Kiesler K, Chibidziura-Priesching J, Gugatschka M. Subjective breathing impairment in unilateral vocal fold paralysis. *Folia phoniatrica et logopaedica : official organ of the International Association of Logopedics and Phoniatrics (IALP).* 2011;63(3):142-146.

72. Perie S, Roubeau B, Liesenfelt I, Chaigneau-Debono G, Bruel M, St Guily JL. Role of medialization in the improvement of breath control in unilateral vocal fold paralysis. *The Annals of otology, rhinology, and laryngology.* 2002;111(11):1026-1033.

73. Azadarmaki R, Mirza N, Soliman AM. Unilateral true vocal fold synkinesis presenting with airway obstruction. *The Annals of otology, rhinology, and laryngology.* 2009;118(8):587-591.

74. Fasano V, Raiteri L, Bucchioni E, et al. Increased frequency dependence of specific airway resistance in patients with laryngeal hemiplegia. *European Respiratory Journal.* 2001;18(6):1003-1008.

75. Bohlender J. Diagnostic and therapeutic pitfalls in benign vocal fold diseases. *GMS current topics in otorhinolaryngology, head and neck surgery.* 2013;12:Doc01.

76. Francis DO, McKiever ME, Garrett CG, Jacobson B, Penson DF. Assessment of patient experience with unilateral vocal fold immobility: a preliminary study. *Journal of voice : official journal of the Voice Foundation.* 2014;28(5):636-643.

77. Beaty MM, Hoffman HT. Impact of laryngeal paralysis and its treatment on the glottic aperture and upper airway flow characteristics during exercise. *Otolaryngol Head Neck Surg.* 1999;120(6):819-823.

78. Saarinen A, Rihkanen H, Lehikoinen-Soderlund S, Sovijarvi AR. Airway flow dynamics and voice acoustics after autologous fascia augmentation of paralyzed vocal fold. *The Annals of otology, rhinology, and laryngology.* 2000;109(6):563-567.

79. Kashima HK. Documentation of upper airway obstruction in unilateral vocal cord paralysis: flow-volume loop studies in 43 subjects. *Laryngoscope.* 1984;94(7):923-937.

80. Asik MB, Karasimav O, Birkent H, Merati AL, Gerek M, Yildiz Y. Airway and Respiration Parameters Improve Following Vocal Fold Medialization: A Prospective Study. *The Annals of otology, rhinology, and laryngology.* 2015;124(12):972-977.

81. Lim R, Zavou MJ, Milton PL, et al. Measuring respiratory function in mice using unrestrained whole-body plethysmography. *J Vis Exp.* 2014(90):e51755.

82. Yuan H, Silberstein SD. Vagus Nerve and Vagus Nerve Stimulation, a Comprehensive Review: Part I. *Headache.* 2016;56(1):71-78.

83. Schneider R, Przybyl J, Pliquett U, et al. A new vagal anchor electrode for real-time monitoring of the recurrent laryngeal nerve. *American journal of surgery.* 2010;199(4):507-514.

84. Schneider R, Randolph GW, Sekulla C, et al. Continuous intraoperative vagus nerve stimulation for identification of imminent recurrent laryngeal nerve injury. *Head Neck.* 2013;35(11):1591-1598.

85. Schneider R, Machens A, Randolph GW, Kamani D, Lorenz K, Dralle H. Opportunities and challenges of intermittent and continuous intraoperative neural monitoring in thyroid surgery. *Gland Surg.* 2017;6(5):537-545.

86. Pelot NA, Grill WM. Effects of vagal neuromodulation on feeding behavior. *Brain Res.* 2018.

87. Simon B, Blake J. Mechanism of action of non-invasive cervical vagus nerve stimulation for the treatment of primary headaches. *The American journal of managed care.* 2017;23(17 Suppl):S312-s316.

88. Yuan H, Silberstein SD. Vagus Nerve and Vagus Nerve Stimulation, a Comprehensive Review: Part II. *Headache.* 2016;56(2):259-266.

89. Yuan H, Silberstein SD. Vagus Nerve and Vagus Nerve Stimulation, a Comprehensive Review: Part III. *Headache.* 2016;56(3):479-490.

90. Guiraud D, Andreu D, Bonnet S, et al. Vagus nerve stimulation: state of the art of stimulation and recording strategies to address autonomic function neuromodulation. *Journal of neural engineering.* 2016;13(4):041002.

91. Ardesch JJ, Sikken JR, Veltink PH, van der Aa HE, Hageman G, Buschman HP. Vagus nerve stimulation for epilepsy activates the vocal folds maximally at therapeutic levels. *Epilepsy research.* 2010;89(2-3):227-231.

92. Gordon T. Electrical Stimulation to Enhance Axon Regeneration After Peripheral Nerve Injuries in Animal Models and Humans. *Neurotherapeutics.* 2016;13(2):295-310.

93. Sharma N, Marzo SJ, Jones KJ, Foecking EM. Electrical stimulation and testosterone differentially enhance expression of regeneration-associated genes. *Experimental neurology.* 2010;223(1):183-191.

94. Al-Majed AA, Tam SL, Gordon T. Electrical stimulation accelerates and enhances expression of regeneration-associated genes in regenerating rat femoral motoneurons. *Cellular and molecular neurobiology.* 2004;24(3):379-402.

95. Al-Majed AA, Brushart TM, Gordon T. Electrical stimulation accelerates and increases expression of BDNF and trkB mRNA in regenerating rat femoral motoneurons. *The European journal of neuroscience.* 2000;12(12):4381-4390.

96. Brushart TM, Jari R, Verge V, Rohde C, Gordon T. Electrical stimulation restores the specificity of sensory axon regeneration. *Experimental neurology.* 2005;194(1):221-229.

97. Al-Majed AA, Neumann CM, Brushart TM, Gordon T. Brief electrical stimulation promotes the speed and accuracy of motor axonal regeneration. *J Neurosci.* 2000;20(7):2602-2608.

Chapter Two

A SURGICAL MOUSE MODEL FOR ADVANCING LARYNGEAL NERVE REGENERATION STRATEGIES

This chapter has been submitted for publication to the Dysphagia Journal

Contributions include performing RLN transection surgeries and laryngoscopy procedures, laryngoscopy analysis, RLN crush and vagal nerve stimulation procedures, as well as aiding in the drafting of the manuscript and review of multiple revisions.

Alexis Mok[1§], Jakob Allen[2§], Megan M. Haney[3], Ian Deninger[4], Brayton Ballenger[4], Victoria Caywood[4], Kate L. Osman[4], Bradford Zitsch[2], Bridget L. Hopewell[4], Aaron Thiessen[4], Marlena Szewczyk[2], Daniel Ohlhausen[4], Christopher I. Newberry[2], Emily Leary[5], Teresa E. Lever[4]

[1]University of Missouri School of Health Professions, Department of Communication Science and Disorders, Columbia, Missouri

[2]University of Missouri School of Medicine, Department of Medicine, Columbia, Missouri

[3]University of Missouri College of Veterinary Medicine, Department of Veterinary Pathobiology, Columbia, Missouri

[4]University of Missouri School of Medicine, Department of Otolaryngology - Head & Neck Surgery, Columbia, Missouri

[5]University of Missouri School of Medicine, Department of Orthopedic Surgery, Columbia, Missouri

[§]These authors equally contributed to this work.

2.1 Abstract

Objectives: Iatrogenic recurrent laryngeal nerve (RLN) injury is a morbid complication of anterior neck surgical procedures. Existing treatments are predominantly symptomatic, ranging from behavioral therapy to a variety of surgical approaches. Though laryngeal reinnervation strategies often provide muscle tone to the paralyzed vocal fold (VF), which may improve outcomes, there is no clinical intervention that reliably restores true physiologic VF movement. Moreover, existing interventions neglect the full cascade of molecular events that affect the entire neuromuscular pathway after RLN injury, including the intrinsic laryngeal muscles, synaptic connections within the central nervous system, and laryngeal nerve anastomoses. Systematic investigations of this pathway are essential to develop better RLN regenerative strategies. Our aim was to develop a translational mouse model for this purpose, which will permit longitudinal investigations of the pathophysiology of iatrogenic RLN injury and potential therapeutic interventions.

Methods: C57BL/6J mice were divided into 4 surgical transection groups (unilateral RLN, n=10; bilateral RLN, n=2; unilateral SLN, n=10; bilateral SLN, n=10) and a sham surgical group (n=10). Miniaturized transoral laryngoscopy was used to assess vocal fold (VF) mobility over time, and swallowing was assessed using serial videofluoroscopy. Histological assays were conducted 3 months post-surgery for anatomical investigation of the larynx and laryngeal nerves. Eight additional mice underwent unilateral RLN crush injury, half of which received intraoperative vagal nerve stimulation (iVNS). These 8 mice underwent weekly transoral laryngoscopy to investigate VF recovery patterns.

Results: Unilateral RLN injury resulted in chronic VF immobility but only acute dysphagia. Bilateral RLN injury caused intraoperative asphyxiation and death. VF mobility was unaffected by SLN transection (unilateral or bilateral), and dysphagia (transient) was evident only after bilateral SLN transection. The sham surgery group retained normal VF mobility and swallow function. Mice that underwent RLN crush injury and iVNS treatment demonstrated accelerated and improved VF recovery.

Conclusions: We successfully developed a mouse model of iatrogenic RLN injury with impaired VF mobility and swallowing function that can serve as a clinically relevant platform to develop translational neuroregenerative strategies for RLN injury.

2.2 Introduction

Iatrogenic recurrent laryngeal nerve (RLN) injury, a complication of anterior neck surgical procedures, results in ipsilateral vocal fold (VF) immobility and associated dysphagia, dysphonia, and dyspnea.[1-3] Although the RLN may spontaneously regenerate after injury, recovery may take several months to years, and full return of normal function rarely occurs.[2,4,5] Poor outcomes are largely attributed to pathological reinnervation of the intrinsic laryngeal muscles, either by preferential reinnervation of laryngeal adductors by regenerating RLN fibers or by collateral reinnervation by the superior laryngeal nerve (SLN).[2,6,7] While pathological reinnervation may mitigate laryngeal muscle atrophy, VF movement typically remains ineffective and unsynchronized.[6,8,9] Older individuals are particularly at risk for worse outcomes, as aged peripheral nerves have reduced regenerative capacity.[10-12] This biological deficiency is especially concerning for the increasingly aging population undergoing anterior neck procedures.[13,14]

Existing treatments for RLN injury are predominantly symptomatic, ranging from behavioral therapy to a variety of surgical approaches. Though laryngeal reinnervation strategies often provide muscle tone to the paralyzed VF, which may improve functional outcomes, there is no clinical intervention that reliably restores true physiologic VF movement.[15-19] Moreover, existing interventions neglect the full cascade of molecular events that affect the entire neuromuscular pathway after RLN injury, including the intrinsic laryngeal muscles, synaptic connections within the central nervous system, and laryngeal nerve anastomoses. Systematic investigations of this pathway are essential to develop better RLN regenerative

strategies. Animal models such as pigs,[20-25] dogs,[26] cats,[27] rats,[28,29] and rabbits[15] provide suitable platforms for this purpose. Rats, in particular, are at the forefront of an emerging treatment for nerve regeneration -- electrical stimulation applied proximal to the nerve injury site. This approach has shown promising effects after facial nerve[30,31] and RLN[29] injury. However, these studies have predominantly focused on infant or young adult rats whose developing nervous systems bear little resemblance to mature humans. Moreover, no animal study of RLN injury has integrated basic science techniques with the clinical gold standard combination of endoscopy and videofluoroscopy for clinicopathological investigation of the aerodigestive tract.

The goal of this study was to develop a mouse surgical model of iatrogenic RLN injury to accelerate scientific discovery. We chose the C57BL/6J mouse because it is an established translational model for investigations of swallowing[32] and laryngeal biology.[33] The short life-span of the mouse permits high throughput, longitudinal investigations in aged populations more representative of anterior neck surgical patients. However, its small size (**Figure 2.1**) has been prohibitive to the development of directly translatable functional outcome measures for correlation with histological findings.[34] Here, we have overcome this challenge by using our “miniaturized” endoscopic[35] and fluoroscopic[32,36] imaging methodology to develop a translational mouse model of iatrogenic RLN injury.

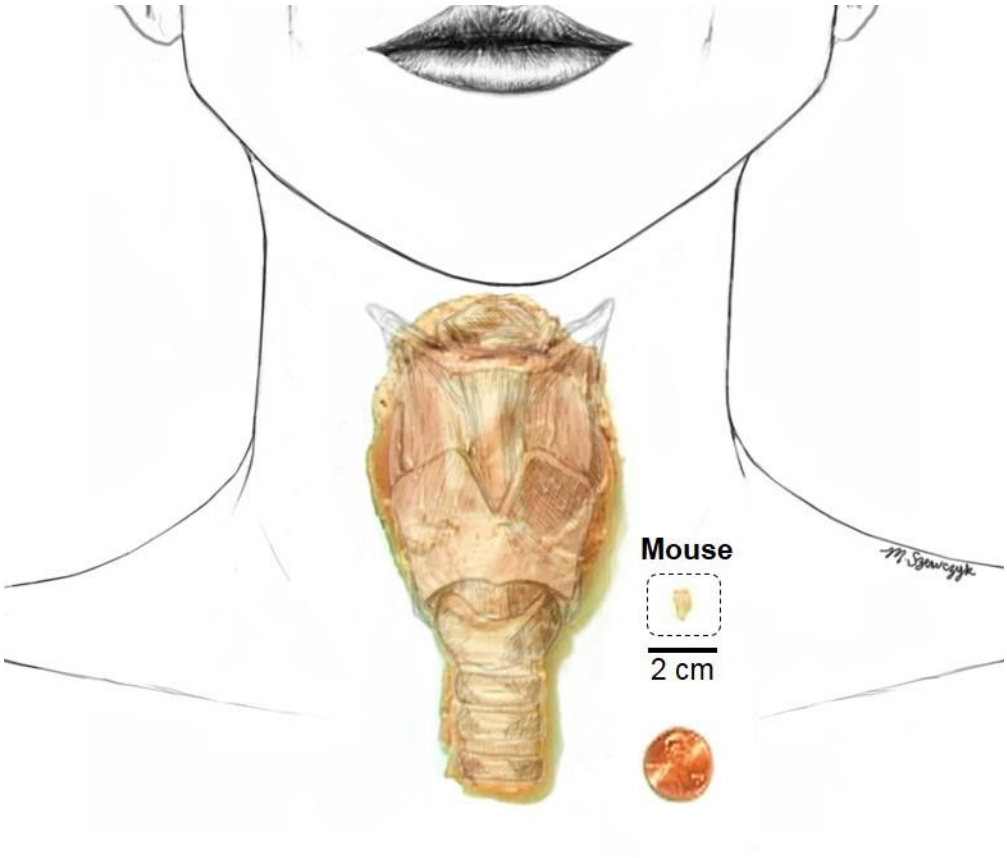

Figure 2.1. Size Comparison between a Human and Mouse Larynx. A photograph of side-by-side specimens of a human and mouse larynx next to a US penny (approximately 1.9 cm diameter), overlaid on a proportionately scaled schematic of a human head and neck. The cartilaginous/bony framework is drawn on both specimens for anatomical clarity. A 2 cm scale bar is shown for added size perspective.

Our first endeavor was to ensure the fidelity of the laryngeal innervation pattern and functional outcomes between humans and mice. We focused on transection (neurotmesis) injuries because they are most experimentally replicable,[5] and included the RLN and SLN because of the growing evidence of dual innervation of the intrinsic laryngeal muscles.[37,38] We hypothesized that like humans, RLN transection in mice would cause chronic impairment of VF mobility and dysphagia, whereas SLN transection would result in subtle, transient changes in VF mobility and swallowing function. Furthermore, we expected more severe

symptoms after bilateral injury. Finally, we adapted our model to include a more prevalent crush (axonotmesis) injury,[5] and conducted a feasibility study of intraoperative vagal nerve stimulation (iVNS) as a novel RLN regenerative strategy. In doing so, we expanded upon a recent study in young adult rats in which RLN stimulation accelerated the recovery of VF mobility after RLN crush injury.[29] However, rather than stimulating the RLN, we chose the cervical vagus nerve as a more clinically relevant treatment site to simultaneously target all potentially injured RLN branches and promote widespread regeneration. Moreover, we tested this strategy in aged mice to better correspond to the average age of anterior neck surgical patients, thus highlighting our translational intent.

2.3 Materials and Methods

2.3.1 Animals

Fifty adult C57BL/6 (also known as B6) mice of either sex were included in this study, which was approved by our Institutional Animal Care and Use Committee. The majority of these mice (n=42) were used to develop our surgical model of iatrogenic laryngeal nerve injury (i.e., transection), and the remaining (n=8) were allowed to age for further model refinement (i.e., RLN crush injury and exploratory regenerative treatment). All mice were offspring from our C57BL/6J colony established by mating sibling pairs purchased at 6 weeks of age from The Jackson Laboratory (Bar Harbor, ME). Over a 2-year period, offspring between 3 and 12 months of age were randomly assigned to several surgical cohorts, with

transection injury groups completed before beginning the crush injury component of this investigation.

Mice were group housed (2-4 animals per cage, based on sex and litter) in a standard 12:12 light/dark cycle facility with controlled temperature and humidity conditions. Free access to water and standard rodent food pellets was provided, except during the experimental procedures described below. An enhanced enrichment protocol (e.g., running wheel and chewable treats) was used for all cages to minimize aggression and the need for single housing in our aging B6 colony. Daily monitoring by veterinary and research staff ensured that all mice remained healthy throughout the study.

2.3.2 Surgical Procedures

General Surgical Approach: All 50 mice underwent microsurgery using a midline ventral neck approach, closely following our previously established methods.[39] After a 4-6 hour food restriction, mice were anesthetized with a single subcutaneous injection of ketamine-xylazine (90/11.25 mg/kg), followed by scheduled maintenance doses of ketamine (half the original dose) every 10-20 minutes as needed to maintain a surgical plane of anesthesia (i.e., absence of pedal withdrawal and eye blink reflexes). Eyes were lubricated (Lacrilube®, Allergan, Inc.; Irvine, CA) to prevent drying. The ventral neck was shaved and prepared aseptically for surgery. Next, the head was stabilized in ear bars, with the mouse positioned in dorsal recumbency on a custom surgical platform beneath a surgical microscope (M125; Leica Microsystems, Inc., Buffalo Grove, IL). Core

body temperature was maintained at 37 ± 0.2 ºC using a homeothermic heating system (DC Temperature Controller; FHC, Bowdoin, ME). Mice spontaneously breathed room air during the entire surgical procedure, except during iVNS treatment, when supplemental oxygen was provided (described below).

Immediately prior to the surgical neck incision, laryngoscopy (described below) was performed according to our published protocol[35] to establish baseline VF function. Next, an approximate 2 cm midline skin incision was made from the suprasternal notch to the intersection of the anterior digastric muscles near the mandibular symphysis, using a micro scalpel and micro scissors. The large salivary glands were gently retracted from midline with micro forceps and secured with a pediatric ophthalmic retractor for unobstructed visualization of the surgical field (**Figure 2.2a**). The target laryngeal nerve was visualized within the fascia along the lateral aspect of the larynx (SLN) or trachea (RLN). After careful isolation using micro forceps, laryngeal nerve injury was performed according to experimental group assignment (transection versus crush injury, described below). Immediately following surgical manipulation, laryngoscopy was repeated to assess the effect on VF mobility (described below). Next, soft tissue structures were approximated medially, and the neck incision was closed with 6-0 monocryl suture material (Ethicon™, Johnson & Johnson Company; New Brunswick, NJ) and surgical glue (Tissumend II, Veterinary Products Laboratories; Phoenix, AZ). Postsurgical analgesics (buprenorphine, 0.05 mg/kg; banamine, 2.2 mg/kg) and saline (0.2 mL) were administered subcutaneously prior to transferring mice to a recovery cage warmed to 37 °C on a water-circulating heating pad (Model #TP700,

Stryker Medical, Portage, MI). Mice were returned to their home cage when fully ambulatory, typically within 1 hour after surgery. For 72 hours post-surgery, pain management (buprenorphine, 0.05 mg/kg) was provided every 8-12 hours, and the home cage was kept warm by placing it half way on a 37 °C water-circulating heating pad (Stryker) to prevent anesthesia-related hypothermia. Post-operative monitoring was conducted daily by research staff for 1 week, and then daily health monitoring by animal care staff continued throughout the remainder of the study.

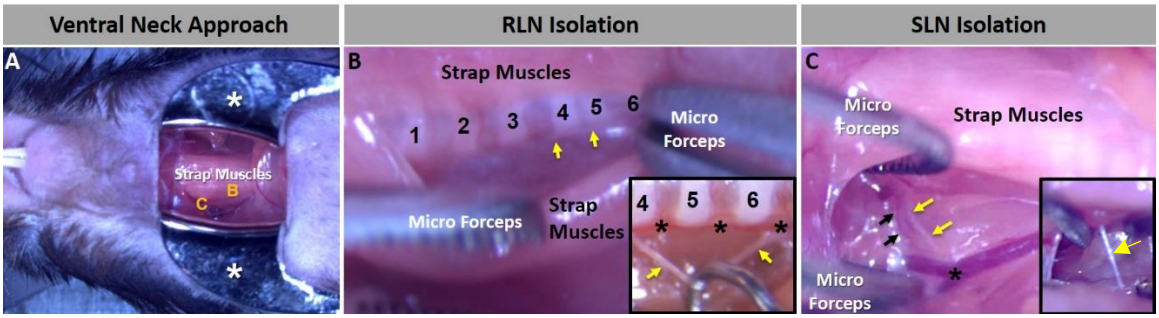

Figure 2.2. Microsurgical Approach. (A) Our microsurgical approach in mice to access the laryngeal nerves via a midline ventral neck incision is typically a bloodless procedure. Micro retractors (white asterisks) are used to maintain the large salivary glands out of the surgical field. The strap muscles obscure the RLN (B) and SLN (C), which are shown at higher magnification in Images B and C, respectively. (B) To access the RLN, the strap muscles are carefully divided along the midline fascia and gently retracted with micro forceps to expose the tracheal rings (numbered) and RLN (yellow arrows).The inset image shows a close-up of the target tracheal ring region, with the RLN (yellow arrows) isolated from the inferior thyroid artery (black asterisks) with a micro hook in preparation for surgical transection. (C) To access the SLN, the strap muscles covering the lateral aspect of the larynx are gently elevated with micro forceps to expose the SLN (yellow arrows) traveling alongside the superior laryngeal artery (black arrows) near the bifurcation of the common carotid artery (black asterisk). The inset image shows a close-up of the SLN (yellow arrow) isolated from the fascia with micro forceps.

Laryngeal Nerve Transection Injury: Mice (n=42) were randomly allocated to one of five surgical groups: unilateral RLN transection (n=10), bilateral RLN transection (n=2, due to anticipated mortality from mechanical asphyxiation), unilateral SLN transection (n=10), bilateral SLN transection (n=10), and sham surgery (n=10). *For*

RLN transection, the strap muscles overlying the trachea were retracted from midline between the 4th and 6th tracheal rings to visualize the RLN running alongside the inferior thyroid artery (**Figure 2.2b**). *For SLN transection*, the SLN was readily identified within the superficial fascia on the lateral aspect of the larynx, traveling alongside the superior laryngeal artery (**Figure 2.2c**). *For the unilateral nerve injury groups*, only the right side was included because it was the most ergonomic for our custom surgical set-up and workflow. The target laryngeal nerve (either SLN or RLN, unilateral or bilateral) was gently isolated from the surrounding fascia and blood vessels with micro forceps. The nerve was then transected with micro scissors and a 1-2 mm section was removed to prevent spontaneous re-attachment of the proximal and distal nerve stumps during recovery. The transection location was always proximal (i.e., closer to the central nervous system) to any visible branches from the main nerve trunk. *Sham surgery mice* underwent all aspects of the surgical procedure, except the laryngeal nerves were visualized within the fascia and isolated, but not transected. For all surgical groups, laryngoscopy was repeated at the end of the procedure to assess the effect of surgical manipulation on VF mobility.

Immediately prior to transection of the SLN, a confirmatory step of brief electrical stimulation (described below) was added to assure that we had indeed identified the correct nerve. Previous work in our lab[39] and others[40] has shown that 40 Hz stimulation of the SLN (main trunk) in mice reliably evokes swallowing. In contrast, RLN stimulation parameters to evoke swallowing in mice have not yet been established, and our preliminary work (unpublished) has shown that 40 Hz

stimulation of the RLN in mice does not reliably evoke swallowing. Therefore, correct targeting of the RLN was confirmed by endoscopic visualization of ipsilateral VF immobility immediately after surgical transection.

For SLN stimulation, we used custom, bipolar hook electrodes (FHC, Bowdoin, ME) made of platinum iridium, with a 300-μm tip diameter, spaced 800 μm apart. The electrodes were positioned near the SLN using a manual micromanipulator (model U-30CF; Narishige, Co, LPD, Setagaya-Ku, Tokyo, Japan), and the SLN was gently draped over the electrodes using micro hooks. Electrical stimulation was delivered continuously for a single 20-second train using our previously published parameters for evoking SLN-stimulated swallowing in mice: 40 Hz, biphasic 0.5 ms square wave pulses, with a 0.1 ms interphase delay, delivered at 800 μA.[39] Stimulation was delivered using a constant current stimulus isolator (model 1101; ADInstruments, Colorado Springs, CO) coupled to an A/D converter (PowerLab 8/30, ADInstruments), with both devices controlled by LabChart software (ADInstruments). Current flow was directed *toward* the brain by positioning the anode electrode distal to the cathode electrode on each nerve, with directionality verified using a current probe (model P6042; Tektronic, Beaverton, OR) and voltage meter (True RMS MultiMeter; Extech Intruments, Waltham, MA). The stimulus shape and intensity were continually verified using a digital oscilloscope (model TDS 2024B; Tektronix) connected to the stimulus isolator. Swallowing events were identified by endoscopic visualization of tongue base retraction in conjunction with observable laryngeal elevation within the surgical site; both events were simultaneously video recorded at 30 frames per second

(fps) via the endoscope camera and surgical microscope camera. If no swallowing events were observed, visible exudate around the SLN was absorbed using paper points (#501; Henry Schein, Inc., Melville, NY), the nerve was repositioned on the bipolar electrode to prevent any contact with the surrounding tissues, and then a 2nd 20-second stimulus train was delivered. For the bilateral SLN transection group, this stimulation approach was performed separately for each side.

RLN Crush Injury and iVNS Treatment: For this feasibility study, we included 8 aged mice (over 12 months old) from our B6 colony to expand the utility and translatability of our surgical model. Rather than a transection (neurotmesis) injury, all 8 mice underwent a right-sided RLN crush (axonotmesis) injury. To do this, the RLN was carefully isolated from the fascia and inferior thyroid artery between the 4th and 6th tracheal rings using micro forceps. Next, a micro hook was used to place the RLN perpendicularly across smooth jaw hemostatic forceps (1 mm tip diameter, 13007-12; FST, Foster City, CA), which were then closed to the second locking position for 30 seconds.[41]

Laryngoscopy was repeated after RLN crush injury to assess the immediate effect on VF mobility. Mice were then randomly allocated to iVNS treatment (n=4) or control (n=4) groups. For the iVNS treatment group, the right cervical vagus nerve was isolated from the carotid sheath and placed on our previously described hook electrodes for continuous electrical stimulation at 20 Hz, as has been used for previous cranial nerve regeneration studies in rats.[29,31,30,42] For the control

group, the vagus nerve was neither isolated nor placed on electrodes after the RLN crush injury.

During iVNS treatment, current flow was directed toward the brain by positioning the anode electrode distal to the cathode electrode on the vagus nerve, with directionality verified as described above. This approach ensured that iVNS-evoked action potentials traveled toward the central nervous system to stimulate the cell bodies of the injured axons, which is essential for triggering upregulation of neurotrophic factors, their receptors, and growth associated proteins that accelerate regeneration at the distal nerve injury site.[43,44] We used our standard stimulus waveform parameters (biphasic 0.5 ms square wave pulses, with a 0.1 ms interphase delay) to deliver 20-second stimulus trains continuously for up to 60 minutes, depending on respiratory tolerance (described below). Stimulus intensity was increased from 0.2 to 0.8 mA in 0.1 mA steps to quickly (within 1-2 minutes) identify the highest subthreshold intensity level that did not evoke swallowing or cause agonal/labored breathing. This subthreshold stimulus level was then used for iVNS treatment, with the waveform morphology (shape and intensity) continually verified via oscilloscope, as described above.

During the additional surgical time required for the iVNS-treated mice, supplemental oxygen was provided via a nose cone at 1 L/min, and respiratory rate was monitored every 10 minutes throughout the treatment duration. If agonal/labored breathing developed during iVNS treatment, the stimulus intensity level was lowered in 0.1 mA steps to quickly (within 1-2 minutes) identify the level at which breathing stabilized; this new subthreshold level was used for the

remainder of the iVNS treatment. If respiratory status was not stabilized by lowering the stimulus intensity, iVNS treatment was immediately stopped to prevent ensuing morbidity or mortality.

2.3.3 Functional Measures

Laryngoscopy and VFSS were conducted at baseline (pre-surgery) and several post-surgical time points to assess VF mobility and swallowing function, respectively, during a three month recovery period, as described below. Post-surgical VFSS was always conducted 3-5 days before laryngoscopy to avoid confounding effects of anesthesia (required for laryngoscopy) on VFSS outcomes.

VF Mobility: To assess VF mobility, laryngoscopy was performed according to our established protocol,[35] with mice under surgical plane of anesthesia while spontaneously breathing room air (**Figure 2.3**). Laryngoscopy was performed twice during the surgical procedure -- immediately before surgical incision (to record baseline bilateral VF movement during spontaneous breathing) and again following surgical manipulation (to determine the immediate effect on VF mobility). Additionally, laryngoscopy was performed at multiple post-surgical time points with mice under brief (<15 minutes), surgical-level sedation. Mice allocated to the transection protocol underwent post-operative laryngoscopy at 1 week and 3 months post-surgery to assess acute versus chronic effects, respectively, on VF mobility. Mice allocated to the RLN crush/iVNS protocol underwent laryngoscopy

more frequently (i.e., weekly) to better characterize the pattern of spontaneous functional recovery versus treatment efficacy.

Our laryngoscopy protocol entailed securing anesthetized mice in ear bars in dorsal recumbency on our custom surgical platform. Next, a sialendoscope (R11573A; Karl Storz) with a custom laryngoscope was inserted transorally and advanced via a custom micromanipulator to visualize the larynx on a Storz Tele Pack X monitor (Karl Storz Endoskope, Tuttlingen, Germany). The endoscope was slowly advanced until the bilateral VFs filled the entire field of view, and VF movement was video recorded at 30 fps for approximately 1 minute during spontaneous breathing. Videos (MP4 files) were viewed frame-by-frame by two independent reviewers (authors TEL and BZ or MMH) using video editing software (Pinnacle Studio 14, Pinnacle Systems, Inc., Mountain View, CA), and VF mobility was scored using a subjective rating scale: 2 = normal movement, 1 = reduced movement, and 0 = no movement.[28,45] Reviewer discrepancies were resolved by group consensus with the principal investigator (TEL).

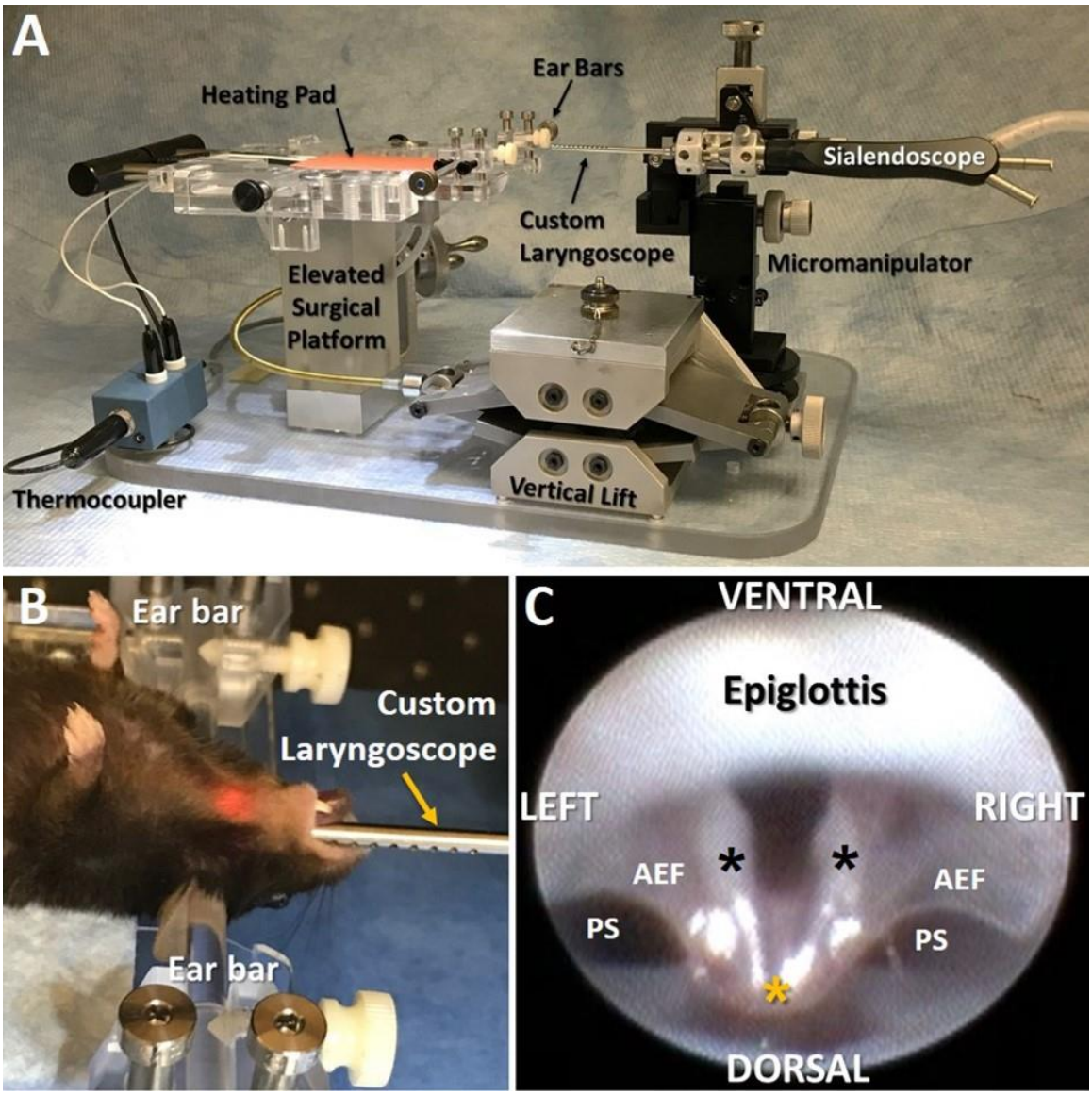

Figure 2.3. Laryngoscopy Assay. (A) Lateral view of our custom endoscopy suite for mice, with labeled components. (B) An anesthetized mouse in dorsal recumbency undergoing laryngoscopy, with the head gently secured in ear bars. The micromanipulator in Image A is used to precisely guide oral insertion, gentle advancement, and precise positioning of the sialendoscope (fitted with a custom laryngoscope) to visualize the larynx. (C) Representative endoscopic image of the murine larynx at maximum VF abduction during spontaneous breathing, taken from a 30 fps video at baseline (i.e., before surgery). Visible laryngeal structures of interest include the bilateral VFs (black asterisks), epiglottis, aryepiglottic folds (AEF), and pyriform sinuses (PS). In contrast to the human larynx, the VFs of mice retain midline proximity at the dorsal commissure (yellow asterisk), and the ventral commissure is consistently obscured by the epiglottis.

Swallow Function: Mice allocated to the transection protocol underwent VFSS testing according to our standard, freely behaving (unanesthetized) protocol[32,36]

(**Figure 2.4**) at 3 time points: baseline (i.e., approximately 1 week prior to surgery) as well as 1 week and 3 months post-surgery to assess acute versus chronic effects, respectively. Mice allocated to the RLN crush/iVNS treatment protocol were not subjected to VFSS testing in order to minimize resources used for this feasibility study.

Beginning two weeks prior to baseline VFSS testing, mice underwent a behavioral conditioning program to assure familiarity and acceptance of the contrast solution and test environment. At each VFSS time point, mice were fluid restricted overnight for 14-16 hours and provided additional chewable enrichment (e.g., nut and seed mix) to motivate voluntary drinking during VFSS testing the following morning. During testing, mice were individually enclosed in a custom VFSS test chamber secured to a custom, remote-controlled lift table within our miniaturized fluoroscope (Glenbrook Technologies, Randolph, NJ). Each mouse was then exposed to approximately 2-3 minutes of low-dose radiation (~30 kV and 0.2 mA) for fluoroscopic examination of swallowing in the lateral plane while freely drinking a species-specific oral contrast agent recipe: Omnipaque (350 mg iodine per mL; GE Healthcare, Inc., Princeton, NJ) diluted to a 25% solution with deionized water and 3% chocolate syrup. The contrast solution was administered through a custom delivery system into a custom bowl positioned immediately above the test chamber floor. To minimize radiation exposure, the fluoroscope was activated only when mice were drinking from the bowl, which was identified by real-time viewing via a webcam (C920 HD Pro Webcam; Logitech International S.A., Lausanne, Switzerland) positioned above the VFSS test chamber. The

oropharyngeal stage of swallowing was visualized first (**Figure 2.4c**), followed by remote-controlled repositioning of the chamber to visualize the entire esophageal stage of swallowing in a single field of view (**Figure 2.4d**). Fluoroscopic videos were captured at 30 fps during real-time viewing via computer monitor.

Videos (AVI files) were subsequently analyzed frame-by-frame by two independent reviewers (authors AM, VC, BB, DO, or ID) using video editing software (Pinnacle Studio 14) to quantify 6 swallow metrics established by our prior work,[32,36] as described in **Table 2.1**. We also quantified airway protection using the standardized 8-point Penetration-Aspiration Scale (PAS) that ranges from 1 (no penetration or aspiration) to 8 (silent aspiration).[46] Reviewer discrepancies were resolved by group consensus with the principal investigator (TEL).

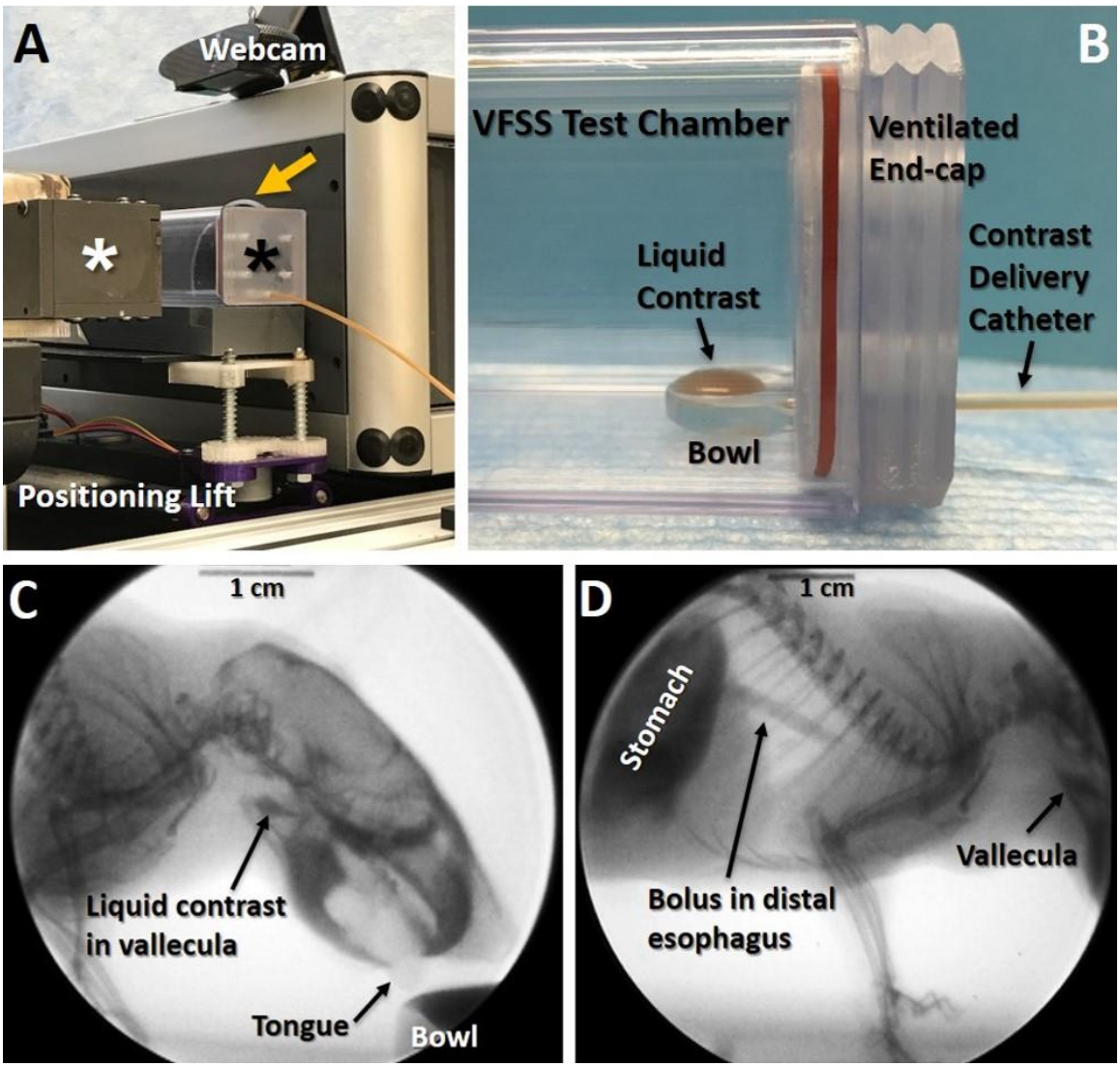

Figure 2.4. Videofluoroscopic Swallow Study (VFSS) Assay. (A) A custom VFSS test chamber (black asterisk) is positioned in lateral view between the X-ray source (white asterisk) and image intensifier (yellow arrow) of our custom, miniaturized c-arm fluoroscope. The X-ray beam is turned on only when mice are actively drinking, identified via a webcam positioned above the test chamber. A remote-controlled positioning lift is used to readily maintain the mouse's aerodigestive tract within the fluoroscopy field of view. (B) Close-up of the VFSS test chamber in Image A, designed to promote voluntary drinking of liquid contrast agent by mice with minimal behavioral distractions. Note the bowl within the test chamber is filled using a syringe delivery system that is manually controlled a few feet away from the fluoroscope. (C and D) Representative X-ray images from a 30 fps video of a mouse drinking in lateral view. Image C shows the oropharyngeal stage of swallowing, immediately prior to triggering of the swallow reflex. Note the liquid contrast agent accumulating in the vallecula within the pharynx, which is the stereotypical swallow trigger point in mice. Image D shows the esophageal stage of swallowing. Note the swallowed bolus traversing the distal esophagus into the stomach while liquid contrast continues to accumulate in the vallecula prior to triggering a subsequent swallow.

Table 2.1. VFSS Metrics to Detect and Quantify Dysphagia in Mice

VFSS Metrics	Operational Definition
Lick Rate	The number of licks per second (30 frames) during uninterrupted drinking. Each lick cycle begins with the jaw maximally opened and tongue protruding. Each subsequent maximal jaw excursion/tongue protrusion is counted as an individual lick cycle.
Swallow Rate	The number of swallows occurring during each 2-second (60 frames) episode of uninterrupted drinking. Each 2-second episode begins at the "rest frame" that immediately precedes triggering of the pharyngeal swallow (i.e., bolus flow from the valleculae to the esophagus).
Inter-Swallow Interval	The time (ms) between two successive, uninterrupted swallows during uninterrupted drinking. The start frame is the ''rest frame'' that immediately precedes triggering of the pharyngeal swallow. The end frame is the ''rest frame'' of the subsequent swallow. The number of frames between the two successive swallows is then divided by 30 frames per second (fps) to convert to time (ms).
Lick-Swallow Ratio	The number of licks during the inter-swallow interval (i.e., between two successive, uninterrupted swallows).
Pharyngeal Transit Time	The time (ms) it takes the bolus to be swallowed through the pharynx. The start frame is the ''rest frame'' that immediately precedes visible transfer of the bolus from the swallow trigger point (i.e., valleculae). The end frame is when the bolus tail enters the esophagus. The number of frames between the start and end frames is divided by 30 fps and converted to ms.
Esophageal Transit Time	The time (ms) it takes the bolus to be swallowed through the esophagus. The start frame is when the bolus tail enters the esophagus (i.e., the PTT end frame). The end frame is when the bolus tail enters the stomach. The number of frames between the start and end frames is divided by 30 fps and converted to milliseconds (ms).

Note: Three to five measures of each VFSS metric are obtained for each mouse.

2.3.4 Histological Investigation

At the study end point (3 months post-surgery), mice were euthanized by transcardial perfusion with saline followed by 4% paraformaldehyde, and relevant tissues were collected for a variety of postmortem assays. For gross anatomical mapping of the laryngeal nerves, a subset of samples (n=10) were collected as whole head and thorax specimens for laryngeal nerve mapping using a modified Sihler staining protocol.[47-50] This lengthy (~6 months) 8-step technique, summarized in **Table 2.2**, rendered the entire specimen transparent while staining myelinated nerves a dark purple color. Stained specimens were examined under

a dissection microscope (LM80; Leica) and carefully trimmed to remove soft tissue overlying the laryngeal nerves for improved visualization. Specimens were then placed on an X-ray light box beneath our surgical microscope (M125; Leica) for trans-illumination and digital imaging (Pixelink E421CU camera, Ottawa, Canada).

Another subset of samples (n=10) was subjected to post-mortem dissection of the laryngeal nerves using our surgical (M125; Leica) and dissection (LM80; Leica) microscopes. A separate subset of samples (n=4) underwent paraffin processing and embedding, sectioning by microtome (10 µm serial transverse sections), hematoxylin and eosin (H&E) staining, and light microscopy (DM4000, Leica), according to our standard protocols.[39,51] Color processing of digital images via Photoshop CS5 (Adobe Systems, San Jose, CA) was used to enhance visualization of the anatomical regions of interest. For the remaining samples, the larynx and brain were collected to establish histological methods for subsequent use in a larger RLN crush injury/iVNS study.

Table 2.2. Sihler Staining Protocol for Nerve Mapping

Processing Step	Duration	Target Reaction
4% paraformaldehyde; change solution once a week	50-55 days	Tissue fixation
3% potassium hydroxide (KOH) with 3 drops of 3% v/v hydrogen peroxide per 100 mL; change solution twice a week	50-60 days	Maceration and depigmentation. Endpoint: specimen becomes translucent and nerves can be clearly seen as white fibers under a transilluminated microscope.
Sihler I solution; change solution twice a week	30 days	Decalcification
Sihler II solution; change solution every other week or more often if solution changes from dark blue to purple.	30-40 days	Staining. Endpoint: nerves become dark blue.

Sihler I solution (with agitation); change solution 1-2 times as needed when it becomes blue or purple.	24 hours	Destaining. Endpoint: nerves become dark purple but all other tissues become a transparent lavender color under a transilluminated microscope; check every 2-3 hours.
0.05% lithium carbonate (with agitation)	2 hours	Neutralizing. Endpoint: Nerves turn from purple to deep blue; check every 30 minutes under a transilluminated microscope.
50% glycerine	4 days	Clearing. Endpoint: when the finest nerve twigs can be seen clearly under a transilluminated microscope; check daily.
100% glycerine with thymol crystals	n/a	Long-term preservation

Note: Perform water washes between steps: rinse 5 times, incubate with agitation for 1 hour, then rinse again 5 times.

2.3.5 Statistics

Basic summary statistics were calculated for each outcome measure of interest for each component of this investigation: laryngeal nerve transection injury (i.e., model development) and RLN crush/iVNS treatment (i.e., model refinement and therapeutic investigation). For the transection component, analysis was focused on three clinically-relevant time points: 1) baseline (1 week prior to surgery), 2) 1 week post-surgery to capture acute functional changes in VF mobility and swallowing, and 3) at the end of the surgical recovery period (i.e., 3 months post-surgery; chronic recovery stage) to capture any functional improvement or progression of the surgical injury. One-way repeated measures ANOVAs and one-way ANOVAs were used to demonstrate differences in outcome measures across time and between surgical groups. Two-sample t-tests were used to assess mean differences between a treated group and control. Some analyses used change scores rather than the original data values; change scores were calculated using the difference from each measure at each time point (acute or chronic recovery surgery), compared to baseline. If warranted, post-hoc testing was performed

using Tukey HSD. For the RLN crush/iVNS component, the small sample size (n=3 per group) precluded rigorous statistical analyses. All statistics were calculated using SPSS v24 with a two-sided alpha of 0.05 to determine statistical significance.

2.4 Results

Six of the 50 mice (12%) included in this study died during the surgical procedure. Four of the 6 mice died unexpectedly from intra-operative respiratory distress: unilateral SLN transection (n=1), unilateral RLN transection (n=1), and RLN crush/iVNS (n=1 in the 60-minute treatment group, and n=1 in the no treatment group). As expected, the 2 mice in the bilateral RLN transection group died from mechanical asphyxiation (i.e., VFs fixed in the median position) immediately after the 2nd RLN was transected. These 6 mice were excluded from statistical analysis, as no post-operative data were collected. Below, the results for the surviving 44 mice are summarized separately for the model development (i.e., transection injury, n=38) and model refinement (i.e., RLN crush injury and iVNS treatment, n=6) aims of this study.

2.4.1 Model Development: Laryngeal Nerve Transection Injury

Descriptive statistics for the 4 surgical groups are shown in **Table 2.3**. All 38 mice underwent functional testing of VF mobility (i.e., laryngoscopy) and swallowing (i.e., VFSS) as planned at each time point, with results described below.

Table 2.3. Sample Size, Age, and Body Weight for Surgical Groups at the Study Start and End Points.

SURGICAL GROUPS	Group Sample Size	START OF STUDY				END OF STUDY			
		MALES		FEMALES		MALES		FEMALES	
		Age	Body Weight	Age	Body Weight	Age	Body Weight	Age	Body Weight
RLN Transection (Unilateral)	**9** (4M, 5F)	6.85 (0.45)	31.35 (2.09)	7.30 (0.00)	24.02 (0.53)	11.55 (0.45)	31.85 (2.68)	11.20 (0.12)	25.47 (0.69)
SLN Transection (Unilateral)	**9** (4M, 5F)	4.25 (0.03)	24.93 (1.03)	5.24 (.27)	20.80 (0.77)	7.75 (.03)	28.64 (0.89)	8.8 (0.29)	22.29 (0.64)
SLN Transection (Bilateral)	**10** (3M, 7F)	3.20 (0.16)	27.67 (2.07)	3.27 (0.09)	20.92 (0.39)	7.05 (.42)	30.92 (0.97)	6.67 (0.08)	23.80 (0.70)
Sham Surgery	**10** (6M, 4F)	3.87 (0.08)	26.33 (0.99)	4.00 (2.00)	22.92 (1.17)	7.62 (0.19)	31.58 (0.91)	7.60 (0.21)	25.11 (1.76)

Note: Age = months (standard error of the mean); body weight = grams (standard error of the mean); M = males; F = females.

VF Mobility: A total of 152 laryngoscopy videos (38 mice X 4 time points) were manually analyzed using a 3-point rating scale. Only RLN transection injury had an effect on VF mobility. Specifically, unilateral RLN transection resulted in immediate, ipsilateral VF immobility (i.e., fixation in the paramedian position; score = 0, **Figure 2.5**) that persisted at the acute (1 week) and chronic (3 month) post-surgical time points. In contrast, SLN transection (unilateral or bilateral) had no effect on VF mobility, as the score remained unchanged (i.e., 2 = normal) across time points. Similarly, the sham surgery itself did not impair VF mobility. Change scores in VF mobility at the acute (1 week) versus chronic (3 month) post-surgical time points (compared to baseline function) are shown in **Table 2.4**. However, statistical analysis could not be performed because there was no variability in the data within treatment groups (i.e., standard deviation = 0).

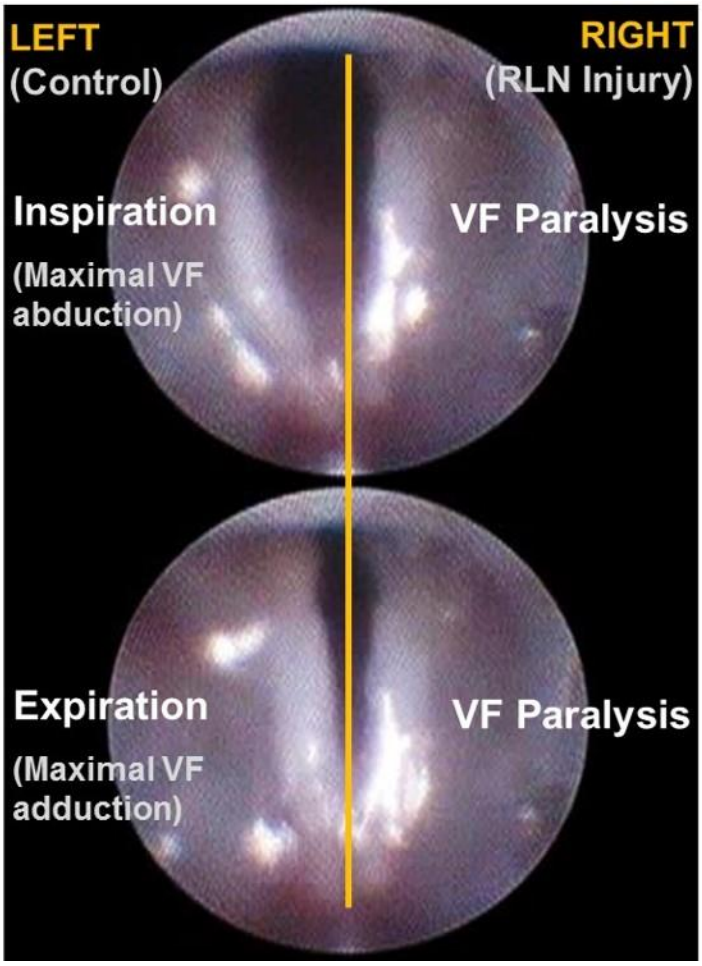

Figure 2.5. VF Immobility after RLN Transection. Endoscopic images showing the bilateral VFs of an anesthetized mouse during spontaneous breathing of room air after transection of the right RLN. Top: Maximal VF abduction during inspiration. Bottom: Maximal VF adduction during expiration. Note the paralyzed (immobile) right VF during the inspiratory and expiratory phases of the respiratory cycle.

Table 2.4. Change in VF Mobility after Surgical Injury

Change Score	Mean Change Score (Standard Deviation)			
	RLN Transection (Unilateral)	SLN Transection		Sham Surgery
		Unilateral	Bilateral	
1 week post-surgery minus baseline	-2 (0)	0 (0)	0 (0)	0 (0)
3 months post-surgery minus baseline	-2 (0)	0 (0)	0 (0)	0 (0)

Swallow Function: A total of 114 VFSS videos (38 mice X 3 time points) were manually analyzed to calculate 6 VFSS metrics as well as to assign a penetration-aspiration score for each mouse at each time point. Descriptive statistics are provided in **Table 2.5**. We first assessed the effect of the surgical injury itself (i.e., without laryngeal nerve transection) using a one-way repeated measures ANOVA. Results revealed that the mean value for each variable was not statistically different between time points, thus validating that the surgical procedure does not cause dysphagia.

Three VFSS metrics (swallow rate, lick-swallow ratio, and inter-swallow interval) were problematic for hypothesis testing because mean values for both SLN transection groups were statistically different from the RLN transection and sham surgical groups at baseline, but not at post-surgical time points. Therefore, we conducted separate one-way ANOVAs at each time point (rather than using change scores which utilizes baseline values) at the 1 week and 3 month post-surgery time points to facilitate model development. No statistically significant differences were identified between surgical groups for each of these 3 VFSS metrics, which suggests these metrics may not be useful for detecting post-surgical dysphagia in this model.

In contrast, the group means for lick rate (i.e., tongue motility), pharyngeal transit time, and esophageal transit time were similar at baseline but different at the post-surgical time points, as shown in **Figure 2.6**. ANOVAs based on change scores revealed statistically significant ($p<0.05$) differences in lick rate and pharyngeal transit time, but not esophageal transit time, ($F_{3,34} = 4.470$, $p=0.009$;

$F_{3,34}$ = 3.956, p=0.016 respectively) at the acute recovery time point (**Table 2.6**). No significant differences in swallow function were evident at the chronic recovery time point (**Table 2.7**), indicating that acute changes in swallow function had returned to normal by 3 months post-surgery. Post-hoc t-tests were conducted only for the two significant acute recovery ANOVA change scores (i.e., lick rate and pharyngeal transit time). Results revealed that lick rate was significantly slower after unilateral RLN transection compared to unilateral SLN transection ($diff_{\Delta uRLN-\Delta uSLN}$=-0.522; p=0.035), bilateral SLN transection ($diff_{\Delta uRLN-\Delta bSLN}$=-0.992; p=0.011), and sham surgery ($diff_{\Delta uRLN-\Delta sham}$=-0.835; p=0.047), whereas pharyngeal transit time was significantly longer after bilateral SLN transection compared to unilateral SLN transection ($diff_{\Delta bSLN-\Delta uSLN}$=0.003; p=0.009). All other group comparisons for these two VFSS metrics were not statistically different (p>0.05). Although not statistically different, esophageal transit time was noticeably longer for the unilateral RLN and bilateral SLN transection groups at the 1 week post-surgery time point.

The final VFSS metric under investigation was PAS. At each time point, all mice in each of the four surgical groups had a score of 1 (i.e., no evidence of penetration or aspiration). Therefore, statistical analysis was not performed for this metric because there was no variability in the data (i.e., standard deviation = 0).

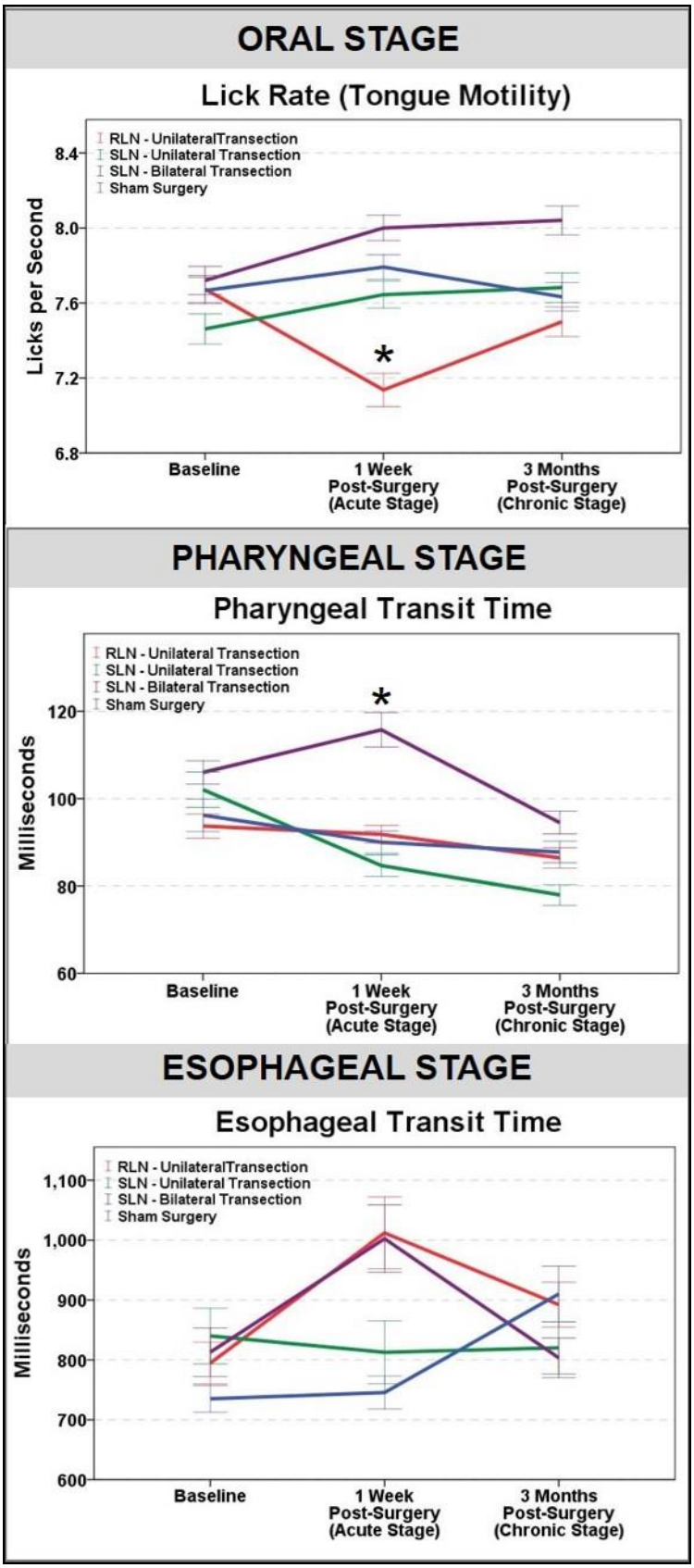

Figure 2.6. Effect of Laryngeal Nerve Transection Injury on Swallow Function. Of the four surgical groups investigated, only unilateral RLN transection and bilateral SLN transection had a statistically significant effect on swallow function. At the acute (1 week post-surgery) time point, lick rate (i.e., tongue motility) was significantly slower after unilateral RLN transection (red line, Oral Stage – top panel), and pharyngeal transit time was significantly longer after bilateral SLN transection (purple line, Pharyngeal Stage – middle panel). In addition, esophageal transit time was longer for the unilateral RLN and bilateral SLN transection groups (red and purple lines, respectively, Esophageal Stage – bottom panel); however, results did not reach statistical significance. At the chronic (3 month post-surgery) time point, swallow function was not significantly different from baseline function. Asterisk denotes statistical significance ($p<0.05$) based on change scores; error bars = ±1 SEM.

Table 2.5. Descriptive Statistics for VFSS Metrics

RLN TRANSECTION - UNILATERAL												
VFSS METRICS (units)	**Baseline**				**1 Week Post-Surgery**				**3 Months Post-Surgery**			
	min	**max**	$\bar{x}$	**SD**	**min**	**max**	$\bar{x}$	**SD**	**min**	**max**	$\bar{x}$	**SD**
Lick Rate (# per second)	7.00	8.00	7.67	0.47	6.00	8.00	7.14	0.59	7.00	8.00	7.50	0.51
Swallow rate (# per 2 sec)	2.00	6.00	3.70	0.86	2.00	6.00	3.66	0.75	2.00	6.00	3.74	0.96
Inter-swallow Interval (sec)	0.23	1.30	0.65	0.21	0.27	1.03	0.64	0.17	0.37	1.30	0.62	0.24
Lick-swallow Ratio (licks/swallow)	1.00	10.00	4.47	1.84	1.00	9.00	4.09	1.55	2.00	10.00	4.12	2.18
PTT (seconds)	0.07	0.13	0.09	0.02	0.07	0.10	0.09	0.01	0.07	0.10	0.09	0.02
ETT (seconds)	0.57	1.43	0.79	0.22	0.60	2.23	1.01	0.40	0.57	1.50	0.89	0.25

SLN TRANSECTION - UNILATERAL												
VFSS METRICS (units)	**Baseline**				**1 Week Post-Surgery**				**3 Months Post-Surgery**			
	min	**max**	$\bar{x}$	**SD**	**min**	**max**	$\bar{x}$	**SD**	**min**	**max**	$\bar{x}$	**SD**
Lick Rate (# per second)	7.00	8.00	7.46	0.51	7.00	8.00	7.64	0.48	7.00	9.00	7.68	0.52
Swallow rate (# per 2 sec)	2.00	5.00	3.18	0.89	2.00	6.00	4.04	0.95	2.00	6.00	3.91	0.83
Inter-swallow Interval (sec)	0.33	1.47	0.77	0.29	0.37	1.20	0.59	0.19	0.27	1.03	0.62	0.18
Lick-swallow Ratio (licks/swallow)	2.00	10.00	5.51	2.37	2.00	9.00	3.96	1.60	1.00	7.00	4.16	1.51
PTT (seconds)	0.07	0.17	0.10	0.03	0.07	0.13	0.08	0.02	0.03	0.10	0.08	0.02
ETT (seconds)	0.53	1.50	0.84	0.30	0.53	2.23	0.81	0.35	0.60	2.07	0.82	0.29

SLN TRANSECTION - BILATERAL												
VFSS METRICS (units)	**Baseline**				**1 Week Post-Surgery**				**3 Months Post-Surgery**			
	min	**max**	$\bar{x}$	**SD**	**min**	**max**	$\bar{x}$	**SD**	**min**	**max**	$\bar{x}$	**SD**
Lick Rate (# per second)	7.00	9.00	7.72	0.54	7.00	9.00	8.00	0.47	7.00	9.00	8.04	0.54
Swallow rate (# per 2 sec)	3.00	8.00	4.92	1.05	3.00	7.00	4.26	0.92	2.00	6.00	4.06	1.04
Inter-swallow Interval (sec)	0.23	0.87	0.47	0.14	0.23	0.87	.55	0.13	0.33	1.20	0.59	0.17
Lick-swallow Ratio (licks/swallow)	1.00	6.00	3.18	1.16	1.00	7.00	3.91	1.25	2.00	9.00	4.16	1.56
PTT (seconds)	0.07	0.13	0.11	0.02	0.03	0.20	0.12	0.03	0.07	0.13	0.09	0.02
ETT (seconds)	0.50	1.77	0.81	0.29	0.63	2.27	1.00	0.40	0.57	1.43	0.80	0.22

SHAM SURGERY												
VFSS METRICS (units)	**Baseline**				**1 Week Post-Surgery**				**3 Months Post-Surgery**			
	min	**max**	$\bar{x}$	**SD**	**min**	**max**	$\bar{x}$	**SD**	**min**	**max**	$\bar{x}$	**SD**
Lick Rate (# per second)	7.00	8.00	7.67	0.48	7.00	9.00	7.79	0.46	7.00	9.00	7.63	0.53
Swallow rate (# per 2 sec)	2.00	6.00	3.87	0.94	0.00	7.00	3.89	1.67	2.00	7.00	4.18	1.11
Inter-swallow Interval (sec)	0.27	1.07	0.57	0.19	0.23	1.07	0.56	0.20	0.23	1.00	0.56	0.19
Lick-swallow Ratio (licks/swallow)	1.00	8.00	3.93	1.63	0.00	8.00	3.35	1.95	1.00	7.00	3.55	1.61
PTT (sec)	0.07	0.17	0.10	0.03	0.07	0.13	0.09	0.02	0.07	0.13	0.09	0.02
ETT (sec)	0.53	1.40	0.74	0.16	0.53	1.40	0.75	0.19	0.43	1.70	0.91	0.33

Note: PTT = pharyngeal transit time; ETT = esophageal transit time; VFSS metric values represent min (minimum), max (maximum), $\bar{x}$ (mean), and SD (standard deviation).

Table 2.6. Acute Changes in Swallow Function

VFSS Metrics (units)	**Mean Change Score: 1 week post-surgery minus baseline (standard deviation)**				***p*-value ANOVA**
	RLN Transection (Unilateral)	**SLN Transection**		**Sham Surgery**	
		Unilateral	**Bilateral**		
Tongue motility (licks per second)	-0.5 (0.6)	0.18 (0.5)	0.3 (0.5)	0.1 (0.5)	**0.009**
Pharyngeal transit time (ms)	-2.0 (11.7)	-1.7 (17.6)	8.9 (21.1)	-5.1 (1.4)	**0.016**
Esophageal transit time (ms)	210.6 (273.2)	-27.9 (318.3)	189.6 (248.7)	17.0 (106.9)	0.103

Note: bold p-values indicate statistical significance; ms = milliseconds.

Table 2.7. Chronic Changes in Swallow Function

VFSS Metrics (units)	Mean Change Score: 3 months post-surgery minus baseline (standard deviation)				*p*-value ANOVA
	RLN Transection (Unilateral)	SLN Transection		Sham Surgery	
		Unilateral	Bilateral		
Tongue motility (licks per second)	-0.2 (0.5)	0.2 (0.4)	0.3 (0.5)	-0.00 (0.6)	0.169
Pharyngeal transit time (ms)	-7.5 (12.9)	-23.8 (14.3)	-11.0 (16.5)	-7.7 (13.5)	0.066
Esophageal transit time (ms)	96.7 (128.5)	-23.6 (248.2)	-20.1 (177.2)	175.6 (224.8)	0.098

Note: ms = milliseconds.

2.4.2 Model Refinement and Therapeutic Investigation: RLN Crush Injury and iVNS Treatment

Descriptive statistics for the two experimental groups (RLN crush without iVNS, and RLN crush with iVNS) are shown in **Table 2.8**. Initially, the four iVNS-treated mice were evenly split into 60-minute (n=2) versus 30-minute (n=2) treatment groups. However, the first mouse in the 60-minute treatment group died intraoperatively due to respiratory distress, and the second mouse developed irregular breathing that was not resolved by lowering the stimulus intensity; therefore treatment was prematurely ended at 50 minutes for this mouse. In contrast, the 30-minute iVNS treatment duration was well-tolerated by the other 2 mice, without adverse events. The 3 surviving iVNS-treated mice (one 50-minute treatment and two 30-minute treatment) were combined into a single iVNS

treatment group for comparison with the control group (n=3, RLN crush without iVNS treatment).

Post-surgery, all 6 mice underwent functional testing of VF mobility (i.e., laryngoscopy) once a week as planned until the study end point (3 months post-surgery). VFSS was not performed on these mice because results from the more severe RLN injury group (i.e., transection) revealed only a transient tongue motility deficit; no other significant swallow-related impairments were identified after RLN injury. Thus, we elected to defer this extremely labor-intensive assay for a subsequent larger RLN crush/iVNS treatment study that will benefit from our VFSS analysis software that is currently under development.

Table 2.8. Sample Size and Age Range for Experimental Groups

Experimental Group	Sample Size			Age (months)
	Group	Sex		
		M	F	
RLN Crush without iVNS (control; no treatment)	3	1	2	14.7 ± 2.3
RLN Crush with iVNS (treatment)	3	1	2	13.3 ± 2.3

Note: Age is expressed as mean ± standard deviation at the time of surgery; M = male; F = female. iVNS = intraoperative vagal nerve stimulation.

VF Mobility: A total of 84 laryngoscopy videos (6 mice X 14 time points) were manually analyzed using a 3-point rating scale. As shown in **Figure 2.7**, RLN crush injury caused immediate, ipsilateral VF immobility (i.e., VF mobility score = 0) in all 6 mice. Beginning at 2 weeks post-injury, iVNS-treated mice demonstrated markedly improved recovery of VF mobility compared to untreated mice. Although the small sample size precluded rigorous statistical analyses, an independent

samples t-test performed at only the final time point (12 weeks post-crush) revealed that treatment recovery after iVNS (mean=1.67 ±0.58, median=2.00, n=3) was significantly different compared to controls (mean=0.34±0.58, median=0.00, n=3), suggesting a beneficial treatment effect (p=0.047).

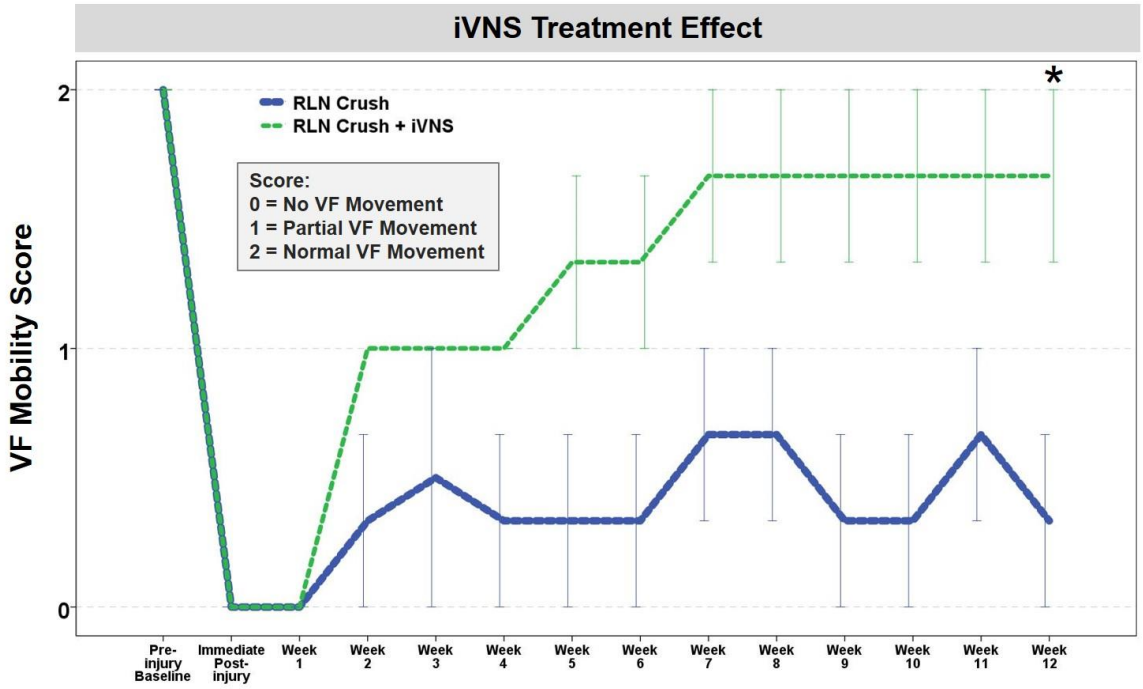

Figure 2.7. Effect of iVNS on VF Mobility after RLN Crush Injury in Aged Mice. VF mobility improved in a stair step pattern after RLN crush injury in iVNS-treated mice >1 year of age. Untreated age-matched mice fluctuated in VF mobility, with minimal improvement after a 12 week post-surgical recovery period. VF mobility was scored using a 3-point Likert scale. Error bars = ±1 SEM; n=3 mice per group. Time points with collapsed error bars indicate no within group variation of VF mobility scores. Asterisk = *p*=0.047, based on a single t-test at the final time point.

2.4.3 Histological Results

Using our Sihler whole mount staining protocol, we were able to grossly map the laryngeal nerves (RLN and SLN) in this small mammal and show that the anatomic pattern is remarkably similar to humans (**Figure 2.8**). This staining method also provided confirmatory evidence that the target laryngeal nerve was

completely transected, without reattachment throughout the post-surgical recovery period. Trans-illumination of Sihler stained specimens under our surgical microscope permitted identification of tiny RLN branches that were not visible during the surgical procedure. RLN branching was also apparent during post-mortem dissections, but only with extreme lateral retraction (**Figure 2.9**). As lateral retraction of the RLN was avoided in our surgical approach, we expect that any existing RLN branches were likely included with the RLN trunk when it was isolated and transected. However, this hypothesis requires histological confirmation in our future studies.

Of the 20 combined specimens subjected to either Sihler staining or post-mortem dissection, most (80%) had 1-2 visible branches emanating from the main RLN trunk bilaterally (but not in a symmetrical pattern), in the vicinity of the 4th to 8th tracheal rings. A few specimens had RLN branching only on the right (n=2) or left (n=1) side, and one specimen did not have any visible RLN branches on either side. All branches disappeared as they approached the larynx, where they became too tiny to visualize using standard light microscopy methods.

A representative H&E stained transverse section of the murine larynx is shown in **Figure 2.10**, which highlights important differences in VF structure and function between the mouse and human. However, striking cross-species similarity of the cartilaginous and muscular framework of the larynx is indeed apparent. For example, like humans, the murine thyroarytenoid muscle consists of medial and lateral bellies, as well as a more ventrally located oblique belly that has only recently been identified in humans.[52]

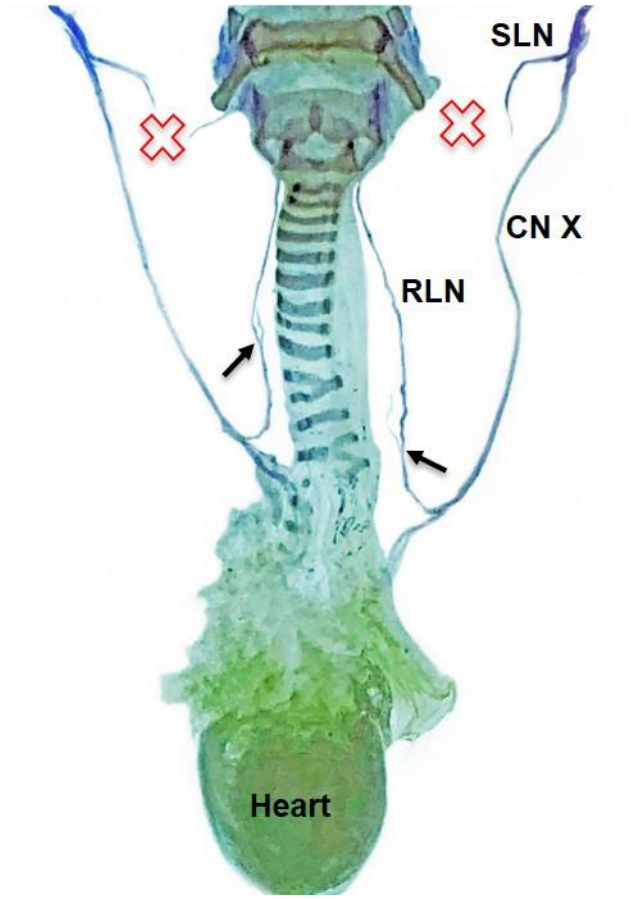

Figure 2.8. Sihler Staining for Laryngeal Nerve Mapping. A representative Sihler stained sample from a mouse in the bilateral SLN transection group demonstrates that the murine laryngeal framework and laryngeal nerve branching pattern are remarkably similar to humans. Red X indicates the location of SLN transection. Black arrows show the origin of nerve branches from the RLN trunk bilaterally. CN X = Cranial Nerve 10 (i.e., vagus nerve); RLN = recurrent laryngeal nerve; SLN = superior laryngeal nerve.

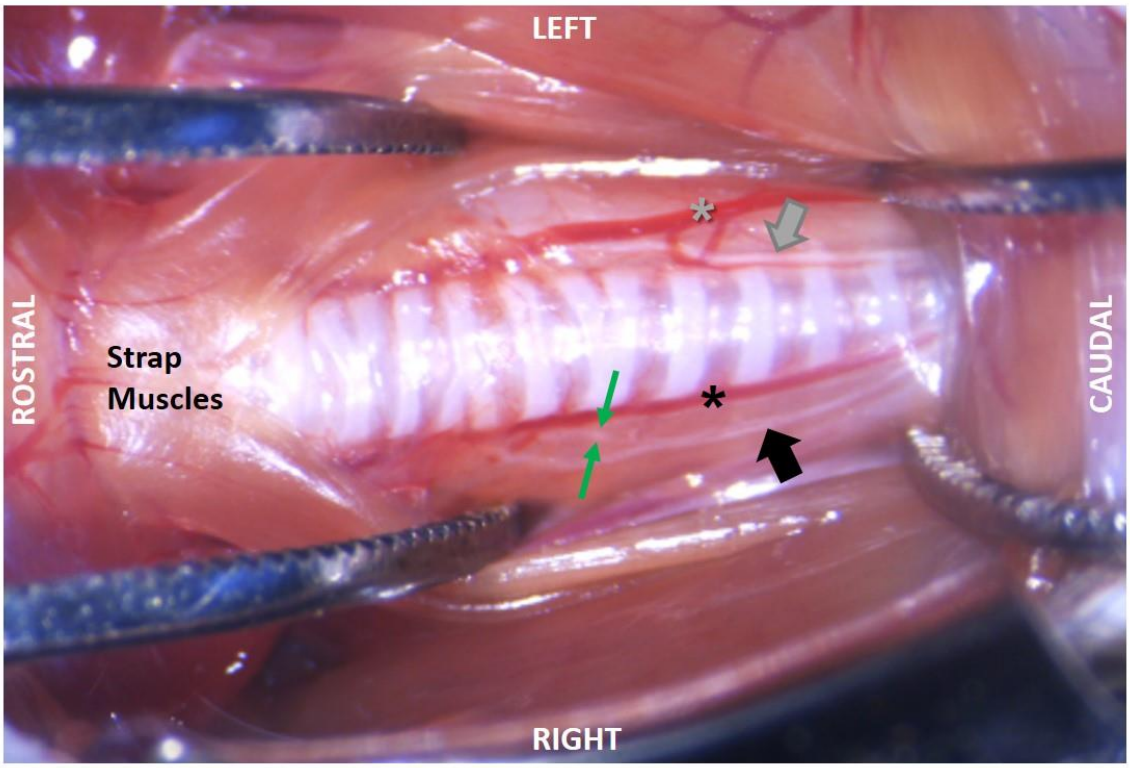

Figure 2.9. Post-mortem Dissection Demonstrating RLN Branching. The left side shows that with minimal retraction of the soft tissues, as is used in our surgical approach, RLN branching is not visible. Instead, only the RLN trunk (gray arrow) can be seen running between the inferior thyroid artery (gray asterisk) and trachea. As shown on the right side, RLN branching is visible only during extreme lateral retraction of the midline strap muscles and fascia. In this specimen, the right RLN trunk (black arrow) has been pulled away from the inferior thyroid artery (black asterisk) to expose a single RLN branch (between the green arrows) near the 6th tracheal ring.

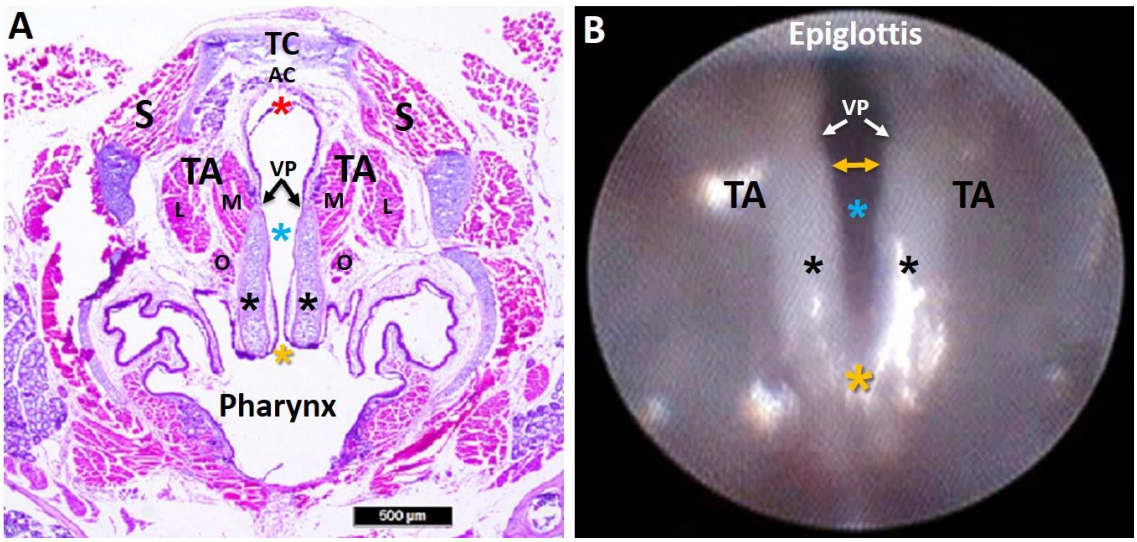

Figure 2.10. Murine Laryngeal Framework. (A) Hematoxylin and eosin (H&E) stained transverse section (10 µm) of a mouse larynx at the level of the VFs, with labeled structures. (B) Endoscopic image of the murine VFs, with corresponding labeled structures from Image A. In contrast to the human larynx, mice have proportionately larger arytenoid cartilages (black asterisks) and a proportionately smaller mucosal region extending beyond the vocal processes (VP) to the ventral commissure (red asterisk). In the mouse, the ventral commissure (which is obscured during laryngoscopy) is framed by a U-shaped alar cartilage (AC) that does not exist in humans. During spontaneous breathing in the mouse, the most dorsal portion of the arytenoids (yellow asterisk; dorsal commissure) remains relatively fixed near midline, serving as a pivot point for VF abduction and adduction. As a result, VF movement in the mouse is more readily apparent at the ventral (yellow bidirectional arrow in Image B) rather than the dorsal (posterior) region as in humans. TC: thyroid cartilage; AC: alar cartilage; VP: vocal process; TA: thyroarytenoid muscle (M: medial belly; L: lateral belly; O: oblique belly); S: strap muscles; blue asterisk: glottis; black asterisk: arytenoid cartilage; yellow asterisk: dorsal commissure; red asterisk: ventral commissure. Scale bar = 500 µm.

2.5 Discussion

We successfully developed a mouse model of iatrogenic RLN injury with impaired VF mobility and swallowing function to serve as a translational platform for investigations of the pathological mechanisms contributing to poor functional outcomes and the development of novel regenerative treatment strategies. We used our “miniaturized” endoscopic[35] and fluoroscopic[32,36] imaging assays to characterize VF mobility and swallow function, respectively, after transection injury. We included the SLN in our model development because of its hypothesized

collateral innervation of intrinsic laryngeal muscles after RLN injury, which presumably contributes to VF synkinesis and resultant poor functional outcomes.[6,2,7] Thus, we investigated the effect of four distinct laryngeal nerve injury patterns: RLN transection (unilateral versus bilateral) and SLN transection (unilateral versus bilateral). We examined four clinically relevant time points for longitudinal assessment of functional outcomes: baseline (1 week prior to surgery), during surgery (immediately post-transection), an acute recovery stage (1 week post-surgery), and a chronic recovery stage (3 months post-surgery). A sham surgical group was included as a negative control. Additionally, we studied a potential therapeutic intervention (iVNS) in aged mice to better correspond to the average age of anterior neck surgical patients. Moreover, the recovery period in our study roughly corresponds to over a decade in human years,[53] thus providing additional translational perspective for human surgical patients with chronic adverse outcomes after iatrogenic RLN injury.

As hypothesized, unilateral RLN transection resulted in immediate, ipsilateral VF paralysis (i.e., immobilization in the paramedian position), suggesting the RLN motor innervation pattern of intrinsic laryngeal muscles in mice is similar to humans. As expected, bilateral RLN transection caused complete airway obstruction from the medialized, immobile vocal folds, resulting in intraoperative mortality. In contrast, SLN transection (unilateral or bilateral) had no visible effects on VF mobility. Importantly, our sham surgery group did not develop impaired VF mobility, thus validating the surgical technique itself had no confounding effects on functional outcomes.

Whereas unilateral RLN transection in mice resulted in chronic impairment of VF mobility, dysphagia was transient and limited to the oral stage of swallowing, specifically affecting lick rate (i.e., tongue motility). This finding is in alignment with a recent report of significant oral stage alterations (e.g., tongue shape and bolus formation) in infant pigs after unilateral RLN transection;[54] however, a related study showed no alteration in piglet suckling rate.[20] We suspect this difference may be because licking (drinking) behavior in adult mice requires marked tongue protrusion that visibly elevates the hyoid bone (and hence larynx), whereas suckling in piglets requires comparatively little movement of the tongue and hyoid. As the tongue is anatomically coupled to the larynx via the hyoid,[55] the resultant VF immobility after unilateral RLN transection in mice may be causing an anchoring effect that hinders normal tongue protrusion during drinking. Alternatively, RLN injury in infant pigs was shown to affect EMG swallowing activity in muscles that are not directly innervated by the RLN, particularly the tongue.[56] In this case, muscle activity was decreased in lesioned animals prior to swallow initiation and during bolus transit, resulting in marked differences in tongue shape, movement, and timing, as well as corresponding differences in the size and shape of the bolus. These findings provide rationale for inclusion of EMG and other kinematic assessments of tongue function to further explore the link between RLN injury and altered lick rate in our model.

Moreover, these findings suggest that an RLN lesion may impact upstream neural connections between the numerous brainstem nuclei and/or cortical regions involved in swallowing.[56] In our study, we suspect the 4 day post-surgical VFSS

time point provided an ample window for Wallerian degeneration, a stereotypical process that initiates degeneration of the myelin sheath and axons within 24-36 after nerve injury, paving the way for nerve regeneration.[57] Moreover, the act of surgically creating the nerve injury generates an immediate burst of action potentials that travel centrally along the injured axons to reach the neuronal cell bodies and their synaptic connections. This nerve injury signal triggers the necessary metabolic processes within the cell bodies to promote nerve regeneration and promote neural plasticity.[58] In the case of the RLN, the “injury signal” travels along the vagus nerve to stimulate the vagal ganglia (i.e., afferent/sensory neurons of the RLN) and the nucleus ambiguus in the brainstem medulla (i.e., efferent/motor neurons of the RLN), and their synaptic connections with the numerous brainstem and cortical regions involved in swallowing. Thus, our mouse model of RLN injury with resultant tongue motility deficit at the 4 day post-surgical time point provides a suitable platform for systematic investigations of the peripheral and central effects of RLN injury and for exploring novel mechanisms to enhance neural plasticity and optimize functional outcomes.

Interestingly, esophageal transit time was noticeably (but not significantly) longer after RLN transection, resembling findings with infant pigs.[20] Given that esophageal dysphagia is a common report in humans after anterior neck surgical procedures,[59,60] we are currently strategizing alternative esophageal outcome measures via VFSS that may be more robust indicators of RLN injury for use in future experiments with this model. We also are exploring the possibility of

performing EMG and manometry in this small animal for better detection and objective quantification of esophageal impairment.

In contrast to humans and other larger animal models of RLN injury, VF paralysis in mice does not result in aspiration during swallowing. As the sensory receptors of the RLN are located below the VFs and there is no aspirated fluid stimulating this region (based on our VFSS findings), the sensory component of the RLN is unlikely to contribute to the overall swallow pathology and recovery in our model. Instead, we suspect the dichotomy in recovery between VF mobility and swallowing function after RLN injury may be due to the mice adopting compensatory behavioral strategies during feeding to maintain adequate nutrition and hydration, as previously described for people.[61-63]

This recovery dichotomy may also be due to technological limitations of our fluoroscope as well as species-related differences in the swallowing mechanism. For example, we have previously shown the pharyngeal stage of swallowing in mice is approximately 10 times faster than humans.[36,32] Therefore, the 30 fps limitation of our fluoroscopy camera prevents sufficient temporal resolution to reliably quantify the numerous rapid events occurring during swallowing. Further, our low energy X-ray system prevents visualization of soft tissue and cartilaginous structures of the larynx and pharynx; therefore, quantification of swallowing function was largely limited to bolus flow dynamics. At no time was there evidence of laryngeal penetration or aspiration of the oral contrast agent, likely because mice are preferential nasal breathers whose larynx resides in the nasopharynx, inherently protected from the path of the bolus during swallowing.[32,36] However,

impaired VF mobility is a significant risk factor for penetration/aspiration in humans, thus highlighting the translational applicability of our mouse model.

Results for the SLN transection groups further support model development. We expected SLN transection would result in subtle, transient changes in VF mobility and swallowing function, which would be more pronounced after bilateral transection. However, VF mobility was unaffected by SLN transection, and dysphagia was evident only after bilateral SLN transection, which resolved by the 3 month post-surgery time point. Only the pharyngeal stage of swallowing was significantly affected by bilateral SLN transection, as evidenced by longer pharyngeal transit times. This finding is congruent with studies of infant pigs, in which SLN transection resulted in increased pharyngeal transit time, as well as increased bolus area and aspiration incidence[21,22] with more severe outcomes for bilateral injuries.[23]

Importantly, we refined our RLN transection (neurotmesis) model to include a more prevalent axonotmesis surgical injury type. We chose a crush injury because it is easier to standardize than experimental traction or thermal approaches. Additionally, because crush injury shows spontaneous recovery over time, treatments targeting accelerated recovery can be assessed. We tested this hypothesis by conducting a feasibility study of intraoperative vagal nerve stimulation (iVNS) as a novel regenerative strategy. In doing so, we expanded upon a recent study in young adult rats, whereby intraoperative RLN stimulation accelerated the recovery of VF mobility after RLN crush injury.[29] However, rather than stimulating the RLN, we chose the cervical vagus nerve as a more clinically

relevant treatment site. Our rationale was based on the highly variable and extensive branching pattern of the RLN which renders it quite challenging, if not impossible, for surgeons to pinpoint the exact site(s) of injury.[2,64,65] Thus, iVNS may circumvent this problem by simultaneously targeting all RLN branches to promote widespread regeneration.

Although our study provides encouraging preliminary data that iVNS may improve recovery after RLN axonotmesis, larger studies must be conducted to establish optimal iVNS treatment parameters (e.g., stimulus frequency and intensity, treatment duration, etc.) and to characterize voice, respiratory, and swallowing outcomes in parallel with VF mobility. Furthermore, effects on RLN fiber types (motor, sensory, and autonomic/parasympathetic) must be considered, as each may require different stimulation parameters for optimal regeneration.[43,44,66] Nevertheless, the high clinical-translational potential of our proposed iVNS treatment strategy is supported by existing FDA-approved vagal nerve stimulation technology, for example continuous intraoperative nerve monitoring (CIONM).[67-69] CIONM enables EMG monitoring of the VFs to detect RLN injury by providing periodic, low-level neuro-stimulation throughout the surgery via an electrode secured around the vagus nerve. Thus, if iVNS proves to be effective in promoting RLN regeneration, we propose the CIONM software could be modified to include settings appropriate for iVNS treatment, thereby expanding this technology from purely an RLN monitoring device into a robust therapeutic nerve regeneration strategy.

Additionally, we successfully performed laryngeal nerve mapping using post-mortem dissections and a Sihler whole mount staining technique. Results revealed multiple RLN branches terminating along the esophagus and larynx, similar to the variable innervation pattern described for the human RLN.[70-73] For this reason, our future studies will include histological confirmation in each mouse that all RLN branches at the injury site are effectively targeted, thus providing a methodological control to improve scientific rigor. We also performed basic histologic evaluation of the larynx using H&E staining of transverse sections, which confirmed the previously published, detailed description of the mouse larynx.[33] However, our ability to perform in vivo endoscopic assessment of the larynx for comparison with post-mortem histological assays provides a novel perspective of the similarities and differences between the mouse and human larynx. Given the extremely small size of mice, more in depth microscopic investigations (e.g., immunohistochemistry and transmission electron microscopy) will be essential for detailed laryngeal nerve mapping, as well as objective quantification of normal and pathological neuromuscular innervation and remodeling after laryngeal nerve injury and subsequent treatment interventions such as iVNS.

Other limitations of our study were that we did not investigate simultaneous injury of the RLN and SLN, we included a small sample size in our RLN crush/iVNS feasibility study, we did not include EMG recordings of the laryngeal muscles, nor did we include vocalization and respiratory assays for added translational impact. In addition, sex differences have not yet been explored in this model. Larger studies are underway to address each of these limitations.

A final notable limitation of our study involves interpretation of our endoscopic and fluoroscopic videos. For endoscopy, we used a qualitative Likert scoring system that introduces subjectivity; whereas, for fluoroscopy, we used a frame-by-frame manual analysis approach that is highly objective, but extremely labor intensive and therefore significantly slows the scientific discovery process. To overcome these limitations, we have developed custom software for semi-automated analysis of endoscopic[74] and fluoroscopic videos; validation studies are currently underway. We expect automation will permit high throughput, objective quantification of the fast-paced breathing[35] and drinking[32,36] behaviors observed in mice. Further, subtle changes in VF motion and swallowing function in mice that are difficult to detect with the human eye may be clinically relevant, as small changes in this small animal may in fact be large changes in humans. In addition, in human medicine, subjectivity is a known limitation of the “gold standard” endoscopic and fluoroscopic swallow tests, which results in poor inter- and intra-rater reliability.[75-80] Thus, we are in the process of adapting our software for validation with endoscopic and fluoroscopic videos obtained from humans, to further facilitate our translational research agenda.

In summary, we successfully developed a translational mouse model of iatrogenic RLN injury that demonstrates laryngeal (chronic) and swallowing (acute) dysfunction. We developed this model using our established endoscopic and fluoroscopic assays that permit longitudinal assessment in mice. We anticipate this new model will serve as a clinically relevant platform to: 1) develop intraoperative strategies for RLN injury prevention, 2) elucidate the functional roles of the RLN

versus SLN under normal versus lesioned conditions, 3) hasten our understanding of the molecular mechanisms contributing to poor functional outcomes after RLN injury, and 4) develop innovative regenerative treatment strategies to significantly accelerate and improve functional recovery of swallowing, voice, and breathing, which are all negatively impacted by RLN injury.

2.6 Acknowledgments

We graciously thank Dr. Christina Goldstein for providing translational surgical insight from an orthopedic perspective. Alex Hackworth and Connor (Beau) Burkett assisted with post-mortem laryngeal nerve dissections in mice. Marc Trautmann performed microtome sectioning of paraffin-embedded murine laryngeal specimens. We also acknowledge Roderic Schlotzhauer (MU Physics Machine Shop) for contribution to design and construction of the custom surgical table and laryngoscope tips essential to this study.

2.7 References

1. Chandrasekhar SS, Randolph GW, Seidman MD, Rosenfeld RM, Angelos P, Barkmeier-Kraemer J, Benninger MS, Blumin JH, Dennis G, Hanks J, Haymart MR, Kloos RT, Seals B, Schreibstein JM, Thomas MA, Waddington C, Warren B, Robertson PJ, Surgery AAoO-HaN (2013) Clinical practice guideline: improving voice outcomes after thyroid surgery. Otolaryngol Head Neck Surg 148 (6 Suppl):S1-37. doi:10.1177/0194599813487301

2. Mattsson P, Hydman J, Svensson M (2015) Recovery of laryngeal function after intraoperative injury to the recurrent laryngeal nerve. Gland Surg 4 (1):27-35. doi:10.3978/j.issn.2227-684X.2015.01.10

3. Brunner E, Friedrich G, Kiesler K, Chibidziura-Priesching J, Gugatschka M (2011) Subjective breathing impairment in unilateral vocal fold paralysis. Folia Phoniatr Logop 63 (3):142-146. doi:10.1159/000316320

4. Wang B, Yuan J, Chen X, Xu J, Li Y, Dong P (2016) Functional regeneration of the transected recurrent laryngeal nerve using a collagen scaffold loaded with laminin and laminin-binding BDNF and GDNF. Sci Rep 6:32292. doi:10.1038/srep32292

5. Dionigi G, Wu CW, Kim HY, Rausei S, Boni L, Chiang FY (2016) Severity of Recurrent Laryngeal Nerve Injuries in Thyroid Surgery. World J Surg 40 (6):1373-1381. doi:10.1007/s00268-016-3415-3

6. Crumley RL (2000) Laryngeal synkinesis revisited. Ann Otol Rhinol Laryngol 109 (4):365-371. doi:10.1177/000348940010900405

7. Hydman J, Mattsson P (2008) Collateral reinnervation by the superior laryngeal nerve after recurrent laryngeal nerve injury. Muscle Nerve 38 (4):1280-1289. doi:10.1002/mus.21124

8. Crumley RL (1979) Mechanisms of synkinesis. Laryngoscope 89 (11):1847-1854. doi:10.1288/00005537-197911000-00020

9. Crumley RL (1994) Unilateral recurrent laryngeal nerve paralysis. J Voice 8 (1):79-83

10. Kovacic U, Sketelj J, Bajrović FF (2009) Chapter 26: Age-related differences in the reinnervation after peripheral nerve injury. Int Rev Neurobiol 87:465-482. doi:10.1016/S0074-7742(09)87026-8

11. Verdú E, Butí M, Navarro X (1995) The effect of aging on efferent nerve fibers regeneration in mice. Brain Res 696 (1-2):76-82

12. Tanaka K, Zhang QL, Webster HD (1992) Myelinated fiber regeneration after sciatic nerve crush: morphometric observations in young adult and aging mice and the effects of macrophage suppression and conditioning lesions. Exp Neurol 118 (1):53-61

13. Marawar S, Girardi FP, Sama AA, Ma Y, Gaber-Baylis LK, Besculides MC, Memtsoudis SG (2010) National trends in anterior cervical fusion procedures. Spine (Phila Pa 1976) 35 (15):1454-1459. doi:10.1097/BRS.0b013e3181bef3cb

14. Howlader N, Noone A, Krapcho M, Miller D, Bishop K, Kosary C, Yu M, Ruh lJ, Tatalovich Z, Mariotto A, Lewis D, Chen H, Feuer E, Cronin K (2016) SEER Cancer Statistics Review, 1975-2014 , National Cancer Institute. Bethesda, MD. https://seer.cancer.gov/csr/1975_2014/. 2017

15. Choi JS, Oh SH, An HY, Kim YM, Lee JH, Lim JY (2014) Functional regeneration of recurrent laryngeal nerve injury during thyroid surgery using an asymmetrically porous nerve guide conduit in an animal model. Thyroid 24 (1):52-59. doi:10.1089/thy.2013.0338

16. Kupfer RA, Old MO, Oh SS, Feldman EL, Hogikyan ND (2013) Spontaneous laryngeal reinnervation following chronic recurrent laryngeal nerve injury. Laryngoscope 123 (9):2216-2227. doi:10.1002/lary.24049

17. Rosko AJ, Kupfer RA, Oh SS, Haring CT, Feldman EL, Hogikyan ND (2018) Immunohistologic analysis of spontaneous recurrent laryngeal nerve reinnervation in a rat model. Laryngoscope 128 (3):E117-e122. doi:10.1002/lary.27004

18. Nishimoto K, Kumai Y, Yumoto E (2014) Paradoxical movement of rat vocal folds following recurrent laryngeal nerve injury. Acta oto-laryngologica 134 (11):1164-1171. doi:10.3109/00016489.2014.936625

19. Old MO, Oh SS, Feldman E, Hogikyan ND (2011) Novel model to assess laryngeal function, innervation, and reinnervation. Ann Otol Rhinol Laryngol 120 (5):331-338. doi:10.1177/000348941112000509

20. Gould FD, Lammers AR, Ohlemacher J, Ballester A, Fraley L, Gross A, German RZ (2015) The Physiologic Impact of Unilateral Recurrent Laryngeal Nerve (RLN) Lesion on Infant Oropharyngeal and Esophageal Performance. Dysphagia 30 (6):714-722. doi:10.1007/s00455-015-9648-8

21. Ding P, Campbell-Malone R, Holman SD, Lukasik SL, Fukuhara T, Gierbolini-Norat EM, Thexton AJ, German RZ (2013) Unilateral superior laryngeal nerve lesion in an animal model of dysphagia and its effect on sucking and swallowing. Dysphagia 28 (3):404-412. doi:10.1007/s00455-013-9448-y

22. Ding P, Campbell-Malone R, Holman SD, Lukasik SL, Thexton AJ, German RZ (2013) The effect of unilateral superior laryngeal nerve lesion on swallowing threshold volume. Laryngoscope 123 (8):1942-1947. doi:10.1002/lary.24051

23. Ding P, Fung GS, Lin M, Holman SD, German RZ (2015) The effect of bilateral superior laryngeal nerve lesion on swallowing: a novel method to quantitate aspirated volume and pharyngeal threshold in videofluoroscopy. Dysphagia 30 (1):47-56. doi:10.1007/s00455-014-9572-3

24. Lin YC, Dionigi G, Randolph GW, Lu IC, Chang PY, Tsai SY, Kim HY, Lee HY, Tufano RP, Sun H, Liu X, Chiang FY, Wu CW (2015) Electrophysiologic monitoring correlates of recurrent laryngeal nerve heat thermal injury in a porcine model. Laryngoscope 125 (8):E283-290. doi:10.1002/lary.25362

25. Kwak HY, Dionigi G, Kim D, Lee HY, Son GS, Lee JB, Bae JW, Kim HY (2015) Thermal injury of the recurrent laryngeal nerve by THUNDERBEAT during thyroid surgery: findings from continuous intraoperative neuromonitoring in a porcine model. J Surg Res. doi:10.1016/j.jss.2015.06.066

26. Paniello RC, Rich JT, Debnath NL (2015) Laryngeal adductor function in experimental models of recurrent laryngeal nerve injury. Laryngoscope 125 (2):E67-72. doi:10.1002/lary.24947

27. Woodson GE (2007) Spontaneous laryngeal reinnervation after recurrent laryngeal or vagus nerve injury. Ann Otol Rhinol Laryngol 116 (1):57-65. doi:10.1177/000348940711600110

28. Wang B, Yuan J, Xu J, Xie J, Wang G, Dong P (2016) Neurotrophin expression and laryngeal muscle pathophysiology following recurrent laryngeal nerve transection. Mol Med Rep 13 (2):1234-1242. doi:10.3892/mmr.2015.4684

29. Monaco GN, Brown TJ, Burgette RC, Fargo KN, Akst LM, Jones KJ, Foecking EM (2015) Electrical stimulation and testosterone enhance recovery from recurrent laryngeal nerve crush. Restor Neurol Neurosci 33 (4):571-578. doi:10.3233/RNN-130334

30. Sharma N, Moeller CW, Marzo SJ, Jones KJ, Foecking EM (2010) Combinatorial treatments enhance recovery following facial nerve crush. Laryngoscope 120 (8):1523-1530. doi:10.1002/lary.20997

31. Foecking EM, Fargo KN, Coughlin LM, Kim JT, Marzo SJ, Jones KJ (2012) Single session of brief electrical stimulation immediately following crush injury enhances functional recovery of rat facial nerve. J Rehabil Res Dev 49 (3):451-458

32. Lever TE, Braun SM, Brooks RT, Harris RA, Littrell LL, Neff RM, Hinkel CJ, Allen MJ, Ulsas MA (2015) Adapting human videofluoroscopic swallow study methods to detect and characterize dysphagia in murine disease models. J Vis Exp (97). doi:10.3791/52319

33. Thomas LB, Stemple JC, Andreatta RD, Andrade FH (2009) Establishing a new animal model for the study of laryngeal biology and disease: an anatomic study of the mouse larynx. J Speech Lang Hear Res 52 (3):802-811. doi:10.1044/1092-4388(2008/08-0087)

34. Kingham PJ, Birchall MA, Burt R, Jones A, Terenghi G (2005) Reinnervation of laryngeal muscles: a study of changes in myosin heavy chain expression. Muscle Nerve 32 (6):761-766. doi:10.1002/mus.20409

35. Shock LA, Gallemore BC, Hinkel CJ, Szewczyk MM, Hopewell BL, Allen MJ, Thombs LA, Lever TE (2015) Improving the Utility of Laryngeal Adductor Reflex Testing: A Translational Tale of Mice and Men. Otolaryngol Head Neck Surg 153 (1):94-101. doi:10.1177/0194599815578103

36. Lever T, Brooks R, Thombs L, Littrell L, Harris R, Allen M, Kadosh M, Robbins K (2015) Videofluoroscopic Validation of a Translational Murine Model of Presbyphagia. Dysphagia

37. Björck G, Margolin G, Måbäck GM, Persson JK, Mattsson P, Hydman J (2012) New animal model for assessment of functional laryngeal motor innervation. Ann Otol Rhinol Laryngol 121 (10):695-699. doi:10.1177/000348941212101013

38. Paskhover B, Wadie M, Sasaki CT (2015) Thyroarytenoid cross-innervation by the external branch of the superior laryngeal nerve in the porcine model. Laryngoscope 125 (1):177-179. doi:10.1002/lary.24888

39. Lever TE, Simon E, Cox KT, Capra NF, O'Brien KF, Hough MS, Murashov AK (2010) A mouse model of pharyngeal dysphagia in amyotrophic lateral sclerosis. Dysphagia 25 (2):112-126. doi:10.1007/s00455-009-9232-1

40. Sang Q, Goyal RK (2001) Swallowing reflex and brain stem neurons activated by superior laryngeal nerve stimulation in the mouse. Am J Physiol Gastrointest Liver Physiol 280 (2):G191-200

41. Bridge PM, Ball DJ, Mackinnon SE, Nakao Y, Brandt K, Hunter DA, Hertl C (1994) Nerve crush injuries--a model for axonotmesis. Exp Neurol 127 (2):284-290. doi:10.1006/exnr.1994.1104

42. Hetzler LE, Sharma N, Tanzer L, Wurster RD, Leonetti J, Marzo SJ, Jones KJ, Foecking EM (2008) Accelerating functional recovery after rat facial nerve injury: Effects of gonadal steroids and electrical stimulation. Otolaryngol Head Neck Surg 139 (1):62-67. doi:10.1016/j.otohns.2008.02.006

43. Al-Majed AA, Neumann CM, Brushart TM, Gordon T (2000) Brief electrical stimulation promotes the speed and accuracy of motor axonal regeneration. J Neurosci 20 (7):2602-2608

44. Gordon T, Udina E, Verge VM, de Chaves EI (2009) Brief electrical stimulation accelerates axon regeneration in the peripheral nervous system and promotes sensory axon regeneration in the central nervous system. Motor Control 13 (4):412-441

45. Hernández-Morato I, Valderrama-Canales FJ, Berdugo G, Arias G, McHanwell S, Sañudo J, Vázquez T, Pascual-Font A (2013) Reorganization of laryngeal motoneurons after crush injury in the recurrent laryngeal nerve of the rat. J Anat 222 (4):451-461. doi:10.1111/joa.12031

46. Rosenbek JC, Robbins JA, Roecker EB, Coyle JL, Wood JL (1996) A penetration-aspiration scale. Dysphagia 11 (2):93-98

47. Mu L, Sanders I (2000) Sensory nerve supply of the human oro- and laryngopharynx: a preliminary study. Anat Rec 258 (4):406-420. doi:10.1002/(SICI)1097-0185(20000401)258:4<406::AID-AR9>3.0.CO;2-5 [pii]

48. Mu L, Sanders I (2010) Sihler's whole mount nerve staining technique: a review. Biotech Histochem 85 (1):19-42. doi:10.3109/10520290903048384

49. Su WF, Liu SC, Wang SD, Su WY, Ma KH, Huang TT (2015) Nerve branches to the posterior cricoarytenoid muscle may complicate the laryngeal reinnervation procedure. Laryngoscope 125 (2):419-423. doi:10.1002/lary.24944

50. Mu L, Sanders I (2009) The human cricothyroid muscle: three muscle bellies and their innervation patterns. J Voice 23 (1):21-28. doi:10.1016/j.jvoice.2007.08.001

51. Lever TE, Gorsek A, Cox KT, O'Brien KF, Capra NF, Hough MS, Murashov AK (2009) An animal model of oral dysphagia in amyotrophic lateral sclerosis. Dysphagia 24 (2):180-195. doi:10.1007/s00455-008-9190-z

52. Lee SH, Koh KS, Song WC (2018) Oblique thyroarytenoid muscle in humans: An independent muscle or an accessory belly? Laryngoscope 128 (7):1634-1638. doi:10.1002/lary.27090

53. Dutta S, Sengupta P (2015) Men and mice: Relating their ages. Life Sci. doi:10.1016/j.lfs.2015.10.025

54. Gould FDH, Yglesias B, Ohlemacher J, German RZ (2017) Pre-pharyngeal Swallow Effects of Recurrent Laryngeal Nerve Lesion on Bolus Shape and Airway Protection in an Infant Pig Model. Dysphagia 32 (3):362-373. doi:10.1007/s00455-016-9762-2

55. Duffy JR (2005) Motor speech disorders: substrates, differential diagnosis, and management.

56. DeLozier KR, Gould FDH, Ohlemacher J, Thexton AJ, German RZ (2018) Impact of recurrent laryngeal nerve lesion on oropharyngeal muscle activity and sensorimotor integration in an infant pig model. Journal of applied physiology (Bethesda, Md : 1985) 125 (1):159-166. doi:10.1152/japplphysiol.00963.2017

57. Gong L, Zhu Y, Xu X, Li H, Guo W, Zhao Q, Yao D (2014) The effects of claudin 14 during early Wallerian degeneration after sciatic nerve injury. Neural Regen Res 9 (24):2151-2158. doi:10.4103/1673-5374.147946

58. Wu D, Murashov AK (2013) Molecular mechanisms of peripheral nerve regeneration: emerging roles of microRNAs. Front Physiol 4:55. doi:10.3389/fphys.2013.00055

59. Scerrino G, Tudisca C, Bonventre S, Raspanti C, Picone D, Porrello C, Paladino NC, Vernuccio F, Cupido F, Cocorullo G, Lo Re G, Gulotta G (2017) Swallowing disorders after thyroidectomy: What we know and where we are. A systematic review. Int J Surg 41 Suppl 1:S94-S102. doi:10.1016/j.ijsu.2017.03.078

60. Shriver MF, Lewis DJ, Kshettry VR, Rosenbaum BP, Benzel EC, Mroz TE (2017) Dysphagia Rates after Anterior Cervical Diskectomy and Fusion: A Systematic Review and Meta-Analysis. Global Spine J 7 (1):95-103. doi:10.1055/s-0036-1583944

61. Logemann JA, Larsen K (2012) Oropharyngeal dysphagia: pathophysiology and diagnosis for the anniversary issue of Diseases of the Esophagus. Dis Esophagus 25 (4):299-304. doi:10.1111/j.1442-2050.2011.01210.x

62. Anderson KK, Arnold PM (2013) Oropharyngeal Dysphagia after anterior cervical spine surgery: a review. Global Spine J 3 (4):273-286. doi:10.1055/s-0033-1354253

63. Yue WM, Brodner W, Highland TR (2005) Persistent swallowing and voice problems after anterior cervical discectomy and fusion with allograft and plating: a 5- to 11-year follow-up study. Eur Spine J 14 (7):677-682. doi:10.1007/s00586-004-0849-3

64. Henry BM, Vikse J, Graves MJ, Sanna S, Sanna B, Tomaszewska IM, Tubbs RS, Tomaszewski KA (2016) Extralaryngeal branching of the recurrent laryngeal nerve: a meta-analysis of 28,387 nerves. Langenbeck's Archives of Surgery 401 (7):913-923. doi:10.1007/s00423-016-1455-7

65. Cetin F, Gurleyik E, Dogan S (2016) Morphology and Functional Anatomy of the Recurrent Laryngeal Nerve with Extralaryngeal Terminal Bifurcation. Anatomy research international 2016:9503170. doi:10.1155/2016/9503170

66. Wong JN, Olson JL, Morhart MJ, Chan KM (2015) Electrical stimulation enhances sensory recovery: a randomized controlled trial. Ann Neurol 77 (6):996-1006. doi:10.1002/ana.24397

67. Schneider R, Randolph GW, Barczynski M, Dionigi G, Wu CW, Chiang FY, Machens A, Kamani D, Dralle H (2016) Continuous intraoperative neural monitoring of the recurrent nerves in thyroid surgery: a quantum leap in technology. Gland Surg 5 (6):607-616. doi:10.21037/gs.2016.11.10

68. Anuwong A, Lavazza M, Kim HY, Wu CW, Rausei S, Pappalardo V, Ferrari CC, Inversini D, Leotta A, Biondi A, Chiang FY, Dionigi G (2016) Recurrent laryngeal nerve management in thyroid surgery: consequences of routine visualization, application of intermittent, standardized and continuous nerve monitoring. Updates in surgery 68 (4):331-341. doi:10.1007/s13304-016-0393-9

69. Deniwar A, Bhatia P, Kandil E (2015) Electrophysiological neuromonitoring of the laryngeal nerves in thyroid and parathyroid surgery: A review. World J Exp Med 5 (2):120-123. doi:10.5493/wjem.v5.i2.120

70. Barczyński M, Stopa M, Konturek A, Nowak W (2016) The Overwhelming Majority but not All Motor Fibers of the Bifid Recurrent Laryngeal Nerve are Located in the Anterior Extralaryngeal Branch. World J Surg 40 (3):629-635. doi:10.1007/s00268-015-3257-4

71. Miyauchi A, Masuoka H, Nakayama A, Higashiyama T (2016) Innervation of the cricothyroid muscle by extralaryngeal branches of the recurrent laryngeal nerve. Laryngoscope 126 (5):1157-1162. doi:10.1002/lary.25691

72. Tang WJ, Sun SQ, Wang XL, Sun YX, Huang HX (2012) An applied anatomical study on the recurrent laryngeal nerve and inferior thyroid artery. Surg Radiol Anat 34 (4):325-332. doi:10.1007/s00276-011-0905-8

73. Chiang FY, Lu IC, Chen HC, Chen HY, Tsai CJ, Hsiao PJ, Lee KW, Wu CW (2010) Anatomical variations of recurrent laryngeal nerve during thyroid surgery: how to identify and handle the variations with intraoperative neuromonitoring. Kaohsiung J Med Sci 26 (11):575-583. doi:10.1016/S1607-551X(10)70089-9

74. Haney MM, Hamad A, Leary E, Bunyak F, Lever TE (2018) Automated Quantification of Vocal Fold Motion in a Recurrent Laryngeal Nerve Injury Mouse Model. Laryngoscope. doi:10.1002/lary.27609

75. Kelly AM, Leslie P, Beale T, Payten C, Drinnan MJ (2006) Fibreoptic endoscopic evaluation of swallowing and videofluoroscopy: does examination type influence perception of pharyngeal residue severity? Clin Otolaryngol 31 (5):425-432. doi:10.1111/j.1749-4486.2006.01292.x

76. Kelly AM, Drinnan MJ, Leslie P (2007) Assessing penetration and aspiration: how do videofluoroscopy and fiberoptic endoscopic evaluation of swallowing compare? Laryngoscope 117 (10):1723-1727. doi:10.1097/MLG.0b013e318123ee6a

77. Scott A, Perry A, Bench J (1998) A study of interrater reliability when using videofluoroscopy as an assessment of swallowing. Dysphagia 13 (4):223-227. doi:10.1007/PL00009576

78. Kuhlemeier KV, Yates P, Palmer JB (1998) Intra- and interrater variation in the evaluation of videofluorographic swallowing studies. Dysphagia 13 (3):142-147. doi:10.1007/PL00009564

79. Lee JW, Randall DR, Evangelista LM, Kuhn MA, Belafsky PC (2017) Subjective Assessment of Videofluoroscopic Swallow Studies. Otolaryngol Head Neck Surg 156 (5):901-905. doi:10.1177/0194599817691276

80. Tohara H, Nakane A, Murata S, Mikushi S, Ouchi Y, Wakasugi Y, Takashima M, Chiba Y, Uematsu H (2010) Inter- and intra-rater reliability in fibroptic endoscopic evaluation of swallowing. J Oral Rehabil 37 (12):884-891. doi:10.1111/j.1365-2842.2010.02116.x

Chapter Three

AUTOMATED QUANTIFICATION OF VOCAL FOLD MOTION IN A RECURRENT LARYNGEAL NERVE INJURY MOUSE MODEL

This chapter has been accepted for publication in The Laryngoscope and has been reprinted with permission.

Megan M Haney[1], Ali Hamad[2], Emily Leary[3], Filiz Bunyak[2],

Teresa E Lever[4]

[1]Veterinary Pathobiology, University of Missouri, Columbia, Missouri

[2]Electrical Engineering & Computer Science, University of Missouri, Columbia, Missouri

[3]Orthopaedic Biostatistics, University of Missouri, Columbia, Missouri

[4]Otolaryngology-Head and Neck Surgery, University of Missouri, Columbia, Missouri

3.1 Abstract

Objectives: The goal of this study was to objectively examine vocal fold (VF) motion dynamics after iatrogenic recurrent laryngeal nerve (RLN) injury in a mouse surgical model. Furthermore, we sought to identify a method of inducing injury with a consistent recovery pattern from which we can begin to evaluate spontaneous recovery and test therapeutic interventions.

Methods: The right RLN in C57BL/6J mice was crushed for 30 seconds using an aneurysm clip with 1.3 Newtons closing force. Transoral laryngoscopy enabled visualization of VF movement prior to surgery, immediately post-crush, and at two endpoints: 3 days (n=5) and 2 weeks (n=5). VF motion was quantified with our custom motion analysis software. At each endpoint, RLN samples were collected for transmission electron microscopy (TEM) for correlation with VF motion dynamics.

Results: Our VF tracking software permitted automated quantification of several measures of VF dynamics, such as range and frequency of motion. By 2 weeks post-injury, the frequency of VF movement on the right (injured) side equaled the left, yet range of motion only partially recovered. These objective outcome measures enabled detection of VF dysfunction that persisted at 2 weeks post-crush. TEM images revealed RLN degeneration 3 days post-crush, and partial regeneration at 2 weeks, consistent with functional results obtained with automated VF tracking.

Conclusions: Our motion analysis software provides novel objective, quantitative, and repeatable metrics to detect and describe subtle VF dysfunction in mice that

corresponds with underlying RLN degeneration and recovery. Adaptation of our tracking software for use with human patients is underway.

3.2 Introduction

Iatrogenic recurrent laryngeal nerve (RLN) injury is a common complication of anterior neck surgical procedures, such as cervical spinal surgery or thyroidectomy.[1-3] Injury to the RLN results in ipsilateral vocal fold (VF) paralysis that may contribute to dysphagia, dysphonia, and/or dyspnea (i.e., swallow, voice, and respiratory dysfunction, respectively).[4-7] These conditions are devastating for patients, especially if chronically persistent, as they are associated with poor quality of life, major depression, increased financial burden, and decreased general health.[3,7-9] Furthermore, effective treatment options to promote RLN regeneration and restore full functionality of the injured VF are lacking.[4,7,10-12]

Unfortunately, RLN injury and associated sequelae are impossible to systematically investigate in human patients. Therefore, a consistent animal model that mimics iatrogenic RLN injury is required in order to investigate the responsible mechanisms and explore potential therapeutics.[13] Indeed, work in animal models has shown that unilateral RLN injury causes ipsilateral VF paralysis, as it does in humans.[11,14-18] Though other translatable outcome measures such as voice, respiratory, and swallow function remain to be comprehensively examined, VF motion dynamics have provided robust and direct information in regard to RLN injury and subsequent recovery in these animal models. However, current methods often rely on subjective rating scales[15,16,19-21] that do not permit thorough and

meticulous evaluation of VF motion dynamics. As a result, VF mobility scores may vary between observers, and minute improvements (or deteriorations) in VF motion are likely overlooked or misidentified.

Due to the inherent concerns with subjective VF analysis, efforts have been attempted to objectively quantify VF movement. One strategy involves measuring the angle between VFs during maximum abduction and maximum adduction using still-frame images.[14-16] However, angles may vary slightly within an individual animal, as total range of spontaneous VF movement during breathing depends on factors such as depth of anesthesia and ventilatory drive. Unlike human patients, anesthesia is necessary to immobilize rodent species to record VF movement. Thus, even “normal” VF movement in a single animal can vary between each laryngoscopic procedure, making longitudinal comparisons difficult with this analysis technique.

Another method for objective quantification utilizes examination of glottal area, where the area of the glottic space between midline and the VF mucosa is calculated for the injured and uninjured sides.[11,17] In this case, determining midline remains quite subjective unless there is clear visualization of both the anterior and posterior commissures, which is a challenging view to obtain in rodents. Even if midline is identified accurately, the measurements are again affected by the total range of movement of the VFs under anesthesia, which is variable between anesthetic episodes. In addition, the fluctuating distance of the camera from the glottic space between procedures also contributes to variation in the area measured. To overcome this concern, measurements of the right VF have been

compared to the left VF as a ratio to normalize VF function for each video recording.[11,17] However, this technique, as well as other manual analysis methods are time-consuming and therefore prohibitive to high-throughput data analysis in research or clinical practice.

Another major limitation of these analysis techniques is that they rely on still-frame images representing only two time points of VF movement (maximum abduction and maximum adduction), revealing little about VF motion dynamics as a whole. Therefore, with static images, it is impossible to demonstrate how the VFs are moving in relation to each other. Are the VFs moving symmetrically and in synchrony with one another? Is the motion fluid or uneven? Is there intermittent or paradoxical movement of the VFs? At what rate are the VFs moving? Is there compensation of the uninjured VF? These questions cannot be answered with still-frame images alone.

To alleviate the limitations of still-frame image analysis, we have developed custom computational video analysis software that includes two components: VFTrack and VFQuantify. VFTrack is a VF motion tracker software, whereas VFQuantify is an analytics module that computes a set of objective, quantitative outcome measures describing VF motion dynamics, enabling objective comparisons across time and populations. These measures quantify aspects of motion behavior pertaining to healthy and paralyzed VFs, such as amplitude, frequency, range, symmetry, etc. In this study, two measures, Mean Motion Range Ratio (MMRR) and Open Close Cycle Ratio (OCCR), were developed to begin to objectively assess VF motion dynamics. VFQuantify was also used to calculate the

maximum angle of abduction and the minimum angle during adduction to correlate our findings with previous techniques described in the literature.

To accomplish our primary objective (i.e., demonstration of the utility of our VFTrack and VFQuantify software), we produced a unilateral RLN compression (crush) injury in a mouse model using an aneurysm clip to induce ipsilateral VF dysfunction.[19-23] To visualize VF motion, transoral laryngoscopy was performed prior to and immediately following crush injury, as well as 3 days and 2 weeks post-crush. Our secondary objective was to confirm that this nerve crush methodology and severity of force produces unilateral VF immobility in mice, and to characterize how VF function recovers over time without treatment. In addition to functional analysis, we performed transmission electron microscopy (TEM) to document nerve pathology at each respective endpoint.

3.3 Materials and Methods

3.3.1 Animals

Ten C57BL/6J (B6) mice (n=4 males; 6 females), approximately 4 months of age, were used for this study, which was approved by our Institutional Animal Care and Use Committee. Mice were group housed by sex on a 12:12 light/dark cycle using individually ventilated cages, and had free access to food and water.

3.3.2 RLN Crush Injury Procedure

Mice were anesthetized using a ketamine-xylazine cocktail (90;11.25 mg/kg), prepared aseptically for surgery, and placed in dorsal recumbency on a

customized platform under a surgical microscope. A midline incision (~1-2 cm) was made on the ventral neck, and the salivary glands were retracted laterally to expose the strap muscles overlying the trachea. The right RLN was gently isolated at the level of the 5th tracheal ring and crushed with a Sugita Titanium aneurysm clip (Mizuho, Tokyo, Japan)[19,20,22,23] with a 1.3 N manufacturer-calibrated closing force. The aneurysm clip was closed for 30 seconds to induce a 1 mm injury[24] in all mice (**Figure 3.1**). The left RLN served as an internal control for this study.

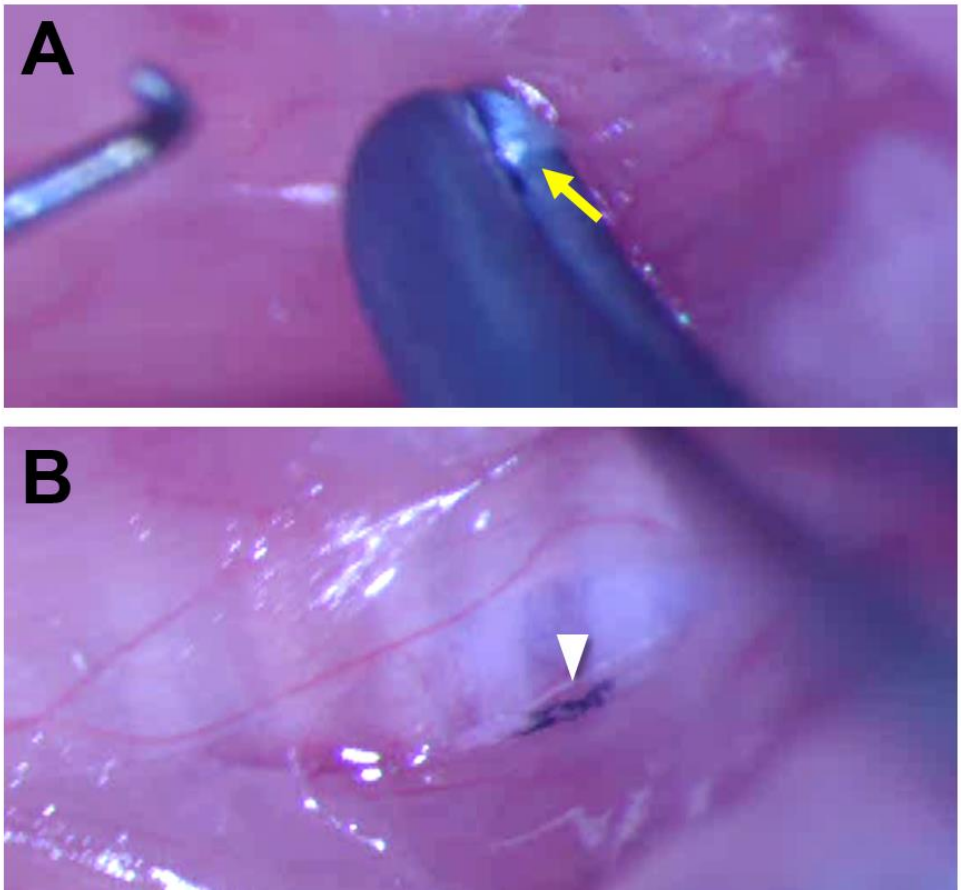

Figure 3.1. A Sugita titanium aneurysm clip with a 1.3-N closing force was used to crush the right RLN in all mice at the level of the fifth tracheal ring. (A) The aneurysm clip (1 mm wide) was closed for 30 seconds to induce injury. Arrow indicates the RLN. (B) Ultraviolet sterilized carbon powder was placed on the crush tool to mark the site of injury on the RLN for postmortem identification, indicated by arrowhead. The right strap muscle is retracted laterally to allow visualization of the RLN. RLN = recurrent laryngeal nerve.

3.3.3 Transoral Laryngoscopy

Transoral laryngoscopy[25] was performed immediately prior to surgical incision, while the mice were anesthetized, positioned in dorsal recumbency, and immobilized in ear bars. To do so, the tongue was retracted with a cotton swab and gentle finger-grip, and a micromanipulator-controlled sialendoscope with a customized laryngoscope sheath was gently inserted into the oral cavity to visualize baseline VF movement. In mice, VF movement is spontaneous with breathing, rather than an evoked response. Immediately post-crush, laryngoscopy was performed again to confirm ipsilateral VF paralysis. After repeat laryngoscopy, the incision was sutured closed, and the mouse was recovered. Laryngoscopy was performed once more at 3 days post-crush (n=5) or 2 weeks post-crush (n=5), prior to euthanasia and tissue collection. Laryngoscopy video recordings (30 frames per second; approximately 1-3 minutes long) were subjectively analyzed by two trained, blinded reviewers using a Likert scoring system (0 = no VF movement, 1 = partial VF movement, 2 = normal VF movement).[15,19-21] Additionally, VF movement was tracked bilaterally with our automated motion tracking software, VFTrack. Then VFQuantify was used to measure amplitude- and frequency- based outcome metrics, MMRR and OCCR, respectively, along with VF angle during maximum abduction and adduction, described below.

3.3.4 Automated Analysis with VFTrack and VFQuantify

Our custom, VF motion analytics software package was used to analyze VF motion dynamics. A 10 second clip was selected from each video recording, based

on adequate visualization of the VFs and no aberrant camera movement. On the first video frame in each clip, a pair of points was manually placed on each VF (VF-glottal region boundary) for automated tracking over time using our VFTrack software. Point selection was based on the anatomical structure of the VFs, which were selected on the upper (i.e., ventral) half of each VF to ensure higher sensitivity to small VF motions. Because of the V-shaped nature of the VFs, VF points with higher *y* coordinates result in larger displacements for the same angular motion. Left (L_L) and right (L_R) lines were automatically passed through each pair of tracked points to approximate the medial side of the VF and the ipsilateral arytenoid cartilage in each video frame (**Figure 3.2a**). Three points of interest (p_o, p_L, p_R) were automatically located on the two VF lines (L_L and L_R) in each frame. P_o was the intersection point of the two VF lines, typically located midline, dorsal to the arytenoid cartilages, and p_L and p_R were two points on L_L and L_R, each at the same fixed distance from p_o (determined as the largest distance between the tracked points and p_o) (**Figure 3.2a**). Left and right VF motion ranges and corresponding motion midlines were automatically computed based on displacement (in pixels) of points p_L and p_R (**Figure 3.2b**). VF motion was automatically calculated through displacement of points p_L and p_R with respect to their motion midlines and graphically displayed as a cyclic waveform due to the oscillatory motion of the VFs during breathing (**Figure 3.3**).

Using VFQuantify, motion behavior differences between left and right VFs were measured using two complementary ratios, OCCR (Open Close Cycle Ratio) and MMRR (Mean Motion Range Ratio), to characterize the frequency and

amplitude of VF motion, respectively. The number of motion cycles for each VF was computed as the number of motion midline crossings. OCCR was then computed as the ratio of number of motion cycles for right and left VFs. Motion range of each VF was defined as the distance between the left-most and right-most positions of the VF (i.e., local minima and maxima in **Figure 3.3**) for each cycle. Mean Motion Range (MMR) was computed by averaging motion ranges over all time periods (i.e., each VF cycle within the 10 s video clip). MMRR was defined as MMR_{right}/MMR_{left}, which compares right and left VF motion amplitudes. The described point selection protocol [$p_L(t)$, $p_R(t)$ equidistant from $p_0(t)$] and unitless MMRR ensure robustness against variations in VF size across different subjects and camera distance from the VFs. In addition, the two VF lines, L_L and L_R, were used for automated measurement of VF angle during maximum abduction (maximum angle) and maximum adduction (minimum angle) for each video, without needing to manually acquire still images. The angular range of VF movement for each mouse was calculated by subtracting the minimum angle from the maximum angle measurements.

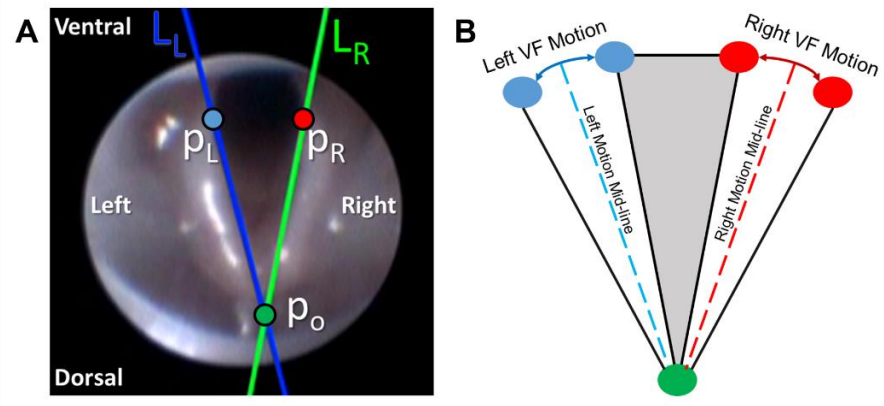

Figure 3.2. (A) Automatically tracked VF lines (LL and LR) and points of interest (po, pL, pR) shown on a sample video frame. (B) Illustration of left/right VF motion ranges and associated motion midlines. VF = vocal fold.

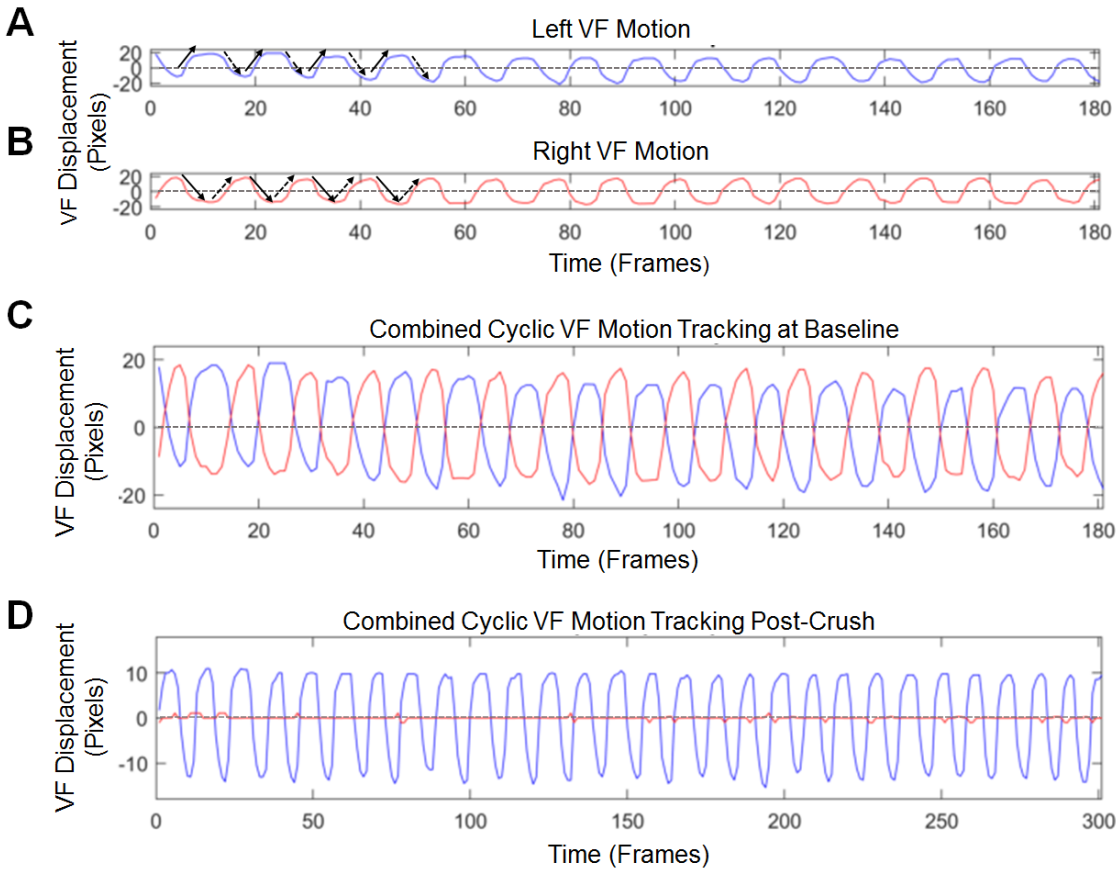

Figure 3.3. (A, B) Displacement of the left (blue) and right (red) VFs individually over time. The x-axis is the video frame number and the y-axis is VF displacement measured in pixels. The graphs display the cyclic movement as the VFs oscillate back and forth across their respective motion midlines (dashed lines) during inspiration and expiration in a normal mouse at baseline under a surgical level of anesthesia. Solid arrows indicate the VF is adducting (closing), whereas dashed arrows indicate the VF is in a state of abduction (opening). (C) The left and right VF displacement graphs from baseline are overlaid with respect to their motion midlines. Right VF range and frequency of motion are similar to the left. (D) Combined right and left VF movement immediately after a right RLN crush injury. There is no right VF movement, compared with normal left VF movement. RLN = recurrent laryngeal nerve; VF = vocal fold.

3.3.5 VFTrack Validation and Performance Evaluation

We validated tracking accuracy of our VFTrack software by comparing the automatically generated tracks from VFTrack to manually generated tracks by two independent reviewers (MH and TL) on a subset of videos (2 out of 5 videos per time point). For each selected video, manual tracks were generated by selecting a

point (x-y coordinate) on each VF boundary and sequentially marking the same boundary coordinate on every frame of each video. Given that different points can be manually selected and tracked on the VF boundary to produce the same line used to compute our outcome measures (MMRR and OCCR), reviewers were asked to track only the x-coordinate on the VF boundary in each frame. The y-coordinate was automatically displayed on each frame, indicated by a blue horizontal line spanning the image. MMRR and OCCR measures were calculated for each video based on the manual points (n=600 per video) placed by each reviewer. VFTrack performance was evaluated by computing (1) the pixel distance between manually and automatically tracked points along the VF boundary; (2) differences in MMRR and OCCR measures produced by these points; and (3) the time needed to generate these points. In addition, VFTrack was ran twice more by two independent reviewers to verify its reliability between reviewers.

3.3.6 Transmission Electron Microscopy

Mice were perfused with saline followed by 4% paraformaldehyde (PFA). RLNs were dissected *en bloc* and post-fixed in 4% PFA / 2% glutaraldehyde in 100 mM sodium cacodylate buffer. Samples were sent to our Electron Microscopy Core for standard tissue processing, embedding, and sectioning (85 nm). High resolution TEM cross-sectional images from the left and right RLNs distal to the crush-site were obtained using a JEOL JEM 1400 TEM microscope at 80 kV with a Gatan Ultrascan 1000 CCD camera.

3.3.7 Statistics

Mice were divided into two groups based on endpoint. Change scores between baseline and endpoint were calculated, and independent samples T-tests were used to separately analyze both outcome metrics (MMRR and OCCR). Spearman's correlations were utilized to compare subjective (Likert scale) and all objective outcome measures (MMRR, OCCR, and VF angle). Pearson's correlations were computed between the calculated angular range of motion and MMRR, to compare traditional objective analysis techniques with our novel objective metrics. Statistics were computed using IBM SPSS Statistics 24 and *p* values of less than 0.05 were considered significant.

3.4 Results

3.4.1 Subjective VF Motion Results

All mice survived the RLN crush surgical procedure and subsequent laryngoscopy recordings. Our subjective analysis of laryngoscopy video recordings revealed that all mice (n=10) had normal, bilaterally-symmetrical VF motion (score = 2) prior to injury. Immediately post-crush, all mice developed complete right-sided (ipsilateral) VF paralysis (score = 0). At the 3 days post-crush endpoint, the right VF remained immobile in all 5 mice. In contrast, mice had partial to full recovery of right VF movement at 2 weeks post crush (n=5; average score = 1.4; std = 0.55) (**Figure 3.4a**).

3.4.2 Objective VF Motion Results

Due to variable total range of VF motion in individual mice between anesthetic episodes, right VF movement was compared to left VF movement and quantified as a ratio (right:left) for our objective outcome measures. Our amplitude-based measure, Mean Motion Range Ratio (MMRR), allows quantification of right (injured) versus left (control) VF range of motion. Our frequency-based measure, Open Close Cycle Ratio (OCCR), quantifies the number of right VF movements compared to the left. At baseline, ratios for both MMRR and OCCR were near 1, signifying that right VF motion dynamics were similar to the left. Immediately post-crush, ratios were virtually 0, indicating complete paralysis of the right VF. At 3 days post-crush, MMRR and OCCR remained near 0, suggesting minimal to no recovery. By 2 weeks, our findings revealed partial recovery of VF range of motion and full recovery of VF frequency (**Figure 3.4b and 3.4c**). Mice at 3 days and 2 weeks post-crush had significantly different change scores for both outcome metrics. In addition, our automated VF angle measurements (**Figure 3.4d**) correlated with MMRR outcomes, signifying our novel, automated MMRR metric corresponds with previously reported angle measurement methods that are based on time-consuming analysis of still-frame images.[14-16] Correlations between outcome measures are displayed in **Tables 3.1 and 3.2**.

In summary, our automated outcome measures, MMRR and OCCR, had statistically significant correlation with our subjective analysis, as well as with angular range of motion, indicating our novel outcome measure detect similar

changes as with historic analysis methods, while providing more objective and informative outcome metrics that can be expanded upon in future studies.

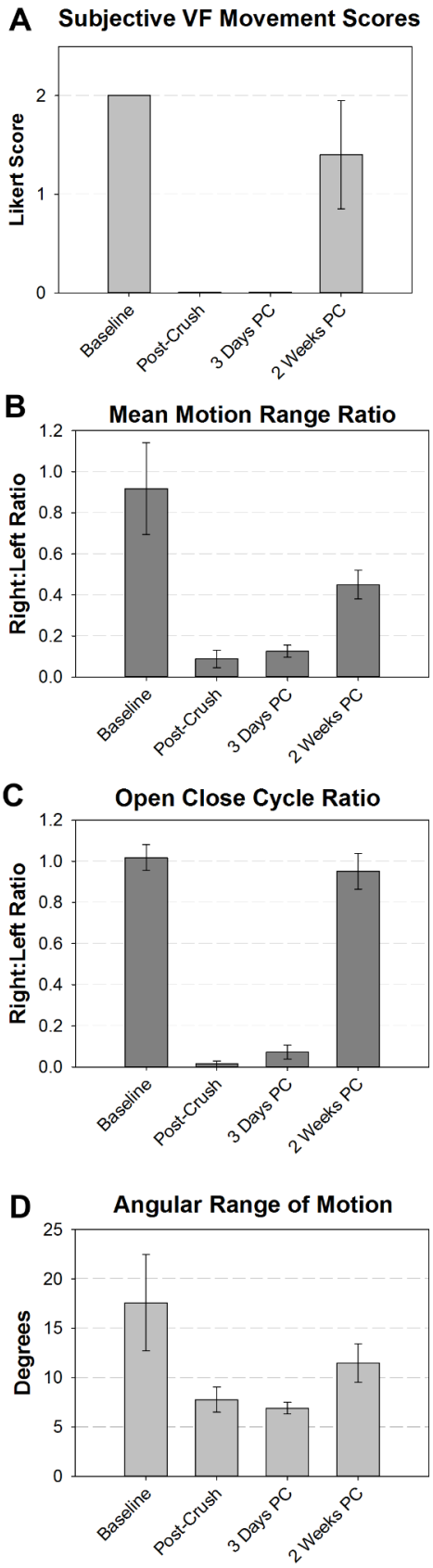

Figure 3.4. VF motion was quantified using (A) subjective and (B–D) objective outcome metrics. In all cases, VF motion was impaired by the RLN crush injury, which partially recovered by 2 weeks post-crush. One video file (immediately post-crush) had poor image quality for automated tracking and was excluded from graphical analysis in (B) and (C). PC = post-crush; RLN = recurrent laryngeal nerve; VF = vocal fold.

Table 3.1. Associations between subjective and objective VF measures using Spearman's correlation.

		MMRR	OCCR	Angular Range of Motion
Subjective Score (n=30)	Correlation Coefficient	0.874**	0.824**	0.886**

**. Correlation is significant at the 0.0001 level (2-tailed).
MMRR = Mean Motion Range Ratio; OCCR = Open Close Cycle Ratio

Table 3.2. Associations between objective measures of VF motion using Pearson correlations.

		MMRR	OCCR	Angular Range of Motion
MMRR (n=30)	Pearson Correlation	1	0.799**	0.817**
OCCR (n=30)	Pearson Correlation	0.799**	1	0.686**
Angular Range of Motion (n=30)	Pearson Correlation	0.817**	0.686**	1

**. Correlation is significant at the 0.0001 level (2-tailed).
MMRR = Mean Motion Range Ratio; OCCR = Open Close Cycle Ratio

3.4.3 VFTrack Validation and Performance Evaluation

To validate our automated tracking software, two reviewers performed manual, frame-by-frame analysis on a subset of videos. The average pixel distance between the automated software and each independent reviewer was 1.94 pixels (sd = 1.16; MH) and 1.88 pixels (sd = 1.10; TL). The average pixel distance between reviewers was 1.59 pixels (sd = 0.40). **Figure 3.5** displays a representative image of pixel error in a single video frame between each reviewer and VFTrack. On average, it took approximately 18 minutes longer to manually track the two VF boundary points compared to our automated process. Thus,

VFTrack drastically decreases the time to collect the MMRR and OCCR measures reported in this study. Calculations of these measures were performed the same for both manual and automated tracks using our VFQuantify software. The average difference in MMRR and OCCR was less than 0.09 and 0.20, respectively, for all three cases. The larger error in OCCR was likely due to inconsistent point selection with manual analysis. Additionally, MMRR and OCCR results did not significantly change when VFTrack was reran by two different reviewers.

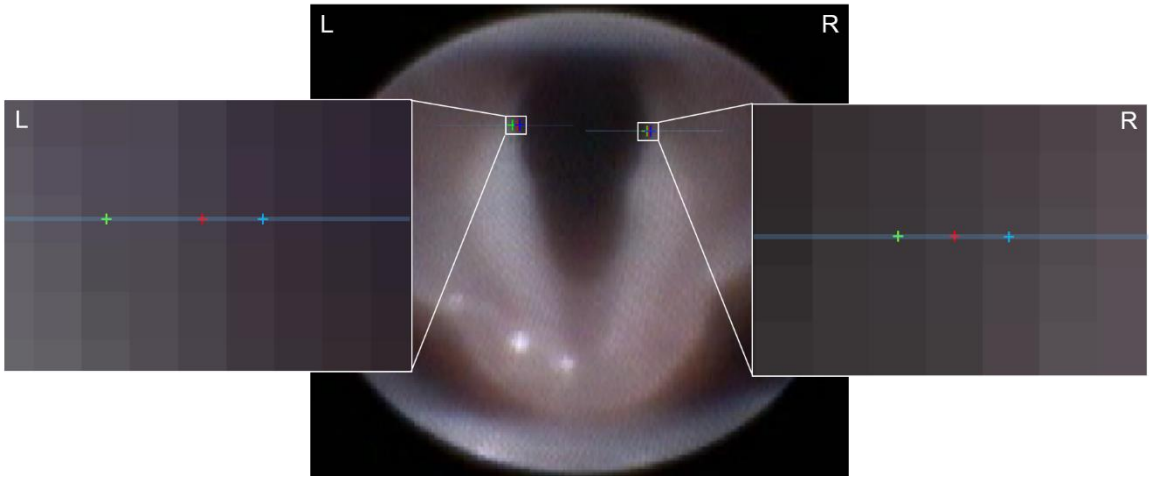

Figure 3.5. Representative image of VFTrack validation process. VF boundaries were tracked with our automated software (red points). Manual points were placed on each frame by 2 independent reviewers (green and blue points). The expanded view of the left and right VF boundaries shows individual pixels and the pixel location of each point along the given blue horizontal line. In this image, both reviewers are no more than 2 pixels away from the automatically tracked point, demonstrating high reliability of our automated tracking software. For perspective, the total endoscopy field of view contains approximately 60,000 pixels. VF = vocal fold.

3.4.4 TEM

Cross-sections of the left (control) RLN in all mice revealed thick axonal myelination with minimal interstitial space between axons. In contrast, there was evidence of extensive axonal degeneration in the right RLN at 3 days post-crush. This degeneration was indicated by collapsed nerve fibers and dense, compressed

myelin debris. At 2 weeks post-crush, the presence of thinly myelinated axons provided evidence of nerve regeneration (**Figure 3.6**).

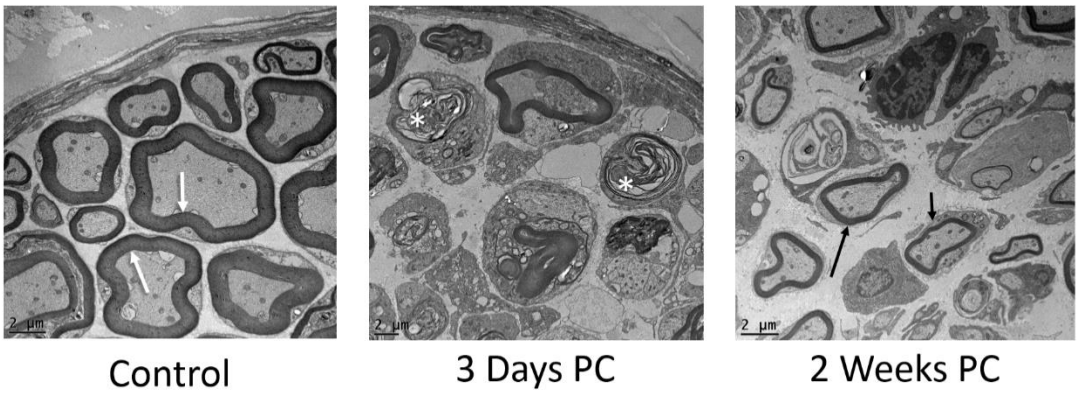

Figure 3.6. Representative TEM images of control and experimental RLN (above; 1,200×). Left (control) nerves showed thick myelination (white arrows) and tightly packed axons. At 3 days post-crush, the right (experimental) RLN showed extensive signs of degeneration, indicated by collapsed fibers and dense, compressed myelin debris (asterisks). At 2 weeks post-crush, regeneration of thinly myelinated axons was evident (arrows) within an expanded perineurial space. PC = post-crush; RLN = recurrent laryngeal nerve; TEM = transmission electron microscopy.

3.5 Discussion

The results from this study show that an aneurysm clip induced method of unilateral RLN compression injury resulted in ipsilateral VF impairment that allowed partial recovery by 2 weeks post-crush. This recovery was objectively evaluated with our custom VF motion analytics software, VFTrack and VFQuantify, to provide novel outcome metrics to detect and quantify subtle changes in VF motion in mice after RLN injury. Our primary objective was to demonstrate the feasibility of our novel software by comparing outcome metrics with previously described methods (i.e., objective angle measurements and subjective scoring). Thus, we have shown that our software can achieve similar results as currently used methods; however, it does so via automated objective quantification

methods, enabling efficient analysis of a high volume of dynamic VF motion recordings, rather than single frame analysis.

The subjective VF recovery results found in this study correlated with the objective measures obtained by our software, which were further validated by semi-automated manual analysis methods. However, our objective measures provide more precise and accurate metrics to quantify longitudinal VF recovery. Not only can our motion analysis software detect the difference between paralyzed and fully functional VFs, but it can detect small, but perhaps clinically important, changes in VF motion. Without VFTrack and VFQuantify, it would be extremely challenging and time consuming to calculate the novel functional outcome measures identified in this study, mean motion range ratio (MMRR) and open close cycle ratio (OCCR). Additionally, with our objective VF tracking there is less variation between mice in each group when compared to subjective scoring methods, which increases the likelihood of detecting significant findings when evaluating different treatments and time points.

Objective tracking allows full visualization of VF motion dynamics throughout the entire video clip, thus overcoming the limitation of quantifying static images at only two positions in the respiratory cycle. The data supplied by our motion analysis software includes both raw measures along with the ratios of right VF dynamics compared to the left. In addition to the metrics quantified in this study, we are searching for additional robust outcome measures that may provide new or complementary information for improved diagnostics and treatment evaluation. These measures can be used to acquire more meaningful information beyond

basic range of motion and quantification of VF angles at maximum adduction and abduction. Possible automated metrics of VF motion dynamics include: rate of VF movement, fluidity of VF motion, VF length/size/area, the amount of VF jitter, and uninjured VF compensation, among many others.

Our VF motion software is a crucial asset for objective and reproducible analysis of VF movement for experimental purposes, but it may have much broader applications beyond a laboratory setting. In fact, we are currently working on using this technology to quantify VF motion dynamics in healthy human patients, along with patients with known laryngeal dysfunction. Besides tracking VF movement with respiration, we have begun tracking more complex laryngeal functions, including the laryngeal adductor reflex and other behavioral tasks, such as sniffing through the nose, taking a deep breath, holding the breath, and vocal diadochokinetic tasks. Once perfected and validated, healthcare professionals can begin to use VFTrack and VFQuantify in a clinical setting in real time to advance diagnostic capabilities. We hope this will allow healthcare professionals to better monitor disease progression and treatment effects over time, enabling them to tailor therapeutic approaches to distinct symptoms and objectively quantify treatment efficacy in individual patients.

3.6 Conclusions

In conclusion, subjective analysis remains crucial for investigators to estimate VF motion dynamics. However, because subjective analysis is inadequate for detecting small changes in VF motion over time, objective, quantitative measures

are needed to fully and accurately assess VF motion dynamics. Furthermore, automation of VF motion quantification allows for high through-put analysis of dynamic VF motion recordings, enabling increased, highly-efficient research with our animal models. Most important, we have been expanding our software capabilities to identify additional outcome metrics that are amenable to automation, and are also clinically relevant (i.e., translatable to humans). As such, our software is currently being tested with human patients to improve diagnosis of VF disorders and enhance monitoring of treatment efficacy.

3.7 Acknowledgments

The authors thank Kate Osman for managing the laboratory and caring for the mouse colony on campus. The authors would also like to acknowledge DeAna Grant at the University of Missouri Electron Microscopy Core for her assistance with processing and imaging nerve samples for TEM. We would also like to acknowledge our funding sources: vocal fold motion tracking software (Coulter Translational Partnership) and post-doctoral training stipend & supplies (NIH T32-5T32OD011126-39).

3.8 References

1. Liu JB, Sosa JA, Grogan RH, et al. Variation of Thyroidectomy-Specific Outcomes Among Hospitals and Their Association With Risk Adjustment and Hospital Performance. *JAMA surgery.* 2018;153(1):e174593.

2. Chen C-C, Huang Y-C, Lee S-T, Chen J-F, Wu C-T, Tu P-H. Long-term result of vocal cord paralysis after anterior cervical disectomy. *European Spine Journal.* 2014;23(3):622-626.

3. Ta JH, Liu YF, Krishna P. Medicolegal Aspects of Iatrogenic Dysphonia and Recurrent Laryngeal Nerve Injury. *Otolaryngol Head Neck Surg.* 2016;154(1):80-86.

4. Rosko AJ, Kupfer RA, Oh SS, Haring CT, Feldman EL, Hogikyan ND. Immunohistologic analysis of spontaneous recurrent laryngeal nerve reinnervation in a rat model. *Laryngoscope.* 2018;128(3):E117-e122.

5. Brunner E, Friedrich G, Kiesler K, Chibidziura-Priesching J, Gugatschka M. Subjective breathing impairment in unilateral vocal fold paralysis. *Folia phoniatrica et logopaedica : official organ of the International Association of Logopedics and Phoniatrics (IALP).* 2011;63(3):142-146.

6. Mattsson P, Hydman J, Svensson M. Recovery of laryngeal function after intraoperative injury to the recurrent laryngeal nerve. *Gland Surg.* 2015;4(1):27-35.

7. Chandrasekhar SS, Randolph GW, Seidman MD, et al. Clinical practice guideline: improving voice outcomes after thyroid surgery. *Otolaryngol Head Neck Surg.* 2013;148(6 Suppl):S1-37.

8. Fang TJ, Li HY, Gliklich RE, Chen YH, Wang PC, Chuang HF. Quality of life measures and predictors for adults with unilateral vocal cord paralysis. *Laryngoscope.* 2008;118(10):1837-1841.

9. Wang W, Chen D, Chen S, et al. Laryngeal Reinnervation Using Ansa Cervicalis for Thyroid Surgery-Related Unilateral Vocal Fold Paralysis: A Long-Term Outcome Analysis of 237 Cases. *PLoS ONE.* 2011;6(4):e19128

10. Lin RJ, Smith LJ, Munin MC, Sridharan S, Rosen CA. Innervation status in chronic vocal fold paralysis and implications for laryngeal reinnervation. *The Laryngoscope.*n/a-n/a.

11. Choi JS, Oh SH, An HY, Kim YM, Lee JH, Lim JY. Functional regeneration of recurrent laryngeal nerve injury during thyroid surgery using an asymmetrically porous nerve guide conduit in an animal model. *Thyroid.* 2014;24(1):52-59.

12. Wang B, Yuan J, Xu J, Xie J, Wang G, Dong P. Neurotrophin expression and laryngeal muscle pathophysiology following recurrent laryngeal nerve transection. *Mol Med Rep.* 2016;13(2):1234-1242.

13. Paniello RC, Rich JT, Debnath NL. Laryngeal Adductor Function in Experimental Models of Recurrent Laryngeal Nerve Injury. *The Laryngoscope.* 2015;125(2):E67-E72.

14. Hernandez-Morato I, Sharma S, Pitman MJ. Changes in neurotrophic factors of adult rat laryngeal muscles during nerve regeneration. *Neuroscience.* 2016;333:44-53.

15. Hernandez-Morato I, Valderrama-Canales FJ, Berdugo G, et al. Reorganization of laryngeal motoneurons after crush injury in the recurrent laryngeal nerve of the rat. *J Anat.* 2013;222(4):451-461.

16. Wang B, Yuan J, Chen X, Xu J, Li Y, Dong P. Functional regeneration of the transected recurrent laryngeal nerve using a collagen scaffold loaded with laminin and laminin-binding BDNF and GDNF. *Scientific reports.* 2016;6:32292.

17. Nishimoto K, Kumai Y, Yumoto E. Paradoxical movement of rat vocal folds following recurrent laryngeal nerve injury. *Acta oto-laryngologica.* 2014;134(11):1164-1171.

18. Abstracts of Scientific Papers 2017 AALAS National Meeting. *Journal of the American Association for Laboratory Animal Science.* 2017;56(5):574-694.

19. Tessema B, Pitman MJ, Roark RM, Berzofsky C, Sharma S, Schaefer SD. Evaluation of functional recovery of recurrent laryngeal nerve using transoral laryngeal bipolar electromyography: a rat model. *The Annals of otology, rhinology, and laryngology.* 2008;117(8):604-608.

20. Tessema B, Roark RM, Pitman MJ, Weissbrod P, Sharma S, Schaefer SD. Observations of recurrent laryngeal nerve injury and recovery using a rat model. *Laryngoscope.* 2009;119(8):1644-1651.

21. Monaco GN, Brown TJ, Burgette RC, et al. Electrical stimulation and testosterone enhance recovery from recurrent laryngeal nerve crush. *Restor Neurol Neurosci.* 2015;33(4):571-578.

22. Sarikcioglu L, Demir N, Demirtop A. A standardized method to create optic nerve crush: Yasargil aneurysm clip. *Experimental eye research.* 2007;84(2):373-377.

23. Sarikcioglu L, Ozkan O. Yasargil-Phynox aneurysm clip: a simple and reliable device for making a peripheral nerve injury. *Int J Neurosci.* 2003;113(4):455-464.

24. Bridge PM, Ball DJ, Mackinnon SE, et al. Nerve crush injuries--a model for axonotmesis. *Experimental neurology.* 1994;127(2):284-290.

25. Shock LA, Gallemore BC, Hinkel CJ, et al. Improving the Utility of Laryngeal Adductor Reflex Testing: A Translational Tale of Mice and Men. *Otolaryngol Head Neck Surg.* 2015;153(1):94-101.

Chapter Four

RECURRENT LARYNGEAL NERVE TRANSECTION RESULTS IN TRANSLATIONAL UPPER AIRWAY COMPLICATIONS

This chapter has been submitted for publication to the

Journal of Comparative Neurology

Megan M Haney[1], Ali Hamad[2], Henok G Woldu[3], Michelle Ciucci[4,5], Nicole Nichols[6], Filiz Bunyak[2], Teresa E Lever[6,7*]

[1]Department of Veterinary Pathobiology, University of Missouri, Columbia, Missouri

[2]Department of Electrical Engineering and Computer Science, University of Missouri, Columbia, Missouri

[3]Department of Health Management & Informatics, University of Missouri, Columbia, Missouri

[4]Department of Communication Sciences and Disorders, University of Wisconsin–Madison, Madison, Wisconsin

[5]Department of Surgery, Division of Otolaryngology, University of Wisconsin-Madison, Madison, Wisconsin

[6]Department of Biomedical Sciences, University of Missouri, Columbia, Missouri

[7]Department of Otolaryngology–Head and Neck Surgery, University of Missouri, Columbia, Missouri

4.1 Abstract

Objectives: The recurrent laryngeal nerve (RLN) is responsible for normal vocal fold (VF) movement, and is at risk for iatrogenic injury during anterior neck surgical procedures in human patients. Injury, resulting in VF paralysis, may contribute to subsequent swallowing, voice, and respiratory dysfunction. Unfortunately, treatment for RLN injury does little to restore physiologic function of the VFs. Thus, we sought to create a mouse model with translational functional outcomes to further investigate RLN regeneration and potential therapeutic interventions.

Methods: To do so, we performed ventral neck surgery in 21 C57BL/6J male mice, divided into two groups: Unilateral RLN Transection (n=11) and Sham Injury (n=10). Mice underwent behavioral assays to determine upper airway function at multiple time points prior to and following surgery. Transoral endoscopy, videofluoroscopy, ultrasonic vocalizations, and whole-body plethysmography were used to assess VF motion, swallow function, vocal function, and respiratory function, respectively. Outcome metrics were identified to increase the translational potential of this model. Additionally, immunohistochemistry was used to investigate neuronal cell death in the nucleus ambiguus.

Results: Results revealed that RLN transection created ipsilateral VF paralysis that did not recover by 13 weeks post-surgery. Furthermore, there was evidence of significant vocal and respiratory dysfunction in the RLN transection group, but not the sham injury group. No significant differences in swallow function or neuronal cell death were found between the two groups.

Conclusions: In conclusion, our mouse model of RLN injury provides several novel functional outcome measures to increase the translational potential of findings in preclinical animal studies. We will use this model and behavioral assays to assess various treatment options in future studies.

4.2 Introduction

Unilateral vocal fold (VF) paralysis is a common complication of iatrogenic recurrent laryngeal nerve (RLN) injury during cervical and thoracic surgeries. In patients with unilateral VF paralysis, 56% experience dysphagia, up to 80% are affected by dysphonia, and 75% encounter dyspnea.[1-3] Moreover, dysphagia may result in life-threatening complications such as aspiration pneumonia, dehydration, and malnutrition,[4] whereas dysphonia can greatly interfere with one's social life and employment, potentially necessitating a career change.[1] In fact, complications due to RLN palsy are among the leading reasons for litigation of healthcare professionals who perform these procedures.[1,3,5,6]

Unfortunately, treatments that restore normal physiologic function after RLN injury are lacking.[1,3,7] Current strategies include voice therapy[4,8-10] and medialization of the impaired VF.[4] Alternative secondary surgeries, such as RLN anastomosis, may increase background muscle activity, but do not guarantee return of normal VF mobility.[3] Thus, more effective neuro-regenerative treatment options are needed. However, to investigate new therapeutic interventions, a translational animal model that consistently replicates the functional outcomes of

RLN injury in humans is essential. In addition, reliable functional assays to quantify these symptoms are critical.

Current models principally use transoral endoscopy to assess VF mobility and evaluate functional impairment and recovery after RLN injury.[11-14] While this methodology provides information on VF movement, it does not concurrently evaluate deficits associated with swallowing, vocalization, or respiration experienced by human patients. As these functions are fundamental to quality of life, it is essential to investigate them in animal models. However, no published study has comprehensively examined each potential complication in a single model.

An infant pig model of RLN injury has provided novel insights concerning the role of the RLN and its neural connections in swallowing behavior. By using videofluoroscopic techniques, RLN injury has been shown to result in compromised airway protection and esophageal dysphagia,[15] alterations in tongue shape,[16] and modified tongue and epiglottis kinematics during swallowing.[17] However, these experiments were performed in neonatal and pre-weanling animals, better representing infants with immature nervous systems. In contrast, many patients undergoing common anterior neck procedures, such as thyroidectomy, belong to an aged population.[1,18] Thus, a more appropriately aged animal with a fully developed nervous system is necessary to evaluate RLN injury and its sequela in this target population.

Of the post-operative complications associated with RLN injury, dysphonia is often the most problematic for the patient. One group assessed audible

vocalizations in a rat model after RLN transection and showed hoarse, deep-pitched, and shorter vocalizations with low amplitudes.[7,13] However, audible vocalizations are not the primary means of rodent communication and are elicited in response to stressful or painful stimuli, whereas ultrasonic vocalizations represent communicative intent.[19] Furthermore, rodent ultrasonic vocalization assays have been well established.[20-22] Social ultrasonic vocalizations are analogous to human vocal communication in many important ways. For example, ultrasonic vocalizations are generated within the larynx[23] and are capable of eliciting change in the behavior of the signal recipient.[24-26] As such, ultrasonic, rather than audible, vocalizations are a more appropriate method to study vocal function in rodents.

Similarly, comparative respiratory function has not been thoroughly assessed in animal models of RLN injury, except in coordination with swallowing in infant pigs.[27] Dyspnea after RLN injury is also under-researched in the human literature, likely because many human patients with unilateral VF paralysis have normal or near normal working respiratory capacity. However, up to ~75% complain of breathing impairment, especially during phonation or physical effort.[2] Of the few studies investigating respiratory parameters following RLN injury, most have noted decreased inspiratory flow rates in patients with unilateral VF paralysis, which may or may not be improved with VF medialization procedures.[28-31]

In this study, we hypothesized that RLN transection would significantly affect VF mobility, swallowing, vocalization, and respiration in an adult mouse model. We chose a transection injury as this is the most experimentally

reproducible injury, and removes severity of injury as a confounding variable. In addition, we performed immunohistochemistry to investigate if neuronal cell death was present in the brainstem motor nucleus, the nucleus ambiguus, after RLN transection, as peripheral nerve injury often results in various percentages of retrograde cell death.[32] We also continued to refine our VF tracking and quantification software[33] to better evaluate and characterize dynamic VF motion. Furthermore, behavioral tests were optimized to identify the most translational outcome measures for application towards human studies. Through this comprehensive behavioral regimen, this study offers the first look at the interplay between unilateral VF paralysis with the consequent somatic manifestations of dysphagia, dysphonia, and dyspnea in a single animal model.

4.3 Materials and Methods

4.3.1 Animals

Animal care was conducted in accordance with the Guide for the Care and Use of Laboratory Animals and all experimental procedures performed in this study were reviewed and approved by the Institutional Animal Care and Use Committee at the University of Missouri, which is USDA-licensed and AAALAC-accredited. Twenty-one male C57BL/6J (B6) mice (age at beginning of study = 7.5 ± 0.6 months; weight = 30.4 ± 2.4 g) were used for this study. Mice were housed in individually ventilated caging (Tecniplast, West Chester, PA) with aspen chip bedding. Mice were group-housed (2-4 mice per cage) whenever possible throughout the study, and had free access to food (Laboratory Rodent Diet 5001,

Purina, St. Louis, MO) and water, except for overnight water restriction for swallow assays, described below. Room temperature was maintained between 20.0 °C and 26.0 °C, relative humidity was between 30% to 70%, and the photoperiod was a 12:12-h standard light:dark cycle (lights on at 7:00 am). Standard enrichment (nestlet), running wheels, and mouse huts were provided to all cages.

All mice were of the same health status and were housed in the same room throughout the study; however, surgical manipulations and behavioral assays were performed in separate rooms of the laboratory, located outside of the vivarium. At the time of the study, serology samples from colony sentinels were tested quarterly and were considered free of the following agents: mouse hepatitis virus, minute virus of mice, mouse parvovirus, Sendai virus, Theiler's murine encephalomyelitis virus, mouse rotavirus, Mycoplasma pulmonis, Pasteurella pneumotropica, Salmonella spp., mouse pneumonia virus, reovirus 3, lymphocytic choriomeningitis virus, Ectromelia, mouse adenovirus 1 and 2, K virus, and polyoma virus. Fecal PCR was used to detect pinworms in sentinel mice, whereas cage PCR (pooled swabs by room) was used to detect fur mites, neither of which were detected.

4.3.2 Experimental Design

Mice were randomized to undergo survival surgery to create an RLN transection injury (n=11), or a sham surgery to visualize, but not injure, the RLN (n=10). Transoral laryngoscopy was performed during surgery immediately prior to incision and immediately after surgery to assess the effect on VF motion. In addition, mice underwent baseline behavioral testing prior to surgery to quantify

normal swallow, vocal, and respiratory function. Testing consisted of videofluoroscopic swallow study, whole-body plethysmography, and ultrasonic vocalization assays. Mice received subsequent behavioral testing at various time points following surgical manipulations (**Figure 4.1**). At 13 weeks post-surgery (WPS), mice were anesthetized to repeat transoral laryngoscopy prior to euthanasia for tissue collection.

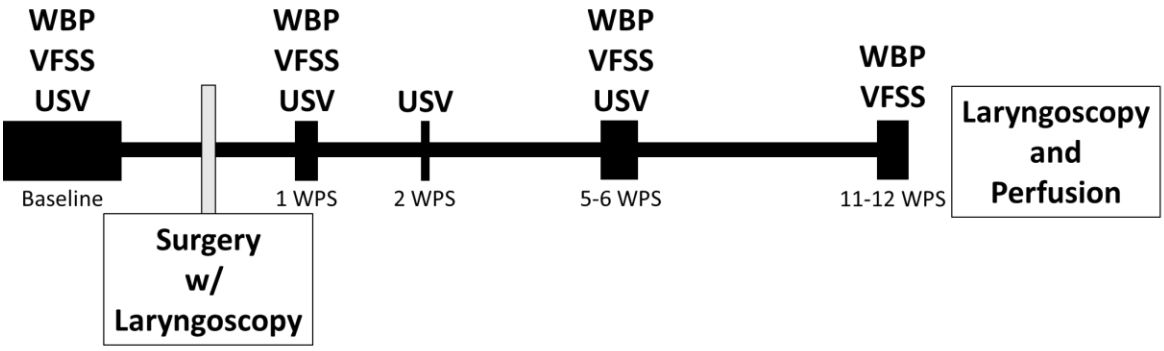

Figure 4.1. Experimental Timeline. Baseline functional testing was performed 2-4 weeks prior to surgery. Additional functional analysis was performed following surgery. Whole body plethysmography was performed at 1,5, and 11 WPS. Videofluoroscopic swallow studies were performed 1, 6, and 12 WPS, and ultrasonic vocalizations were collected at 1, 2, and 5 WPS. Laryngoscopy was performed prior to surgical incision, immediately following surgical manipulation of the RLN, and at 13 WPS prior to perfusion for tissue collection. WPS = weeks post-surgery, WBP = whole body plethysmography, VFSS = videofluoroscopic swallow study, USV = ultrasonic vocalizations.

4.3.3 Surgical Procedures

Mice were anesthetized with ketamine (90 mg/kg; Henry Schein, Melville, NY) and xylazine (11.25 mg/kg; Akorn, Lake Forest, IL), administered subcutaneously (SQ). Half doses of SQ ketamine were given to maintain the surgical plane of anesthesia every 10-20 min, as needed, throughout the procedure. The eyes were lubricated to prevent drying and the ventral neck was

shaved and prepared aseptically for surgery. Mice were positioned in dorsal recumbency on a heated, custom platform beneath a surgical microscope (M125; Leica Microsystems, Inc., Buffalo Grove, IL), and reflexes (toe-pinch) were checked at least every 10-15 minutes.

A midline neck incision was made from the suprasternal notch to the mandible. The salivary glands were gently retracted laterally to expose the strap muscles overlying the trachea. In mice undergoing an RLN transection injury, the right RLN was isolated at the level of the 5th tracheal ring and a small section of nerve (~1-2 mm) was removed to prevent RLN regeneration. The left RLN served as an internal control for this study. Mice in the sham injury group underwent an identical surgical procedure; however, the RLN was only visualized, not isolated or transected.

For both groups, the neck incision was closed with absorbable sutures (6-0 Monocryl, Ethicon, Somerville, NJ) and surgical glue (Tissumend II, Veterinary Products Laboratories; Phoenix, AZ). After suturing was complete, 0.2 ml of warm, sterile saline was administered SQ, along with buprenorphine-SR (1 mg/kg, SQ; Zoopharm, Windsor, CO), flunixin meglumine (2.2 mg/kg, SQ; Merck, Kenilworth, NJ), and atipamezole (0.22 mg/kg, SQ; Zoetis, Parsippany-Troy Hills, NJ) as separate injections for pain control and to reverse anesthesia. Mice were transferred to a clean, heated cage for recovery, and were monitored at least every 10-15 minutes until they were returned to their home cage once fully ambulatory. The home cages were placed half-on/half-off a heated water blanket (Model: TP700, Stryker, Kalamazoo, MI) overnight and returned to the vivarium the

following morning. All mice were monitored daily for 1 week after surgery for any signs of pain, distress, or surgical complications.

4.3.4 Transoral Laryngoscopy

While mice were anesthetized for surgery, transoral laryngoscopy[33,34] was performed immediately prior to surgical incision to establish baseline VF movement and immediately after surgical manipulation to determine the direct effect on VF mobility. To do so, a micromanipulator-controlled sialendoscope (R11573A; Karl Storz, Tuttlingen, Germany) with a customized laryngoscope was inserted into the oral cavity to visualize VF movement on a Storz Tele Pack X monitor (Karl Storz, Tuttlingen, Germany). In mice, VF movement is spontaneous with breathing, rather than an evoked response; therefore, no exogenous stimulus was required to elicit VF movement. Laryngoscopy was performed once more at 13 WPS with mice under anesthesia prior to euthanasia and tissue collection. Laryngoscopy videos were recorded at 30 frames per second (fps) for approximately 1-3 minutes per mouse for analysis.

4.3.5 Automated Vocal Fold Motion Analysis

Ten second clips from each laryngoscopy video were analyzed to detect left and right VF movement using our automated motion tracking software, VFTrack,[33] and outcome metrics were calculated using our custom VFQuantify software.[33] Briefly, points (p_L and p_R) were manually placed on the medial aspect of each VF or arytenoid cartilage on the first frame of each video clip. A third point (p_o), was

placed midline, dorsal to the arytenoid cartilages. Separate lines (L_L and L_R) were automatically drawn from p_L and p_R to p_o to approximate the medial edge of each VF and its associated cartilage (**Figure 4.2a**). The VFs were automatically tracked using points on L_L and L_R at the same fixed distance from p_o. Left and right VF motion ranges and corresponding motion midlines (d_L=0 and d_R=0) were automatically computed based on displacement (in pixels) of the VFs. VF motion was graphically displayed as a cyclic waveform due to the oscillatory motion of the VFs during spontaneous breathing.

In addition to our previously published dynamic VF outcome metrics, Mean Motion Range Ratio and Open Close Cycle Ratio,[33] we developed two additional metrics to characterize paradoxical movement of the right VF and compensation of the left VF, which we have observed in numerous mice after RLN injury. Abnormal, paradoxical movement of the VFs is characterized by the motion of the left and right VFs in the same direction, in contrast to the motion of the left and right VFs in the opposite direction during normal VF opening and closing behavior (**Figure 4.2b**). To differentiate between normal versus paradoxical movement, we have computed the motion correlation coefficient (Mcorr)[35] between the time series of the left and right VF displacements. Mcorr is defined as,

$$Mcorr(d_L, d_R) = \frac{1}{N-1}\sum_{i=1}^{N}\left(\frac{\overline{d_L - \mu_L}}{\sigma_L}\right)\left(\frac{d_R - \mu_R}{\sigma_R}\right)$$

where d_L and d_R are displacements of the left and right VFs, and μ, σ denote mean and standard deviation of the displacement time series. The values of the correlation coefficients can range from -1 to 1, where values close to -1 represent

a negative correlation (i.e., motion in opposite directions; normal function), values close to 1 represent a positive Mcorr (i.e., motion in the same direction; paradoxical VF motion), and values close to 0 represent minimal correlation. Based on the Mcorr values between the left and right VF displacement series, we have defined a VF motion activity index (VFActivity) as follows:

$$VFActivity = \begin{cases} -1 \le Mcorr(d_L, d_R) \le -0.5 & \text{Normal VF motion behavior} \\ -0.5 < Mcorr(d_L, d_R) < 0.5 & \text{Minimal motion correlation} \\ 0.5 \le Mcorr(d_L, d_R) \le 1 & \text{Paradoxical VF motion behavior (Pull or Push)} \end{cases}$$

For the cases of paradoxical motion (VFActivity=Push/Pull), where the left and right VFs were moving in the same direction, further signal analysis was performed to differentiate pushing versus pulling behaviors. Pushing is characterized as the intact left VF pushing the injured right VF during glottal closing (adduction); while pulling is characterized as the intact VF pulling the injured VF during glottal opening (abduction) (**Figure 4.3**). Paradoxical motion is automatically classified as pushing versus pulling using the following processing steps:

1. In this model, the intact left VF moves symmetrically; therefore, its motion midline, d_L=0, is set as the steady state position for the left VF.
2. Left VF steady state crossing times (t_i) are detected as $d_L(t_i)$=0 (black dashed lines in **Figure 4.4a**).
3. Next, the steady state positions of the right, injured VF are determined as positions of the right VF when the left VF is positioned at its steady state (no pulling or pushing behavior by the left VF; dashed yellow lines in **Figure 4.4a**).

4. Pulling versus pushing behaviors are identified by separately computing total displacements of the right VF during positive and negative displacements of the left VF. Positive displacement of the left VF occurs when the left VF moves to the right of its motion midline (d_L=0) during adduction, indicated by positive movement on the displacement plots. Negative displacement of the left VF occurs when the left VF moves to the left of its motion midline (d_L=0), indicated by negative movement on the displacement plots. Larger total absolute displacement by the right VF during positive displacements of the left VF indicates pushing behavior (i.e., the area between the right VF and its steady state during positive displacements is greater than during negative displacements; **Figure 4.4b**). Larger total absolute displacement by the right VF during negative displacements of the left VF indicates pulling behavior (i.e., the area between the right VF and its steady state during negative displacements is greater than during positive displacements; **Figure 4.4c**).

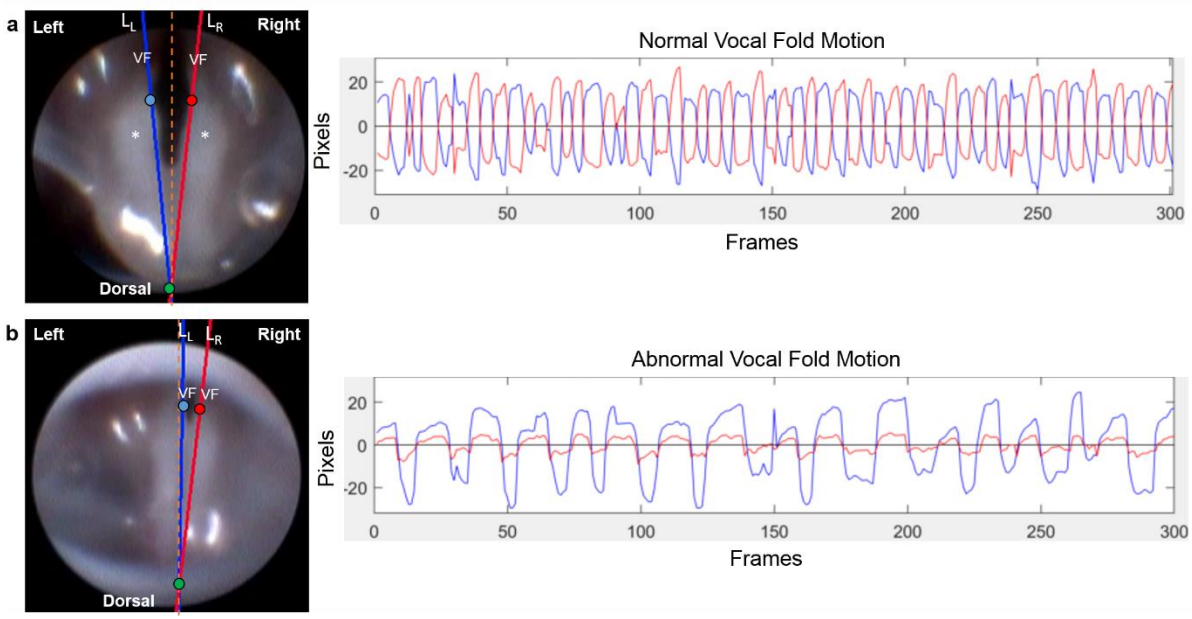

Figure 4.2. Representative still frame images (left) and displacement plots (right) of normal versus abnormal (paradoxical) vocal fold motion. On the first frame of each endoscopic video clip, two points, p_L (blue circle) and p_R (red circle), were manually placed on the medial aspect of each VF and associated arytenoid cartilage, and a third point, p_o (green circle), was placed midline, dorsal to the arytenoid cartilages. Using these manual reference points, separate lines (L_L and L_R) were automatically drawn to approximate the medial edge of each VF/arytenoid for motion tracking analysis, after automatic adjustment to make points p_L and p_R at the same fixed distance from p_o. These still frame images represent the positioning of the VFs in a state of maximum adduction. Note the left and right VF are symmetrical and do not cross the glottal midline in normal VF motion (a). However, in abnormal cases (b), the left VF may cross the glottal midline and contact the right VF, pushing it laterally, such that both VFs are paradoxically moving in the same direction. Alternatively, the left VF may pull the right VF medially during abduction, resulting in a similarly positive correlated displacement plot. VF = vocal fold. Asterisk (*) = arytenoid cartilage. Orange dashed line = glottal midline. Plots show displacement of the intact left (blue) VF and denervated right (red) VF with respect to their motion midline (0 on y-axis) over time. Normal VF motion (a) is represented by oscillatory motion of both VFs in opposite directions (negatively correlated). Abnormal (paradoxical) VF motion (b) is represented by movement of the VFs in the same direction (positively correlated).

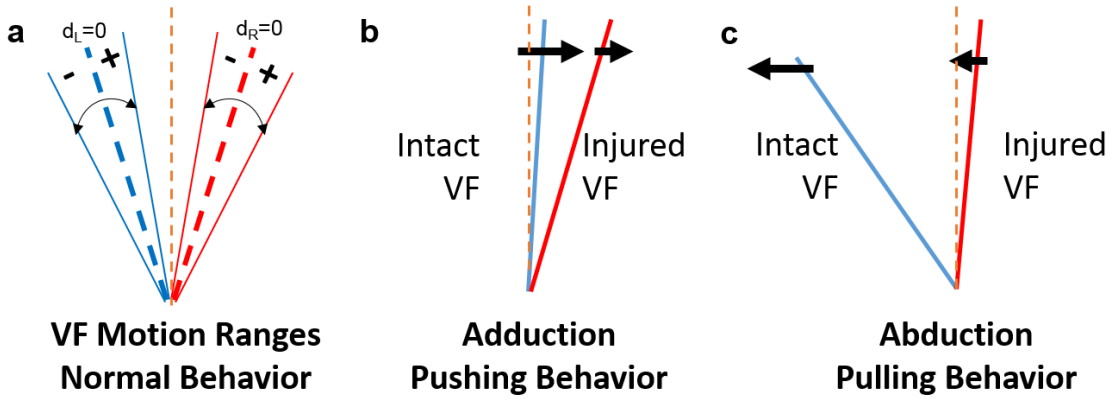

Figure 4.3. Analysis of vocal fold motion behavior. (a) Left and right VF motion ranges; center dashed blue and red lines represents motion midline for each VF (i.e., d_L= displacement of left VF = 0; d_R= displacement of right VF = 0). (b) VF motion during pushing: The intact VF contacts the injured VF to push it laterally in the same direction during VF adduction. (c) VF motion during pulling: The intact VF pulls the injured VF medially in the same direction during abduction. Left VF (blue line) represents the healthy, intact VF; right VF (red line) represents the injured VF. Orange dashed line = glottal midline. VF = vocal fold.

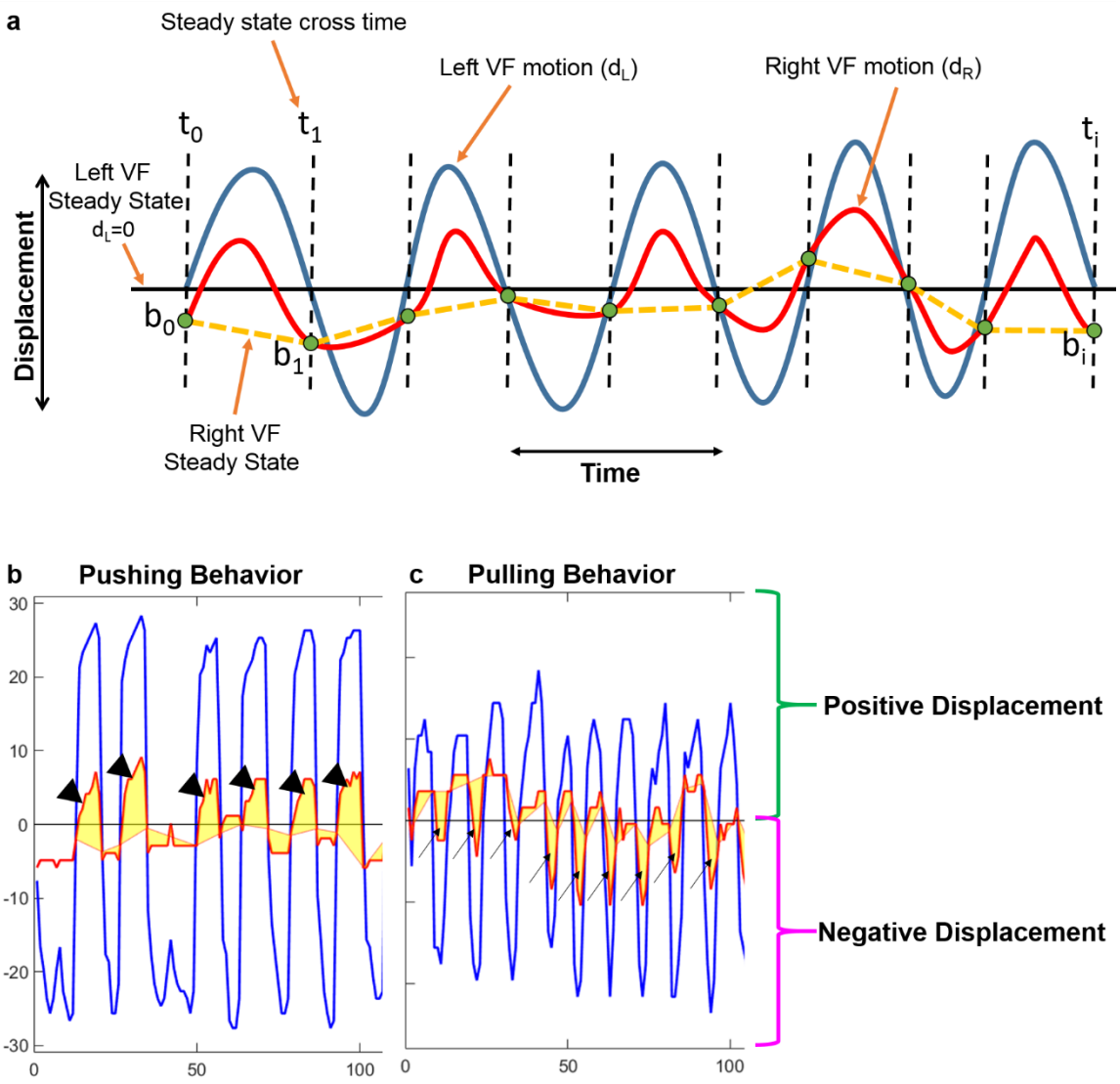

Figure 4.4. Identification of pulling versus pushing behaviors from left and right VF displacement time series. (a) Synthetic plot illustrating analysis of pushing vs. pulling behaviors. Displacement of the left VF with respect to its motion midline is shown in blue. Displacement of the right VF with respect to its motion midline is shown in red. The solid black (horizontal) line illustrates the motion midline and steady state for the left VF. The dashed black (vertical) lines indicate where the left VF crosses its steady state position. The steady state position of the right VF is determined by the positions of the right VF when the left VF is positioned at its baseline (no pulling or pushing by the left VF). The dashed yellow lines denote the steady state positions for the right VF. Pulling versus pushing behaviors are identified by separately computing total displacements of the right VF during positive and negative displacements of the left VF. (b) Representative plot for pushing behavior. Larger total absolute displacement by the right VF during positive displacements (arrowheads) of the left VF indicates pushing behavior. (c) Representative plot for pulling behavior. Larger total absolute displacement by the right VF during negative displacements (arrows) of the left VF indicates pulling behavior.

4.3.6 Videofluoroscopic Swallow Study (VFSS)

To assess swallowing function in awake, freely behaving mice, videofluoroscopic swallow testing was performed using our standard protocol[36,37] at 4 time points: baseline (3 weeks prior to surgery), as well as 4 days post-surgery, 6 WPS, and 12 WPS. Videofluoroscopy was performed the week after whole-body plethysmography and ultrasonic vocalization assays to reduce the amount of testing for a single mouse in a given week. Four days post-surgery was chosen as it was the earliest time point that mice could undergo fluoroscopy without risking confounding effects of post-surgical analgesics.

Prior to baseline swallow testing, mice underwent a behavioral conditioning program to assure familiarity and acceptance of the contrast solution and test chamber. For each time point, mice were fluid restricted overnight for 14-16 hours and provided additional chewable enrichment (e.g., nut and seed mix) to motivate voluntary drinking during testing. During testing, mice were individually enclosed in a custom test chamber positioned on a custom, remote-controlled lift table within a miniaturized fluoroscope (Glenbrook Technologies, Randolph, NJ). Each mouse was then exposed to approximately 2-3 minutes of low-dose radiation (~30 kV and 0.2 mA) for fluoroscopic examination of swallowing in the lateral plane while freely drinking a species-specific oral contrast agent recipe: Omnipaque (350 mg iodine per mL; GE Healthcare, Inc., Princeton, NJ) diluted to a 25% solution with deionized water and 3% chocolate syrup. The contrast solution was administered through a custom delivery system into a custom bowl positioned immediately above the test chamber floor.

To minimize radiation exposure, the fluoroscope was activated and video (30 fps) was recorded only when mice were drinking from the bowl, which was identified by real-time viewing via a webcam (C920 HD Pro Webcam; Logitech International S.A., Lausanne, Switzerland) positioned above the test chamber. Each video (AVI file) was subsequently analyzed frame-by-frame by two independent reviewers using video editing software (Pinnacle Studio 14; Corel Corporation, Ottawa, Ontario, Canada) to quantify several swallow metrics established by our prior work.[36,37] Metrics included lick rate (licks/second), swallow rate (swallows/2 seconds), inter-swallow interval (seconds), lick-swallow ratio (licks/swallow), pharyngeal transit time (seconds), esophageal transit time (seconds), and percentage of esophageal swallow inhibition (%). Three to five measures of each videofluoroscopic swallow metric were obtained for each mouse. Reviewer discrepancies were resolved by group consensus.

4.3.7 Ultrasonic Vocalizations (USV)

As vocal function has been noted to recover shortly after RLN denervation,[38] two acute time points and one chronic time point were selected to assess this functional outcome. Ultrasonic vocalization testing was performed to assess vocal function in mice 1 week prior to surgery and at 1, 2, and 5 WPS. Two to three nights prior to vocalization testing, mice were co-housed with a sexually mature female mouse overnight to sexually experience the male mice, as sexually experienced male mice are likely to produce greater numbers of ultrasonic calls.[39] For study feasibility, estrus cycle of the female mouse was not taken into account.

The night prior to testing, male mice were individually housed in a clean cage to establish a home cage environment for data collection the following day. For testing, the entire home cage was placed in a custom sound insulated chamber. To elicit calls, a random female “intruder” mouse was anesthetized using ketamine and xylazine (90:11.25 mg/kg; SQ) and placed inside the home cage with the test subject.[40] This ensured that male-only vocalizations were obtained. The same intruder mouse was used approximately 4-6 times in succession until anesthetic depth began to lighten. Vocalization recording of the male mouse commenced immediately after placing the anesthetized female mouse in the test cage.

Individual vocalizations from the mice were recorded for 3 minutes using an ultrasonic microphone (CM16, Avisoft, Germany) with 16-bit resolution and a sampling rate of 250-kHz, placed directly over the test cage fitted with a modified wire bar lid.[40-42] Offline acoustic analysis of vocal recordings for each mouse were analyzed using SASLab Pro (Avisoft, Germany). The WAV files were analyzed with Avisoft-generated spectrograms using a Fast Fourier Transform (FFT) of 512 points, frame size of 100%, flat top window, and temporal resolution set to display 75% overlap. A high pass filter was used to eliminate noise below 25 kHz.[42,43] The number of calls was automatically calculated by the Avisoft software and classified as low or high frequency modulated calls for all 4 time points. High frequency modulated calls were defined in the software as any call with a standard deviation of >0.1 for peak frequency of the entire call, whereas low frequency modulated calls had a standard deviation of $\leq$0.1 for peak frequency. These data were used to select the time points for additional in-depth ultrasonic vocalization analysis

consisting of call labeling and acoustic parameters, from which we could identify potential outcome metrics that could be used for future studies in this model.

Using the high frequency modulated call results, baseline and 1 WPS were chosen for additional in depth analysis as follows: a trained reviewer independently classified and quantified all calls in a blinded fashion within the first 90 seconds after the first detected call. Ten call types (i.e., constant, downsweep, upsweep, harmonic, multiple jumps, jump up, jump down, half cycle, full cycle, and two cycle) were identified and grouped accordingly into four call categories based on complexity: simple, complex, jump, and cycle (**Figure 4.5**).[42,43] The following acoustic properties that are common in communication signals among various species, including mice and humans, were measured for each call type and category:[44] percentage of call type (%), bandwidth (kHz), peak frequency (kHz), duration (millisecond, ms), and duration of peak frequency (ms).

Furthermore, mice preferentially produce ultrasonic calls in a repetitive series, which display a regular temporal structure.[45-47] Thus, additional ultrasonic vocalization metrics were used to further characterize potential dysfunction in repetitive calling in this model. To do so, series of calls within the first 90 seconds after the first call were manually identified using spectrogram files with labeled calls. Series of calls were defined as a group of at least four calls spaced no more than 150 ms apart from one another (i.e., an intervocalization interval < 150 ms; **Figure 4.6**).[47] The time in between series of calls was labeled as a pause. The number of call series and the average number of calls within a series, as well as the average length of call series and longest length of call series were calculated.

In addition, the average intervocalization interval within a series was determined. Groups of less than four calls or individual calls were counted as isolated calls within a pause. The average pause length and the average number of isolated calls within a pause were also calculated and compared between groups.

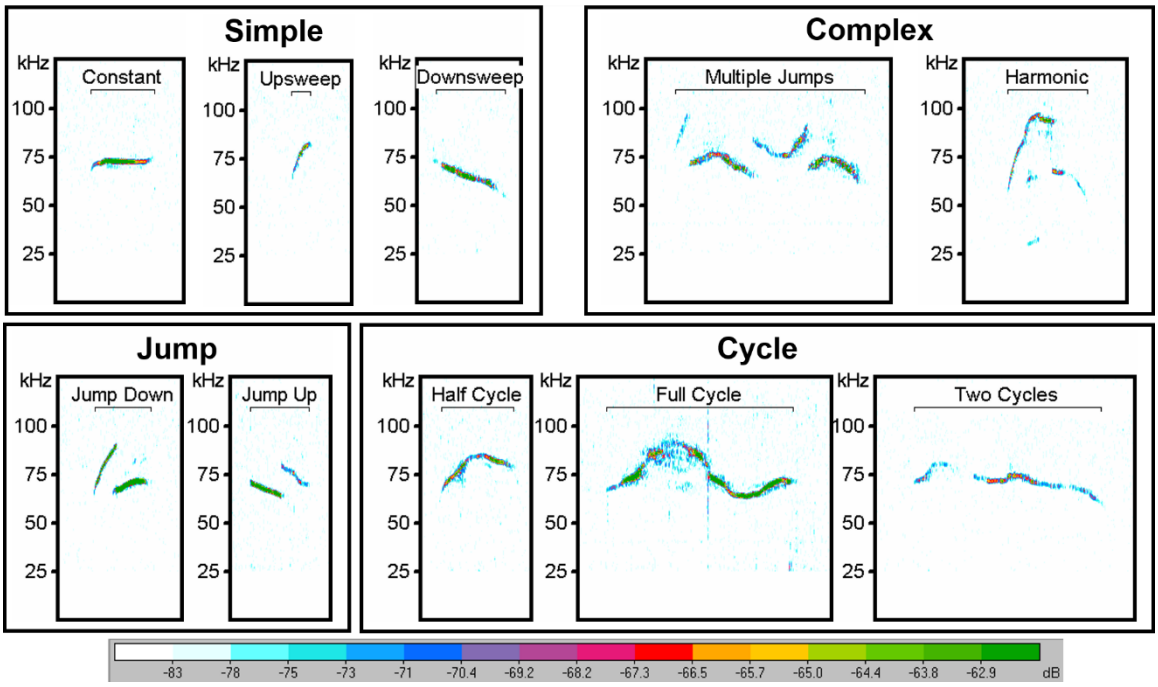

Figure 4.5. Mouse USV Call Classifications. USV call types are classified into 4 call categories: simple, complex, jump, and cycle. Spectrograms are representative of baseline vocalization prior to any surgical manipulation. A high pass filter was used to eliminate noise below 25 kHz. Relative intensity ("vocal loudness") is measured in decibels (dB) and encoded by the color spectrum at the bottom of the image. The y-axis represents frequency of the call in kilohertz (kHz). USV = ultrasonic vocalization.

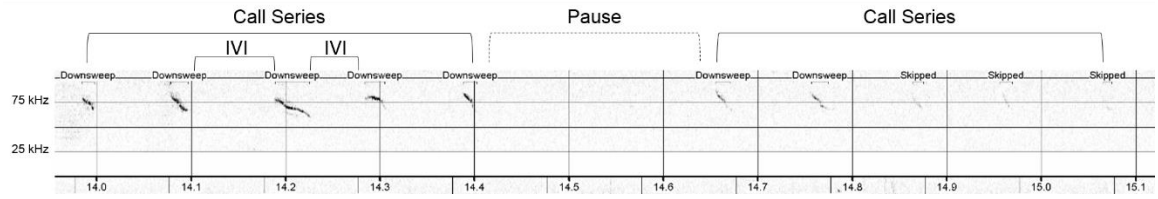

Figure 4.6. Representative image of USV call runs and a pause. USV call series consisted of any group of calls with at least 4 calls spaced no more than 150 ms apart. Time between call series were considered pauses and may or may not have had isolated calls (groups of three or less calls) within the pause. The spectrogram X-axis represents time in seconds; the Y-axis is frequency in kilohertz (kHz). Relative intensity ("vocal loudness") is measured in decibels (dB) and encoded by darkness of the signal; louder is darker. Some calls were not automatically detected by the software. These calls were labeled as "skipped" but were included in call series if they were visually and audibly confirmed by the reviewer. IVI = Intervocalization Interval. USV = ultrasonic vocalizations.

4.3.8 Whole Body Plethysmography (WBP)

Mice underwent baseline whole-body plethysmography within 3 weeks prior to surgery and at 1, 5 and 11 WPS to assess respiratory function. Unrestrained and unanesthetized mice were placed in individual plethysmography chambers (Data Sciences International, St. Paul, Minnesota) and exposed to normoxia (21% O_2) for 30 minutes to allow for unchallenged respiratory assessment. Mice were placed in the same chambers from week to week. Following normoxia, mice underwent a five minute hypercapnia (7% CO_2) and hypoxia (10.5% O_2) challenge.[48-50] As human patients complain of dyspnea with phonation or exercise, this hypercapnic/hypoxic challenge was utilized to obtain respiratory metrics in mice with increased respiratory effort to better correlate with human experiences.

A pressure calibration signal, ambient pressures, and chamber pressures were utilized for automated calculation of breath-by-breath respiratory parameters using Buxco FinePointe Software (Data Sciences International, St. Paul, Minnesota) to determine respiratory frequency (breaths/min), tidal volume (ml), inspiratory and expiratory time (seconds), peak inspiratory flow (ml/second), and

minute ventilation (ml/min) for each mouse during normoxia and during the hypercapnic/hypoxic challenge. In addition, the apnea detection function within FinePointe software was used to identify sighs (2x the average amplitude of the respiratory waveform)[51,52] and apneas. An apnea was defined as the absence of at least two inspirations (i.e., a pause in breathing 2x the average frequency).[53-57] The automatically detected sighs and apneas were manually reviewed for each mouse to verify accuracy and were excluded if not identified correctly, for example, if two shallow breaths were detected as an apnea rather than two individual breaths. The software was also used to calculate the percentage of erratic breathing, which is defined by the software as any breathing that was not classified as a normal breath, sigh, apnea, or sniff (Data Sciences International).

4.3.9 Neuronal Brainstem Histology

Mice were euthanized with an intraperitoneal overdose injection of pentobarbital solution following the final laryngoscopy procedure at 13 WPS, and were perfused with saline followed by 4% paraformaldehyde (PFA). Brainstems were collected from each mouse and post-fixed overnight in 4% PFA at 4 °C. They were then placed in 20% sucrose solution for 3 days, followed by 30% sucrose and stored at 4 °C. Samples were replaced with fresh 30% sucrose solution with 1% sodium azide every 4 weeks until sectioning. Brainstems were sectioned at 40 µm on a freezing-sliding microtome (Leica SM 2010R, Wetzlar, Germany). All sections were stored free-floating at -20 °C in tissue antifreeze solution (30%

ethylene glycol, 30% glycerol, and 40% 1xPBS) in well plates with every 6th section/well.

To investigate if neuronal cell death occurred, one to two wells (randomly selected; containing every 6th section of serial 40 µm brainstem sections) from sham (n=6) and RLN transected (n=7) mice underwent fluorescent immunohistochemistry to identify and count neurons in the left and right nucleus ambiguus, the motor nucleus for the RLN.[58] After washing with 1X PBS and placing in a blocking solution with 5% normal donkey serum (NDS) for 1 hour, sections were incubated overnight in primary antibody, rabbit anti-NeuN (1:500, Abcam, ab177487), to stain neuronal cell bodies. The following day, sections were washed with 1X PBS and then incubated in secondary antibody, anti-rabbit Alexa Fluor 488-conjugated antibody (1:1000; Molecular Probes, #A21206), for 2 hours. Sections were washed a final time in 1X PBS and immediately mounted on positively-charged glass slides. Slides were mounted with Prolong Gold Antifade Mountant with DAPI (ThermoFisher Scientific, # P36931) and allowed to air dry for 1 day in the dark. Slides were stored at -20 °C until quantification of staining was performed using an epifluorescence microscope (Model #:DM4000 B LED; Leica Biosystems, Wetzlar, Germany). Two to four sections containing an easily identifiable left and right nucleus ambiguus were randomly selected for each mouse for quantification (**Figure 4.7**). Sections incubated without primary and secondary antibodies served as negative controls. Stereo Investigator software (MBF Bioscience, Williston, VT) was used to count all neurons with a visible nucleolus within the entire nucleus ambiguus of each randomly selected section.

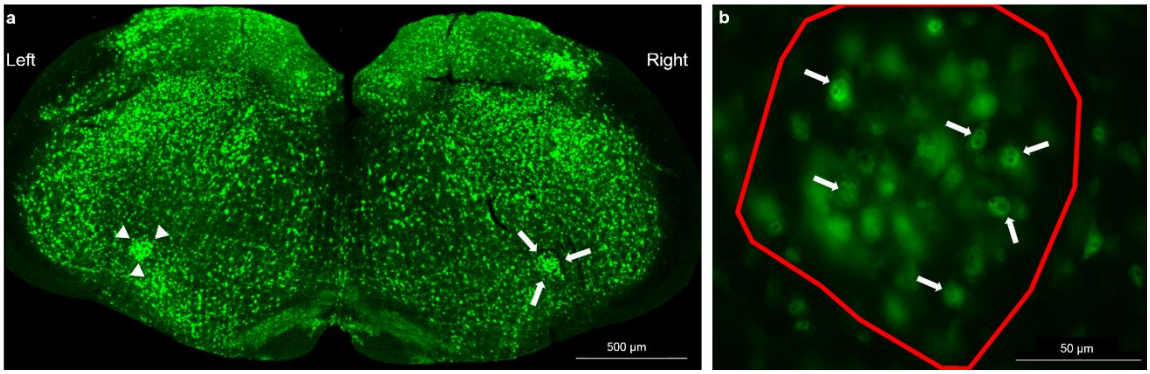

Figure 4.7. Fluorescent immunohistochemistry of the nucleus ambiguus (NA). (a) 40 µm brainstem sections were stained with primary antibody (anti-NeuN; 1:500) followed by an Alexa Fluor 488-conjugated antibody (1:1000). Stereo Investigator software was used to outline the left (arrow heads) and right (arrows) NA with a 2.5x objective that permitted visualization of the entire brainstem section in a single field of view. (b) Neurons with a visible nucleolus (arrows) were counted for each NA (outlined in red) using a 40x objective throughout the entire 40 µm section.

4.3.10 Statistics

For normally distributed data, two-way repeated measures ANOVAs with surgical group (sham vs. transection) and time point as factors were performed using SigmaPlot 14.0 (Systat Software, San Jose, CA). If significant differences were indicated, multiple comparisons were made using a Tukey post hoc test. To take into account for any inherent baseline variability among the mice, a mixed effects model with a random intercept and group as fixed effects term was fitted using SAS 9.4 (SAS Institute, Cary, NC). To assess if the mean difference between the two groups also differed by time, the group*time interaction term was included in each of the fitted models. Post hoc Mann-Whitney U Tests were used to determine significant differences between the two experimental groups at each time point.

Baseline values often differed between groups for ultrasonic vocalization acoustic parameters and call series data, likely due to the inherently high acoustic variability in ultrasonic vocalizations.[59] Thus, we fitted a regression model (Regression Model: Post_Surgery = Bo + B1*Group + B2*BaselineMeasure) using the baseline measurements as a covariate and the post-surgery measures as outcomes using SAS 9.4 (SAS Institute, Cary, NC). In addition, a two-way ANOVA was used to detect significant differences in mean neuron counts between experimental groups and the left and right nucleus ambiguus in each brainstem section. Analysis was performed using SigmaPlot 14.0 (Systat Software, San Jose, CA). *P* values less than or equal to 0.05 were considered significant for all tests.

4.4 Results

4.4.1 Effects of Denervation on Vocal Fold Motion

As hypothesized, RLN transection significantly impaired VF motion compared to sham mice. All transected mice developed immediate right (ipsilateral) VF paralysis, which persisted at 13 WPS. As expected, a two-way repeated measures ANOVA revealed significant differences for the mean motion range ratio and open close cycle ratio (**Figure 4.8a and b**) between groups at both post-surgical time points ($F_{2,38}$ = 181.40, P = < 0.001 and $F_{2,38}$ = 2124.14, P = < 0.001, respectively; Tukey post hoc = P = < 0.001 at both time points), signifying a decreased range and frequency of motion of the injured VF after RLN transection. Upon subjective review of each video, paradoxical movement of the right VF was noted in a subset of videos at both time points. In these cases, the

right VF was moving in the same direction as the left VF, rather than its physiological normal direction (i.e., opposite direction of the left VF). However, the nature of this paradoxical movement was different between the two time points. If this movement was noted during the time immediately post-injury, the left VF appeared to be pulling the right VF, likely due to loss of tension on the injured side. Interestingly, if paradoxical movement was noted at the 13 WPS time point, the left VF seemed to be pushing the right VF, rather than pulling, indicating potential compensation by the left VF.

This paradoxical movement of the right VF contributed to increased range and frequency ratio measures for these mice, making it appear as if the right VF had physiologic movement, despite lack of normal function. Thus, in cases with positively correlated Mcorr values, a “0” was assigned to the mean motion range ratio and the threshold for the open close cycle ratio was manually adjusted within our VFQuantify software to more accurately represent the range and frequency of true physiologic motion of the impaired VF. In addition, we developed two novel outcome metrics to better characterize and document this abnormal movement of the VFs. Our first metric, Mcorr, calculates the correlation of the movement of the left VF compared to the right VF. In normal cases, the VFs are moving in opposite directions and are negatively correlated. In contrast, in instances of visible pushing or pulling motion, the VFs are moving in the same direction and are positively correlated. The sham mice retained a highly negative Mcorr value throughout the study, indicating normal directionality of VF movement. However, the transection mice developed minimally correlative or highly positive correlations at the two post-

surgical time points (**Figure 4.8c**), signifying unilateral paralysis with or without abnormal movement of the injured VF. Mann-Whitney Rank Sum Tests revealed significant differences in Mcorr between the sham and RLN transection groups immediately post-surgery (T_{19} = 55.00, P = < 0.001) and at 13 WPS (T_{19} = 55.00, P = < 0.001). Mice with high positive Mcorr values were then automatically assigned a pushing or pulling activity classification based on the left VF steady state motion, quantified in **Figure 4.8d**.

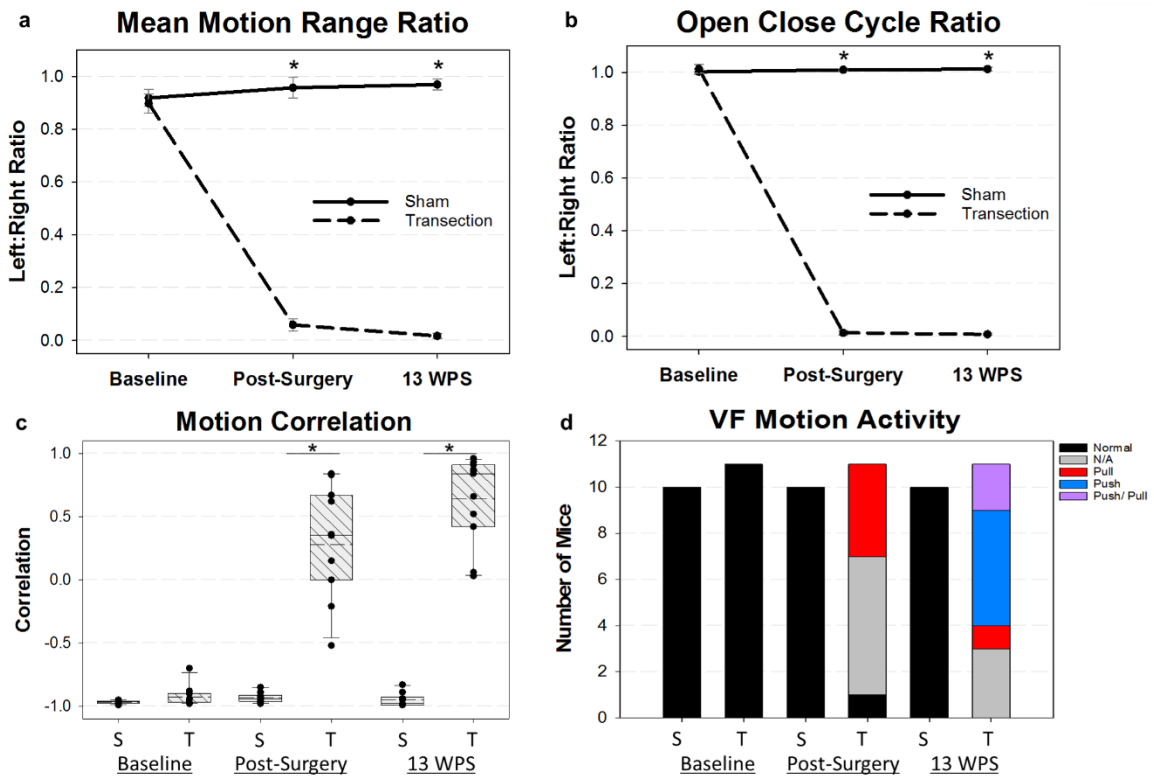

Figure 4.8. Vocal Fold Motion Outcomes. (a) Mean Motion Range Ratio (MMRR) and (b) Open Close Cycle Ratio (OCCR) were significantly impaired in the RLN transected mice immediate post-surgery and at 13 weeks post-surgery (WPS). If mice were detected to have a positive correlation value (paradoxical movement), a 0 was assigned for MMRR. Additionally, the frequency threshold for OCCR was manually adjusted in our VFQuantify software to more accurately represent the true physiologic movement of the injured VF. (c) Vocal fold (VF) activity was assigned using a motion correlation coefficient (Mcorr) value. RLN transection resulted in mice with positive Mcorr values post-surgery and at 13 WPS. Median = solid horizontal line; Mean = dashed horizontal line. (d) VF motion activity was assigned as determined by the Mcorr value in combination with the left VF steady state motion. All mice at baseline had normal VF activity. However, mice undergoing RLN transection displayed abnormal pulling or pushing of the right VF by the left VF at the two post-surgical time points. At 13 WPS, 2 mice in the transection group had evidence of both pushing and pulling motion, and were manually assigned this dual classification. Mice with minimally correlative Mcorr values between -0.5 and 0.5 did not display normal VF motion nor the paradoxical pushing or pulling motion and received an activity classification of “N/A”. An asterisk (*) denotes statistical significance ($p < 0.001$). Error bars = standard error. S = Sham, T = Transection, WPS = Weeks Post Surgery, VF = Vocal Fold

4.4.2 Effects of Denervation on Swallowing

Though we hypothesized that swallow function would be impaired by RLN transection, no significant differences were found between groups for any swallow outcomes ($P > 0.05$). Reviewer discrepancies resolved by group consensus

consisted of less than 15% of all metrics analyzed. Outcomes for each videofluoroscopic swallow study metric are displayed in **Table 4.1**. Interestingly, esophageal transit time was noticeably longer for RLN transected mice, whereas esophageal transit for sham mice was appreciably shorter at 4 days post-surgery (**Figure 4.9**). Although a mixed effects model revealed a Group*Time interaction for esophageal transit time ($F_{3,390}$ = 3.75, P = 0.011), there were no significant differences between groups at 4 days post-surgery (T_{19} = 84.00, P = 0.072) nor the other time points. In addition, laryngeal penetration or aspiration (i.e., contrast entering the airways), which are the most common manifestations of dysphagia in human patients with RLN injury, were not identified in any mice in this study.

Table 4.1. Videofluoroscopic Swallow Study Outcomes

VFSS Metrics units	**Baseline**		**4 DPS**		**6 WPS**		**12 WPS**	
	S	**T**	**S**	**T**	**S**	**T**	**S**	**T**
Lick Rate # per second	7.94 (0.60)	8.09 (0.30)	7.54 (0.57)	7.58 (0.42)	7.98 (0.55)	7.91 (0.50)	7.74 (0.43)	7.62 (0.56)
Swallow Rate # per 2 seconds	4.72 (0.70)	5.02 (0.60)	4.30 (0.76)	4.35 (0.59)	4.49 (0.86)	4.60 (0.61)	4.91 (0.56)	4.62 (0.40)
Inter-Swallow Interval seconds	0.48 (0.09)	0.42 (0.07)	0.53 (0.12)	0.53 (0.08)	0.54 (0.13)	0.49 (0.08)	0.45 (0.06)	0.46 (0.05)
Lick-Swallow Ratio Licks/swallow	3.08 (0.09)	2.75 (0.70)	3.42 (1.21)	3.40 (0.58)	3.76 (1.28)	3.22 (0.73)	2.80 (0.39)	2.80 (0.51)
Pharyngeal Transit Time seconds	0.10 (0.00)	0.10 (0.01)	0.11 (0.01)	0.11 (0.01)	0.11 (0.01)	0.11 (0.01)	0.11 (0.01)	0.11 (0.01)
Esophageal Transit Time seconds	0.90 (0.31)	0.75 (0.12)	0.71 (0.11)	0.86 (0.23)	0.85 (0.17)	0.81 (0.13)	0.89 (0.27)	0.83 (0.19)
Esophageal Swallow Inhibition percentage	36.0 (27.0)	22.0 (23.0)	8.0 (14.0)	15.0 (18.0)	32.0 (25.0)	27.0 (21.0)	32.0 (30.0)	25.0 (27.0)

Note: VFSS = Videofluoroscopic Swallow Study; S = Sham; T = Transection; DPS = Days Post-Surgery; WPS = Weeks Post-Surgery; VFSS metric values represent the mean (standard deviation).

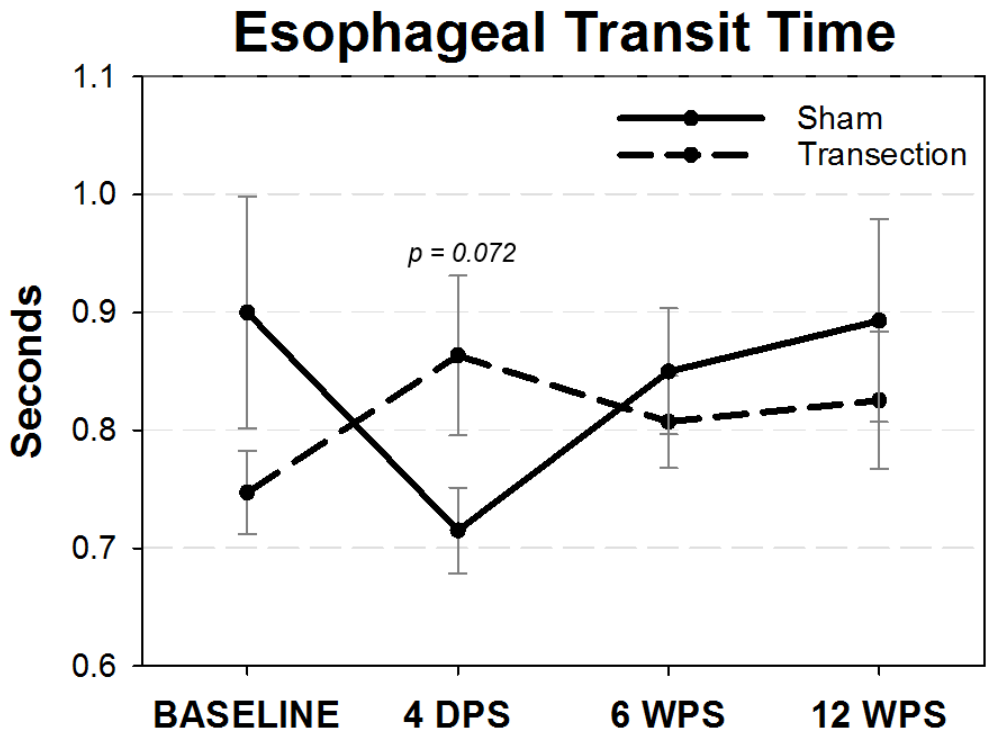

Figure 4.9. Esophageal Transit Time (ETT). Though not statistically significant, mice in the RLN transection group had a trend for increased durations of ETT following surgery that appeared to recover by 6 WPS. On the other hand, sham mice had shortened ETT durations that also returned to baseline values by 6 WPS. WPS = Weeks Post-Surgery, Error bars = standard error.

4.4.3 Effects of Denervation on Vocalization

The total number of calls as well as the percentage of high frequency modulated calls were automatically detected by Avisoft Software and quantified for each group at all 4 time points (baseline, 1, 2, and 5 WPS). A two-way repeated measures ANOVA revealed no significant differences in the total number of calls between groups ($F_{3,57}$ = 1.038, P = 0.38; **Figure 4.10a**); however, a significant group*time interaction existed for the percentage of high frequency modulated calls ($F_{3,35}$ = 3.64, P = 0.022), indicating the mean change over time between the two groups was different. Tukey post-hoc analysis revealed a significant decrease in high frequency modulated calls in the transection group at 1 WPS (P = 0.031;

Figure 4.10b), which corresponded with an increase in the percentage of low frequency modulated calls in this group.

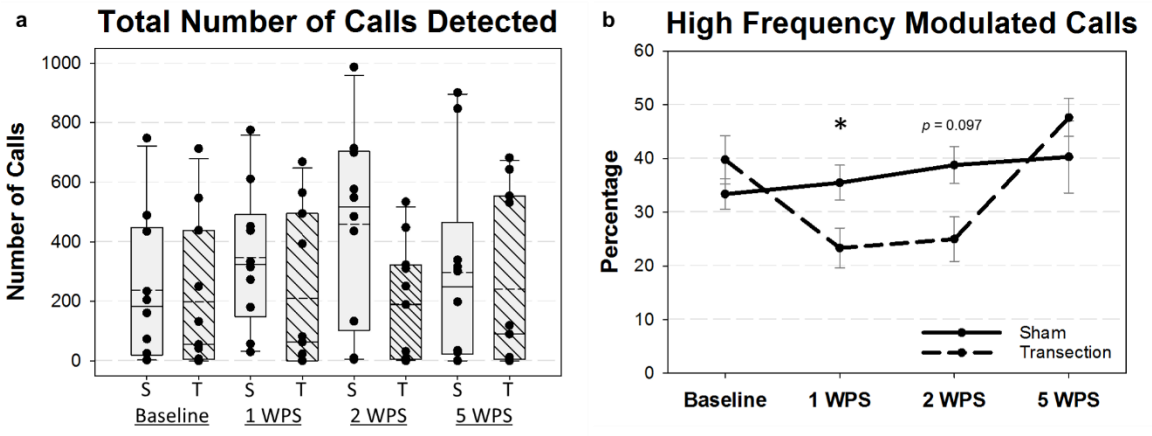

Figure 4.10. Ultrasonic Vocalization (USV) Outcomes for all four time points. a) The total number of USV calls varied widely per group at each time point and were not significantly different between groups. Solid horizontal line = median; dashed horizontal line = mean; S = Sham, T = Transection. b) The percentage of high frequency modulated calls was significantly decreased in the RLN Transection group at 1 WPS, but recovered by 5 WPS. Only mice with greater than 20 calls were included in the analysis of high frequency modulated calls. WPS = Weeks Post-Surgery; S = Sham, T = Transection, Asterisk (*) = p = 0.031.

When comparing the percentage of high frequency modulated calls across all time points, 1 WPS showed significant differences between groups. Therefore, this time point, in addition to baseline, was chosen for additional in depth acoustic analysis. The goal of this analysis was to identify potential outcome metrics that could be used for future studies using this model. As such, all calls within 90 seconds after the 1st detected call were manually classified by a trained reviewer. Baseline measures were taken into account as a covariate to determine statistical significance between the sham and transection groups at 1 WPS for the following acoustic parameters: percentage of call type (%), bandwidth (kHz), duration (ms), peak frequency (kHz), and duration of peak frequency (ms). Results are

summarized in **Table 4.2**. In particular, bandwidth appeared to be the most affected acoustic parameter at 1 WPS, with 3 call types (upsweep, jump down, and half cycle), and 2 subsequent call categories (simple and cycle) significantly affected by RLN transection (**Figure 4.11**). Lastly, we compared a number of outcome metrics related to the repetitive calling nature observed in mice. Though most outcomes were not significantly different between groups, the mean intervocalization interval was significantly longer in the RLN transection group at 1 WPS ($F_{1,12}$ = 7.20, P = 0.02), and denervated mice showed a trend towards an increased number of isolated calls within a pause ($F_{1,12}$ = 3.37, P = 0.091). These results are summarized in **Table 4.3**.

Table 4.2. Ultrasonic Vocalization Acoustic Parameter Outcomes

Percentage of Calls (%)										
Call Type	**Sham (n=10)**				**Transection (n=9)**				**F Value**	**P Value**
	Baseline		**1 WPS**		**Baseline**		**1 WPS**			
	$\bar{x}$	SD	$\bar{x}$	SD	$\bar{x}$	SD	$\bar{x}$	SD		
Simple	38.3	9.8	41.3	13.3	27.7	21.8	27.6	20.2	1.16	0.30
Constant	2.4	3.5	5.1	4.3	4.3	3.4	8.2	11.0	0.46	0.51
Downsweep	3.9	8.0	4.3	9.4	0.7	1.0	0.9	1.2	0.00	0.96
Upsweep	32.0	10.4	31.9	16.4	22.7	18.8	18.6	13.7	1.93	0.18
Jump	35.3	13.2	25.8	8.2	16.5	12.8	24.9	17.1	0.22	0.65
Jump Down	20.5	11.2	17.1	11.1	11.7	12.0	19.2	14.4	2.12	0.17
Jump Up	14.8	15.8	8.6	6.8	4.7	5.3	5.7	5.8	0.37	0.55
Cycle	8.3	7.7	11.4	6.7	12.8	9.2	7.8	7.0	1.45	0.25
Half Cycle	6.1	7.4	7.6	3.9	8.3	9.4	5.3	5.5	0.16	0.70
Full Cycle	1.8	2.2	3.2	2.7	4.2	4.2	2.3	2.2	0.42	0.53
Two Cycles	0.4	0.6	0.5	0.6	0.3	0.6	0.3	0.6	0.20	0.66
Complex	18.1	13.2	21.6	7.5	34.0	28.6	12.4	12.8	0.10	0.76
Multiple Jumps	14.1	11.7	14.2	6.5	29.3	28.7	12.0	12.6	3.74	0.077
Harmonic	3.9	3.4	7.3	4.7	4.6	7.4	0.4	0.7	17.79	**0.0007***

Bandwidth (kHz)										
Call Type	**Sham (n=10)**				**Transection (n=9)**				**F Value**	**P Value**
	Baseline		**1 WPS**		**Baseline**		**1 WPS**			
	$\bar{x}$	SD	$\bar{x}$	SD	$\bar{x}$	SD	$\bar{x}$	SD		
Simple	17.9	3.7	16.3	4.2	17.9	5.6	10.9	3.2	10.94	**0.0048***
Constant	6.9	3.8	5.2	1.2	6.2	1.8	4.2	0.9	3.90	0.08
Downsweep	18.1	10.5	13.9	8.3	11.5	5.5	10.3	3.1	1.46	0.28
Upsweep	18.0	3.9	17.7	4.2	20.0	5.2	13.0	2.8	11.48	**0.0041***
Jump	25.1	8.0	27.9	5.3	27.7	3.8	24.8	3.7	0.45	0.51
Jump Down	26.3	2.9	28.2	4.7	26.7	3.2	22.1	3.7	6.40	**0.026***
Jump Up	25.0	13.5	28.2	8.2	29.0	5.8	29.9	8.7	0.62	0.45
Cycle	23.4	8.1	21.2	5.9	19.6	7.1	14.0	4.8	4.94	**0.046***
Half Cycle	20.7	5.5	21.7	6.0	19.0	6.1	12.7	5.4	6.41	**0.030***
Full Cycle	23.9	8.3	19.7	7.5	18.6	7.3	14.1	3.8	3.39	0.10
Two Cycles	26.6	12.6	22.7	6.9	19.0	7.6	19.5	3.4	n/a	n/a
Complex	45.0	3.0	44.0	4.9	44.8	5.9	36.7	7.0	2.47	0.14
Multiple Jumps	42.8	5.2	43.7	4.1	44.0	6.7	36.8	6.9	2.83	0.12
Harmonic	47.6	6.8	42.5	13.3	45.6	7.5	39.8	13.8	0.07	0.80

Duration of Call (ms)										
Call Type	**Sham (n=10)**				**Transection (n=9)**				**F Value**	**P Value**
	Baseline		**1 WPS**		**Baseline**		**1 WPS**			
	$\bar{x}$	SD	$\bar{x}$	SD	$\bar{x}$	SD	$\bar{x}$	SD		
Simple	19.0	5.2	18.2	3.4	17.7	3.3	16.0	2.6	2.02	0.18
Constant	17.0	8.3	17.0	4.2	19.3	9.6	18.0	3.9	0.02	0.89
Downsweep	32.7	28.3	19.5	11.2	15.2	5.6	20.9	9.4	0.32	0.60
Upsweep	18.3	3.2	18.2	3.1	17.3	1.8	14.5	3.2	7.33	**0.016***
Jump	26.5	11.1	29.0	7.1	34.5	10.1	27.7	8.0	0.16	0.70
Jump Down	27.5	4.7	28.2	7.8	35.0	7.3	27.0	7.7	0.08	0.79
Jump Up	20.5	8.5	29.4	7.4	30.3	14.3	27.0	7.7	0.33	0.58
Cycle	45.9	13.1	35.7	9.9	31.0	9.1	41.9	15.8	0.73	0.41
Half Cycle	38.5	10.0	29.9	7.5	27.8	7.5	35.1	15.6	0.75	0.41
Full Cycle	57.2	21.5	46.9	14.5	38.2	13.4	54.5	12.0	0.00	0.97
Two Cycles	70.4	35.8	72.3	31.9	60.8	45.9	127.3	25.7	n/a	n/a
Complex	47.5	9.3	50.5	15.6	50.3	15.8	59.7	14.7	1.15	0.31
Multiple Jumps	44.1	11.0	48.0	11.8	45.2	9.9	59.5	14.6	1.88	0.20
Harmonic	54.6	14.8	54.7	22.9	72.8	36.4	45.0	15.1	1.93	0.21

Peak Frequency of Call (kHz)										
Call Type	**Sham (n=10)**				**Transection (n=9)**				**F Value**	**P Value**
	Baseline		**1 WPS**		**Baseline**		**1 WPS**			
	$\bar{x}$	SD	$\bar{x}$	SD	$\bar{x}$	SD	$\bar{x}$	SD		
Simple	84.9	5.3	84.1	4.9	83.7	13.1	81.5	4.7	1.28	0.28
Constant	78.0	8.3	75.0	5.4	80.1	3.8	77.9	6.3	0.47	0.51
Downsweep	83.0	9.4	83.2	11.9	89.5	6.4	89.6	10.5	0.89	0.39
Upsweep	85.0	5.5	85.3	5.0	85.1	14.6	83.1	5.3	0.60	0.45
Jump	93.5	8.0	93.4	3.7	94.2	2.0	91.1	3.3	1.14	0.30
Jump Down	95.0	5.1	94.1	5.9	94.7	4.2	88.5	5.1	4.95	**0.046***
Jump Up	93.0	11.0	93.7	7.6	95.9	7.4	94.5	8.4	0.40	0.54
Cycle	90.4	9.5	89.2	4.6	89.1	10.6	83.5	6.2	3.83	0.074
Half Cycle	88.7	6.4	91.0	6.1	91.2	15.1	83.0	8.2	3.72	0.08
Full Cycle	89.2	11.6	85.0	55.5	87.1	8.4	84.8	10.7	0.02	0.90
Two Cycles	89.3	9.4	82.7	7.8	87.2	9.6	84.7	4.2	n/a	n/a
Complex	107.3	3.1	106.7	2.2	105.8	7.5	99.9	7.4	3.82	0.074
Multiple Jumps	106.5	3.9	107.4	4.2	106.1	7.8	100.1	7.1	3.74	0.077
Harmonic	106.4	5.6	101.5	13.6	104.2	8.8	98.8	20.8	0.02	0.90
Duration of Peak Frequency (ms)										
Call Type	**Sham (n=10)**				**Transection (n=9)**				**F Value**	**P Value**
	Baseline		**1 WPS**		**Baseline**		**1 WPS**			
	$\bar{x}$	SD	$\bar{x}$	SD	$\bar{x}$	SD	$\bar{x}$	SD		
Simple	14.6	4.0	14.4	4.6	14.4	2.4	11.3	2.0	10.11	**0.0062***
Constant	12.5	7.5	10.8	4.6	13.4	6.9	9.2	2.1	1.35	0.28
Downsweep	3.6	2.8	2.8	1.7	1.9	1.3	4.5	2.2	1.44	0.28
Upsweep	16.0	3.2	16.3	3.2	15.2	1.6	12.0	2.7	10.81	**0.005***
Jump	13.9	2.5	14.5	4.4	17.8	11.0	11.6	3.0	1.72	0.21
Jump Down	11.8	4.1	11.3	4.7	12.7	2.7	8.7	3.1	0.80	0.39
Jump Up	16.5	5.4	20.5	5.4	21.5	11.1	18.5	4.1	0.10	0.76
Cycle	23.3	11.0	19.0	5.8	15.5	5.1	17.5	7.1	0.01	0.92
Half Cycle	23.6	10.8	16.8	4.7	14.8	2.8	13.6	5.5	0.33	0.58
Full Cycle	20.9	10.8	25.4	11.9	20.1	7.1	21.1	13.0	0.17	0.69
Two Cycles	18.0	14.5	35.3	30.1	16.2	5.4	46.6	33.8	n/a	n/a
Complex	21.1	5.1	21.4	4.0	21.6	4.1	23.8	8.0	0.71	0.42
Multiple Jumps	19.3	3.9	20.4	4.2	20.7	3.4	23.6	7.7	0.84	0.38
Harmonic	24.0	8.8	22.4	8.8	26.2	5.3	27.9	19.9	0.01	0.91

Note: $\bar{x}$ = mean; SD = standard deviation; WPS = weeks post-surgery; kHz = kilohertz; ms = milliseconds; bold values with an asterisk (*) = statistical significance ($p < 0.05$) between Sham and Transection groups at 1 WPS. Two mice from the transection group were excluded due to lack of calls. Outcomes could not be assessed for two cycle calls due to a very low percentage of mice with these types of calls.

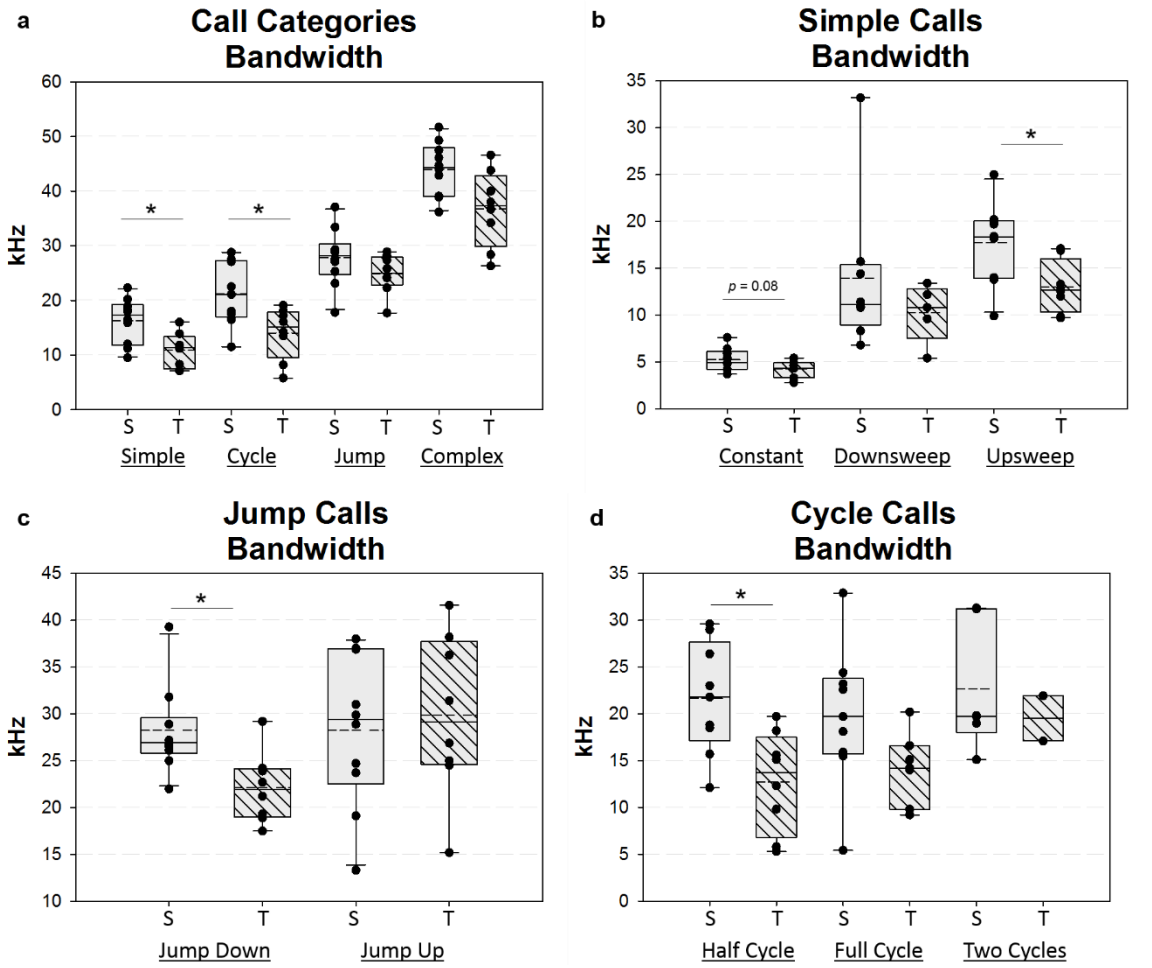

Figure 4.11. Ultrasonic vocalization call bandwidth at 1 WPS. Box and whisker plots showing call bandwidth at 1 WPS for a) call categories, b) simple calls, c) jump calls, and d) cycle calls. Solid horizontal line = median, dashed horizontal line = mean, WPS = Weeks Post-Surgery; S = Sham, T = Transection, Asterisk (*) indicates significant difference between the two groups = $p < 0.05$

Table 4.3. Ultrasonic Vocalization Call Series Outcomes

USV Outcome Measure	Sham (n=10)				Transection (n=9)				F Value	P Value
	Baseline		1 WPS		Baseline		1 WPS			
	$\overline{x}$	SD	$\overline{x}$	SD	$\overline{x}$	SD	$\overline{x}$	SD		
Number of Total Call Series in 90 s	19.0	12.5	24.3	11.2	19.3	15.1	15.9	11.2	1.16	0.30
Number of Calls in a Series	10.5	4.3	11.4	3.7	9.7	2.3	9.3	2.5	0.84	0.38
Length of Series (s)	0.98	0.44	1.11	0.43	0.93	0.24	0.94	0.34	0.19	0.67
Longest Call Series (s)	3.58	4.71	5.55	4.73	3.14	1.96	3.52	3.20	0.75	0.40
Duration of IVI within a Series (ms)	74.5	8.7	71.1	6.5	71.4	5.3	82.0	10.1	7.20	**0.02***
Pause Length (s)	4.33	4.26	2.83	2.59	3.65	3.06	4.52	3.67	0.43	0.52
Number of Calls in a Pause	2.69	1.69	3.11	1.38	3.32	1.55	6.21	3.73	3.37	0.091

Note: $\overline{x}$ = mean; SD = standard deviation; WPS = weeks post-surgery; IVI = intervocalization interval; s = seconds; ms = milliseconds; bold values with an asterisk (*) = statistical significance ($p < 0.05$) between Sham and Transection groups at 1 WPS. Two mice from the transection group were excluded due to lack of calls.

4.4.4 Effects of Denervation on Respiration

Respiratory parameters under normoxic conditions and hypercapnic/ hypoxic conditions were analyzed separately. In normoxia, there were no significant differences in frequency, tidal volume, inspiratory time, expiratory time, peak inspiratory flow, or minute ventilation between groups at any time point (**Table 4.4**). However, during the hypercapnic/hypoxic challenge, transected mice displayed a significant decrease in tidal volume and minute ventilation at 11 WPS compared to sham mice (Tukey post hoc: $P = 0.029$ and 0.047, respectively; **Figure 4.12a and b**). In addition, RLN transected mice displayed a trend for decreased peak inspiratory flows after injury. While there was not a statistically

significant interaction between group and time point ($F_{3,57}$ = 2.473; P = 0.071) for peak inspiratory flow, a two-tailed t-test performed for each individual time point revealed a statistically significant difference between groups at 11 WPS (T_{19} = 2.67, P = 0.015; **Figure 4.12c**). All other respiratory parameters were not significantly different between groups during the hypercapnic/hypoxic challenge (**Table 4.5**).

Table 4.4. Normoxia Respiratory Outcomes

WBP Metrics units	**Baseline**		**1 WPS**		**5 WPS**		**11 WPS**	
	S	**T**	**S**	**T**	**S**	**T**	**S**	**T**
Frequency breaths/minute	304 (44)	290 (44)	285 (67)	292 (68)	340 (44)	346 (42)	371 (23)	366 (28)
Tidal Volume ml	0.36 (0.07)	0.38 (0.05)	0.34 (0.06)	0.37 (0.03)	0.38 (0.06)	0.40 (0.04)	0.42 (0.06)	0.43 (0.03)
Inspiratory Time seconds	0.06 (0.01)	0.06 (0.01)	0.07 (0.02)	0.07 (0.01)	0.05 (0.01)	0.05 (0.01)	0.05 (0.00)	0.05 (0.01)
Expiratory Time seconds	0.16 (0.03)	0.18 (0.03)	0.18 (0.05)	0.18 (0.05)	0.15 (0.03)	0.15 (0.02)	0.13 (0.01)	0.13 (0.01)
Peak Inspiratory Flow ml/second	9.9 (1.7)	10.1 (1.8)	8.9 (2.6)	9.4 (2.1)	11.7 (2.3)	12.3 (1.9)	13.8 (2.6)	13.7 (1.5)
Minute Ventilation ml/minute	106 (21)	109 (20)	96 (28)	105 (25)	131 (30)	140 (22)	155 (27)	155 (15)

Note: WBP = Whole Body Plethysmography; S = Sham; T = Transection; ml = milliliters; WPS = Weeks Post-Surgery; WBP metric values represent the mean (standard deviation).

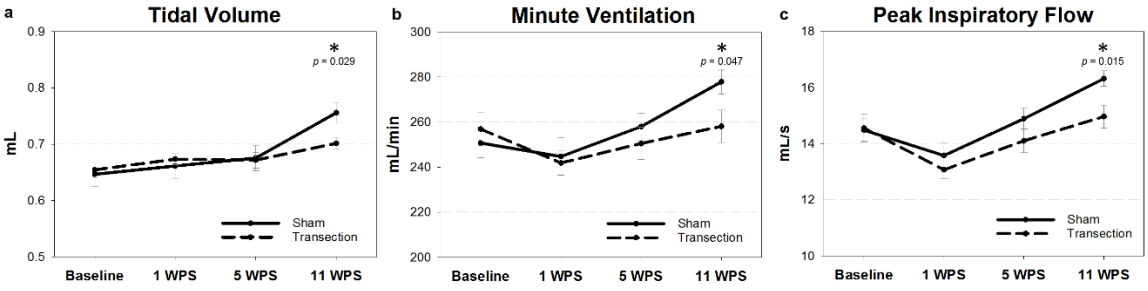

Figure 4.12. Respiratory outcomes during hypercapnic/hypoxic conditions. After normoxic conditions, mice were exposed to a hypercapnic (7% CO2)/hypoxic (10.5% O2) challenge to induce increased respiratory effort. There was a significant difference between groups at 11 WPS for (a) tidal volume, (b) minute ventilation, and (c) peak inspiratory flow. WPS = weeks post-surgery; mL = milliliters; s = seconds; * = significant p value ($p < 0.05$). Error bars = standard error.

Table 4.5. Hypercapnia + Hypoxia Challenge Respiratory Outcomes

WBP Metrics units	Baseline		1 WPS		5 WPS		11 WPS	
	S	**T**	**S**	**T**	**S**	**T**	**S**	**T**
Frequency breaths/minute	393 (38)	397 (39)	373 (33)	362 (33)	387 (33)	376 (39)	370 (22)	369 (24)
Tidal Volume ml	0.65 (0.07)	0.65 (0.04)	0.66 (0.07)	0.67 (0.03)	0.68 (0.07)	0.67 (0.05)	**0.76*** (0.06)	**0.70*** (0.04)
Inspiratory Time seconds	0.07 (0.01)	0.07 (0.01)	0.07 (0.01)	0.08 (0.01)	0.07 (0.01)	0.07 (0.01)	0.07 (0.00)	0.07 (0.01)
Expiratory Time seconds	0.09 (0.01)	0.09 (0.01)	0.09 (0.01)	0.09 (0.01)	0.09 (0.01)	0.09 (0.01)	0.09 (0.01)	0.09 (0.01)
Peak Inspiratory Flow ml/second	14.5 (1.3)	14.6 (1.6)	13.6 (1.4)	13.1 (1.1)	14.9 (1.2)	14.1 (1.4)	**16.3*** (0.09)	**15.0*** (1.4)
Minute Ventilation ml/minute	251 (21)	257 (24)	245 (27)	242 (17)	258 (19)	251 (24)	**278*** (17)	**258*** (24)

Note: WBP = Whole Body Plethysmography; S = Sham; T = Transection; ml = milliliters; WPS = Weeks Post-Surgery; WBP metric values represent the mean (standard deviation). Bold values with an asterisk (*) denotes statistical significance ($p < 0.05$) between groups at the individual time point.

During normoxia, results of the mixed effects model revealed a statistically significant difference in the mean number of apneas between the two groups ($F_{1,57} = 11.64$, $P = 0.0012$). The group by interaction term was significant, indicating the change in the mean number of apneas over time was different between the two groups ($F_{3,57} = 6.88$, $P = 0.0005$). Post hoc Mann-Whitney U Tests showed significant differences between the two groups at all three post-surgical time points ($P < 0.004$ each), but not baseline ($P = 0.769$). Results of the estimated mean number of apneas by group over time is depicted in **Figure 4.13a.** The mixed effects model also detected a statistically significant mean difference between group ($F_{1,57} = 9.30$; $P = 0.0035$) and time point ($F_{3,57} = 20.06$; $P < 0.0001$) for the duration of apneas. There was no group by time interaction noted ($F_{3,57} = 2.29$; $P = 0.0876$), though Mann-Whitney U Tests at each time point revealed a significant decrease in the duration of apneas at 1 and 5 WPS for transected mice ($P = 0.021$

and 0.033, respectively; **Figure 4.13b**). The mean percentage of erratic breathing (**Figure 4.13c**) was also statistically significant between the two groups ($F_{1,57}$ = 19.53, P < 0.001). Mean percentage of erratic breathing was lower in RLN transected mice across the three post-surgical time points (Mann-Whitney U Tests: P = 0.0006, 0.0008, 0.0006, at 1 WPS, 5WPS, and 11 WPS, respectively). In all mice, the number of apneas detected moderately correlated with the percentage of erratic breathing when analyzed using a Pearson Correlation (R = 0.511, P < 0.0001; **Figure 4.13d**). No differences in sighs were detected between groups.

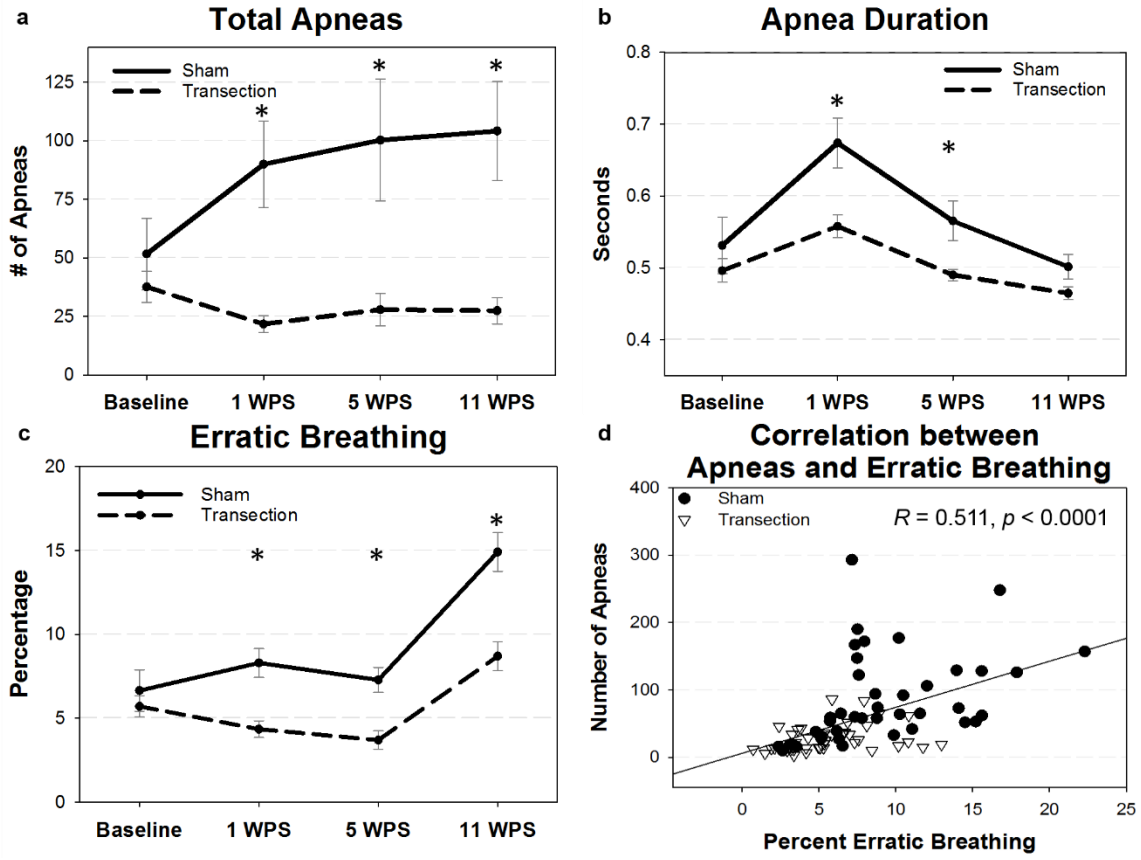

Figure 4.13. Apnea respiratory outcomes. (a and c) RLN transection resulted in significantly less apneas and less erratic breathing in all three post-surgical type points. (b) Apnea duration significantly decreased in transected mice at 1 and 5 WPS as shown. (d) The number of apneas moderately correlated with the percentage of erratic breathing in both groups across all time points. WPS = weeks post-surgery; asterisk (*) denotes statistical significance with p values ≤ 0.05. Error bars = standard error.

4.4.5 Effect of RLN Transection on Motor Neuron Counts in the Nucleus Ambiguus

Each mouse had 2-4 brainstem sections with an easily identifiable left and right nucleus ambiguus for analysis, all within the same brainstem region. On average, sham mice contained 65 (sd = 15) and 70 (sd = 20) neurons in the left and right nucleus ambiguus per section, respectively. RLN denervated mice contained 68 (sd = 14) and 67 (sd = 12) neurons in the left and right nucleus ambiguus per section, respectively. A two-way ANOVA did not detect a significant difference between groups or the left and right neuron counts for each section (F_1 = 0.50, P = 0.48).

4.5 Discussion

In this study, we built upon our previous work[60,61] developing a mouse model of laryngeal nerve injury. We used a holistic approach to successfully create a translational model that mirrors many of the sequela associated with RLN injury in human patients, including VF immobility, as well as vocal and respiratory dysfunction. A combination of behavioral testing, including endoscopic[33] and fluoroscopic[36] imaging assays, along with ultrasonic vocalization and whole-body plethysmography assays allowed exploration of a wide range of potential functional complications (i.e., unilateral VF paralysis, dysphagia, dysphonia, and dyspnea) associated with RLN injury within the same animal. Furthermore, we continued to refine objective quantification of dynamic VF motion, including characterization of compensatory mechanisms of the uninjured VF. This study further validates our automated VF tracking software,[33] and provides novel metrics to elucidate the

mechanics of altered VF motion following RLN damage and subsequent recovery patterns.

As expected, mice experienced immediate unilateral VF paralysis after RLN transection, demonstrated by a decrease in range and frequency of right VF motion. In addition, a subset of denervated mice displayed paradoxical VF motion immediately after injury and at 13 WPS; however, the abnormal movement differed between time points. In both cases, physiological functional movement of the right VF was absent. Consequently, right VF motion appeared passive, such that the intact left VF "pulled" the right VF in an aberrant direction during *abduction* immediately post-transection. In contrast, at 13 WPS, over-*adduction* of the left VF resulted in contact with the right VF, thus displaying a pushing motion. Paradoxical VF movement has been reported in previous animal studies where RLN reinnervation was induced by repairing the transected nerve.[12,62] It is presumable that the thyroarytenoid (adductor) muscle received aberrant reinnervation from former abductor axons, causing abnormal contraction of the intrinsic laryngeal muscles (i.e., synkinesis). Therefore, the paradoxical movement in these studies was likely due to active, but inappropriate muscle contraction, rather than the passive motion generated by the unaffected VF as observed in our current study. In addition, over-adduction of the unaffected VF has been noted in humans with unilateral VF paralysis,[63,64] though its role in functional compensation in patients with unilateral VF paralysis needs further investigation.

In addition to dynamic VF analysis, we continued to investigate dysphagia in this model. Unlike the infant pig model, RLN transection in adult B6 mice had

minimal impact on swallowing behavior, as noted in our previous work.[60,61] This finding is likely due to the anatomical differences between the mouse and human larynx. Yet, while murine laryngeal anatomy limits the assessment of aspiration,[36,37] other outcome metrics, especially those related to esophageal dysphagia, may be affected by RLN injury in this model. As the RLN also provides innervation to the esophagus in addition to the intrinsic laryngeal muscles, the trend for increased esophageal transit time following RLN transection observed in this study is consistent with pharyngoesophageal dysfunction documented in other RLN injury models[15,65,66] and human unilateral VF paralysis patients.[67,68] As such, future studies may benefit by utilizing a higher speed camera or alternative methods, such as manometry, to accurately determine if significant pharyngeal or esophageal dysphagia exists in this small, fast-drinking species.

Next, the effect of RLN injury on murine vocal function was assessed with ultrasonic vocalization analysis. Previous laryngeal nerve transection studies have shown that unilateral RLN injury disrupts ultrasonic vocalizations in rodents.[23,38,69] However, these studies were limited in the acoustic parameters collected and lacked extensive analysis that is more easily performed with current technology. Our study offers the first robust analysis of vocalization acoustics following RLN injury in mice. Surprisingly, the number of calls generated did not differ between groups at any time point. However, high frequency modulated calls were significantly impaired by RLN injury at 1 WPS. Similarly, RLN transection impaired the frequency bandwidth of many call types at 1 WPS. These findings suggest that mice with unilateral VF paralysis lose the ability to modulate the frequency in their

calls, similar to human patients who experience impairment in their phonation frequency (i.e., pitch range) following injury.[70-72] Unilateral VF paralysis patients also demonstrate impaired maximum phonation times,[71] which was observed in the current study as decreased call durations and durations of peak frequency in a collection of call types in RLN transected mice. In addition to acoustic parameters, we examined murine ultrasonic vocalization call series, as patients with unilateral VF paralysis often suffer from vocal fatigue.[73] Indeed, RLN transection resulted in an increased intervocalization interval, requiring more time from the end of one vocalization to the next. An increased intervocalization interval may indicate VF fatigue, requiring more time to rest the VFs in between calls. Moreover, the trend for an increased number of isolated calls within a pause after RLN transection may act as another indicator of fatigue. Thus, we have identified several translational outcome measures to further investigate vocal impairment and recovery in this model.

Interestingly, the percentage of high frequency modulated calls in RLN transected mice recovered by 5 WPS, despite chronic ipsilateral VF paralysis at 13 WPS. The recovery pattern is consistent with previous literature demonstrating the effects of rodent RLN denervation on ultrasonic vocalizations are short-term.[38,69] This recovery of vocalization may be due to a compensatory ability of the intact VF to cross the glottal midline and approximate the paralyzed VF as seen in a subset of mice during our endoscopy analysis. However, this is in contrast to humans, where over-adduction of the intact VF has been shown to result in worse vocal function.[64] Thus, further work is necessary to establish the true

compensatory nature of the intact VF and the exact mechanism of spontaneous vocal recovery in unilateral VF paralysis.

Lastly, this is the first animal study investigating the direct effect of RLN injury on respiratory function. Under normoxic conditions, respiratory parameters did not differ between groups. This was expected, as the majority of patients with unilateral VF paralysis do not develop significant abnormalities in their respiratory capacity.[2] However, many patients do complain of breathing difficulty during increased respiratory effort, such as during conversation and physical activity.[73] As such, denervated mice exposed to a hypercapnic/hypoxic challenge to maximally increase their respiratory effort developed significantly impaired inspiratory flow, tidal volume, and minute ventilation at 11 WPS. Consistent with previous literature, inspiratory flow rate is often the most compromised spirometric parameter in human patients with unilateral VF paralysis.[29] This outcome may be due to an increasingly atrophied VF that weakens over time and becomes flaccid and drawn into the inspiratory airstream, causing the VF to collapse and partially obstruct the airway. The obstruction of inspiratory flow would in turn limit tidal volume and minute ventilation. However, future studies utilizing EMG and/or histological assessments of the laryngeal muscles are necessary to confirm a lack of muscle tone and flaccid paralysis to support this hypothesis.

Furthermore, patients with unilateral VF paralysis report the inability to hold their breath and have an impaired ability to perform a valsalva maneuver,[73] congruent with dysfunctional laryngeal closure. Thus, for this study, B6 mice were chosen as they have a propensity for dysrhythmic breathing contributing to

spontaneous apneas (i.e., pauses in breathing) during wakefulness.[55,56] As apneas in this strain of mice have been associated with active laryngeal closure,[56] we hypothesized that ipsilateral VF paralysis induced by RLN injury would prevent laryngeal closure and inhibit the ability to generate and sustain apneic episodes. In this study, RLN transection significantly decreased the number and duration of apneas, which correlated with a decrease in erratic breathing. This “stabilized” breathing pattern may suggest a central compensatory mechanism to ensure adequate ventilation with a dysfunctional VF. However, this observation may simply be a mechanical consequence of the inability of the mice to actively close their larynx, leading to less spontaneous apneas and less variation in their breathing patterns. It is interesting to note that some of the mice in our study that were found to have left VF compensation (pushing motion seen with laryngoscopy) also generated the most apneas within the RLN transection group at 11 WPS. Though a small sample size precludes statistical analysis, future studies may investigate if the compensatory contact (i.e., laryngeal closure) from the left VF contributes to increased apneas. The correlation between VF compensation and apnea production may be a useful outcome metric to determine whether a stabilized breathing pattern following RLN injury is due to central neurologic processes versus an anatomical laryngeal closure mechanism.

In addition to our behavioral analysis, we performed immunohistochemistry of the nucleus ambiguus to investigate neuronal cell counts at 13 WPS. Peripheral nerve injury often results in various percentages of retrograde cell death due to disruption in axon continuity.[32] As the nucleus ambiguus is the motor nucleus

containing cell bodies for the RLN, cell death may have occurred in the right nucleus ambiguus of the transection group. However, cell counts did not significantly differ between left and right sides nor between treatment groups, likely because post-lesion cell death depends on numerous variables, such as age, severity of injury, and proximity of the injury to the soma.[32] Though we utilized the severest injury type (i.e., transection), our adult mice with fully developed nervous systems are less susceptible to cell death than those with immature neurons.[74,75] Moreover, a distal injury, such as in our study, is often associated with no or limited cell death.[76] Thus, the lack of cell death in the right nucleus ambiguus in RLN transected mice is congruent with current literature.

In conclusion, we have identified several translational outcome measures in our mouse model of RLN injury, which we aim to utilize to objectively assess injury and subsequent recovery after RLN injury of various injury types and with different therapeutic interventions in future studies. In fact, we have begun work in a more prevalent RLN crush injury model to investigate electrical nerve stimulation as a potential treatment option. In this work,[77] we have had preliminary success utilizing intraoperative vagal nerve stimulation as a clinically relevant treatment, though larger scale studies are necessary to establish optimal stimulation parameters. Furthermore, it is necessary to characterize the effects of intraoperative vagal nerve stimulation on all relative outcomes associated with swallowing, voice, and breathing as identified by this study, to understand its true translational potential.

4.6 Acknowledgements

This study was funded in part by National Institutes of Health Grant support (NIH T32-5T32OD011126-39 and NIH K99/R00 HL119606) and by the University of Missouri Coulter Translational Partnership. We graciously acknowledge Ian Deninger and John Szot for their assistance with ultrasonic vocalization analysis, as well as Victoria Caywood for videofluoroscopic swallow study analysis. We would also like to acknowledge Amy Keilholz and Lori Lind for their assistance in brainstem sectioning and training in IHC and neuronal cell counting, respectively. Lastly, we would like to thank Kate Osman for her diligent care and management of the rodent colony for this study.

4.7 References

1. Chandrasekhar SS, Randolph GW, Seidman MD, et al. Clinical practice guideline: improving voice outcomes after thyroid surgery. *Otolaryngol Head Neck Surg.* 2013;148(6 Suppl):S1-37.

2. Brunner E, Friedrich G, Kiesler K, Chibidziura-Priesching J, Gugatschka M. Subjective breathing impairment in unilateral vocal fold paralysis. *Folia phoniatrica et logopaedica : official organ of the International Association of Logopedics and Phoniatrics (IALP).* 2011;63(3):142-146.

3. Choi JS, Oh SH, An HY, Kim YM, Lee JH, Lim JY. Functional regeneration of recurrent laryngeal nerve injury during thyroid surgery using an asymmetrically porous nerve guide conduit in an animal model. *Thyroid.* 2014;24(1):52-59.

4. Anderson KK, Arnold PM. Oropharyngeal Dysphagia after anterior cervical spine surgery: a review. *Global Spine J.* 2013;3(4):273-286.

5. Ta JH, Liu YF, Krishna P. Medicolegal Aspects of Iatrogenic Dysphonia and Recurrent Laryngeal Nerve Injury. *Otolaryngol Head Neck Surg.* 2016;154(1):80-86.

6. Aynehchi BB, McCoul ED, Sundaram K. Systematic review of laryngeal reinnervation techniques. *Otolaryngol Head Neck Surg.* 2010;143(6):749-759.

7. Wang B, Yuan J, Xu J, Xie J, Wang G, Dong P. Neurotrophin expression and laryngeal muscle pathophysiology following recurrent laryngeal nerve transection. *Mol Med Rep.* 2016;13(2):1234-1242.

8. Neel HB, Harner SG, Benninger MS, et al. Evaluation and Treatment of the Unilateral Paralyzed Vocal Fold. *Otolaryngology -- Head and Neck Surgery.* 1994;111(4):497-508.

9. Araki K, Shiotani A, Watabe K, Saito K, Moro K, Ogawa K. Adenoviral GDNF gene transfer enhances neurofunctional recovery after recurrent laryngeal nerve injury. *Gene Ther.* 2006;13(4):296-303.

10. Broniatowski M, Moore NZ, Grundfest-Broniatowski S, et al. Paced glottic closure for controlling aspiration pneumonia in patients with neurologic deficits of various causes. *The Annals of otology, rhinology, and laryngology.* 2010;119(3):141-149.

11. Hernandez-Morato I, Sharma S, Pitman MJ. Changes in neurotrophic factors of adult rat laryngeal muscles during nerve regeneration. *Neuroscience.* 2016;333:44-53.

12. Nishimoto K, Kumai Y, Yumoto E. Paradoxical movement of rat vocal folds following recurrent laryngeal nerve injury. *Acta oto-laryngologica.* 2014;134(11):1164-1171.

13. Wang B, Yuan J, Chen X, Xu J, Li Y, Dong P. Functional regeneration of the transected recurrent laryngeal nerve using a collagen scaffold loaded with laminin and laminin-binding BDNF and GDNF. *Scientific reports.* 2016;6:32292.

14. Tessema B, Roark RM, Pitman MJ, Weissbrod P, Sharma S, Schaefer SD. Observations of recurrent laryngeal nerve injury and recovery using a rat model. *Laryngoscope.* 2009;119(8):1644-1651.

15. Gould FDH, Lammers AR, Ohlemacher J, et al. The physiologic impact of unilateral recurrent laryngeal nerve (RLN) lesion on infant oropharyngeal and esophageal performance. *Dysphagia.* 2015;30(6):714-722.

16. Gould FDH, Yglesias B, Ohlemacher J, German RZ. Pre-pharyngeal Swallow Effects of Recurrent Laryngeal Nerve Lesion on Bolus Shape and Airway Protection in an Infant Pig Model. *Dysphagia.* 2017;32(3):362-373.

17. Gould FD, Ohlemacher J, Lammers AR, et al. Central nervous system integration of sensorimotor signals in oral and pharyngeal structures: oropharyngeal kinematics response to recurrent laryngeal nerve lesion. *Journal of applied physiology (Bethesda, Md : 1985).* 2016;120(5):495-502.

18. Marawar S, Girardi FP, Sama AA, et al. National trends in anterior cervical fusion procedures. *Spine (Phila Pa 1976).* 2010;35(15):1454-1459.

19. Lahvis GP, Alleva E, Scattoni ML. Translating Mouse Vocalizations: Prosody and Frequency Modulation. *Genes, brain, and behavior.* 2011;10(1):4-16.

20. Portfors CV. Types and functions of ultrasonic vocalizations in laboratory rats and mice. *Journal of the American Association for Laboratory Animal Science.* 2007;46(1):28-34.

21. Blanchard RJ, Agullana R, McGee L, Weiss S, Blanchard DC. Sex differences in the incidence and sonographic characteristics of antipredator ultrasonic cries in the laboratory rat (Rattus norvegicus). *Journal of comparative psychology (Washington, DC : 1983).* 1992;106(3):270-277.

22. White NR, Prasad M, Barfield RJ, Nyby JG. 40- and 70-kHz vocalizations of mice (Mus musculus) during copulation. *Physiol Behav.* 1998;63(4):467-473.

23. Roberts LH. Evidence for the laryngeal source of ultrasonic and audible cries of rodents. *Journal of Zoology.* 1975;175(2):243-257.

24. Brudzynski SM, Pniak A. Social contacts and production of 50-kHz short ultrasonic calls in adult rats. *Journal of comparative psychology (Washington, DC : 1983).* 2002;116(1):73-82.

25. Wohr M, Houx B, Schwarting RK, Spruijt B. Effects of experience and context on 50-kHz vocalizations in rats. *Physiol Behav.* 2008;93(4-5):766-776.

26. Brudzynski SM. Principles of rat communication: quantitative parameters of ultrasonic calls in rats. *Behavior genetics.* 2005;35(1):85-92.

27. Ballester A, Gould F, Bond L, et al. Maturation of the Coordination Between Respiration and Deglutition with and Without Recurrent Laryngeal Nerve Lesion in an Animal Model. *Dysphagia.* 2018.

28. Perie S, Roubeau B, Liesenfelt I, Chaigneau-Debono G, Bruel M, St Guily JL. Role of medialization in the improvement of breath control in unilateral vocal fold paralysis. *The Annals of otology, rhinology, and laryngology.* 2002;111(11):1026-1033.

29. Asik MB, Karasimav O, Birkent H, Merati AL, Gerek M, Yildiz Y. Airway and Respiration Parameters Improve Following Vocal Fold Medialization: A Prospective Study. *The Annals of otology, rhinology, and laryngology.* 2015;124(12):972-977.

30. Saarinen A, Rihkanen H, Lehikoinen-Soderlund S, Sovijarvi AR. Airway flow dynamics and voice acoustics after autologous fascia augmentation of paralyzed vocal fold. *The Annals of otology, rhinology, and laryngology.* 2000;109(6):563-567.

31. Kashima HK. Documentation of upper airway obstruction in unilateral vocal cord paralysis: flow-volume loop studies in 43 subjects. *Laryngoscope.* 1984;94(7):923-937.

32. Navarro X, Vivo M, Valero-Cabre A. Neural plasticity after peripheral nerve injury and regeneration. *Progress in neurobiology.* 2007;82(4):163-201.

33. Haney MM, Hamad A, Leary E, Bunyak F, Lever TE. Automated Quantification of Vocal Fold Motion in a Recurrent Laryngeal Nerve Injury Mouse Model. *Laryngoscope.* 2018.

34. Shock LA, Gallemore BC, Hinkel CJ, et al. Improving the Utility of Laryngeal Adductor Reflex Testing: A Translational Tale of Mice and Men. *Otolaryngol Head Neck Surg.* 2015;153(1):94-101.

35. Kendall MG. *The Advanced Theory of Statistics.* Vol 4th Ed: Macmillan; 1979.

36. Lever TE, Braun SM, Brooks RT, et al. Adapting human videofluoroscopic swallow study methods to detect and characterize dysphagia in murine disease models. *J Vis Exp.* 2015(97).

37. Lever TE, Brooks RT, Thombs LA, et al. Videofluoroscopic Validation of a Translational Murine Model of Presbyphagia. *Dysphagia.* 2015;30(3):328-342.

38. Nunez AA, Pomerantz SM, Bean NJ, Youngstrom TG. Effects of laryngeal denervation on ultrasound production and male sexual behavior in rodents. *Physiol Behav.* 1985;34(6):901-905.

39. Chabout J, Jones-Macopson J, Jarvis ED. Eliciting and Analyzing Male Mouse Ultrasonic Vocalization (USV) Songs. *Jove.* 2017(123):e54137.

40. Hammerschmidt K, Radyushkin K, Ehrenreich H, Fischer J. The structure and usage of female and male mouse ultrasonic vocalizations reveal only minor differences. *PLoS One.* 2012;7(7):e41133.

41. Grant LM, Kelm-Nelson CA, Hilby BL, et al. Evidence for early and progressive ultrasonic vocalization and oromotor deficits in a PINK1 gene knockout rat model of Parkinson's disease. *J Neurosci Res.* 2015;93(11):1713-1727.

42. Grant LM, Richter F, Miller JE, et al. Vocalization deficits in mice over-expressing alpha-synuclein, a model of pre-manifest Parkinson’s disease. *Behavioral neuroscience.* 2014;128(2):110-121.

43. Kelm-Nelson CA, Brauer AFL, Barth KJ, et al. Characterization of early-onset motor deficits in the Pink1-/- mouse model of Parkinson disease. *Brain Res.* 2018;1680:1-12.

44. Basken JN, Connor NP, Ciucci MR. Effect of aging on ultrasonic vocalizations and laryngeal sensorimotor neurons in rats. *Exp Brain Res.* 2012;219(3):351-361.

45. Castellucci GA, Calbick D, McCormick D. The temporal organization of mouse ultrasonic vocalizations. *PLOS ONE.* 2018;13(10):e0199929.

46. Sirotin YB, Costa ME, Laplagne DA. Rodent ultrasonic vocalizations are bound to active sniffing behavior. *Front Behav Neurosci.* 2014;8:399.

47. Castellucci GA, McGinley MJ, McCormick DA. Knockout of Foxp2 disrupts vocal development in mice. *Scientific reports.* 2016;6:23305.

48. Lovett-Barr MR, Satriotomo I, Muir GD, et al. Repetitive intermittent hypoxia induces respiratory and somatic motor recovery after chronic cervical spinal injury. *J Neurosci.* 2012;32(11):3591-3600.

49. Nichols NL, Gowing G, Satriotomo I, et al. Intermittent hypoxia and stem cell implants preserve breathing capacity in a rodent model of amyotrophic lateral sclerosis. *Am J Respir Crit Care Med.* 2013;187(5):535-542.

50. Nichols NL, Punzo AM, Duncan ID, Mitchell GS, Johnson RA. Cervical spinal demyelination with ethidium bromide impairs respiratory (phrenic) activity and forelimb motor behavior in rats. *Neuroscience.* 2013;229:77-87.

51. Yamauchi M, Ocak H, Dostal J, Jacono FJ, Loparo KA, Strohl KP. Post-sigh breathing behavior and spontaneous pauses in the C57BL/6J (B6) mouse. *Respir Physiol Neurobiol.* 2008;162(2):117-125.

52. Real C, Popa D, Seif I, et al. Sleep Apneas are Increased in Mice Lacking Monoamine Oxidase A. *Sleep.* 2007;30(10):1295-1302.

53. Matrot B, Durand E, Dauger S, Vardon G, Gaultier C, Gallego J. Automatic classification of activity and apneas using whole body plethysmography in newborn mice. *Journal of applied physiology (Bethesda, Md : 1985).* 2005;98(1):365-370.

54. Moore MW, Akladious A, Hu Y, Azzam S, Feng P, Strohl KP. Effects of orexin 2 receptor activation on apnea in the C57BL/6J mouse. *Respir Physiol Neurobiol.* 2014;200:118-125.

55. Stettner GM, Zanella S, Hilaire G, Dutschmann M. 8-OH-DPAT suppresses spontaneous central apneas in the C57BL/6J mouse strain. *Respir Physiol Neurobiol.* 2008;161(1):10-15.

56. Stettner GM, Zanella S, Huppke P, Gartner J, Hilaire G, Dutschmann M. Spontaneous central apneas occur in the C57BL/6J mouse strain. *Respir Physiol Neurobiol.* 2008;160(1):21-27.

57. Yamauchi M, Kimura H, Strohl KP. Mouse models of apnea: strain differences in apnea expression and its pharmacologic and genetic modification. *Adv Exp Med Biol.* 2010;669:303-307.

58. Yuan H, Silberstein SD. Vagus Nerve and Vagus Nerve Stimulation, a Comprehensive Review: Part I. *Headache.* 2016;56(1):71-78.

59. Riede T. Subglottal pressure, tracheal airflow, and intrinsic laryngeal muscle activity during rat ultrasound vocalization. *J Neurophysiol.* 2011;106(5):2580-2592.

60. Newberry CI LT, Allen J, Thiessen A, Hopewell B. A surgical mouse model of iatrogenic laryngeal nerve injury. *Dysphagia.* 2016;31:786-845.

61. Allen J TA, Robbins KL, Deninger I, Flynn K, Caywood V, Lever TE. A surgical mouse model of iatrogenic laryngeal nerve injury. *Otolaryngology - Head and Neck Surgery.* 2016;155(1):89-98.

62. Nomura K, Kunibe I, Katada A, et al. Bilateral motion restored to the paralyzed canine larynx with implantable stimulator. *Laryngoscope.* 2010;120(12):2399-2409.

63. Tanaka S, Chijiwa K, Hirano M. *Study on Over-Adduction of Unaffected Vocal Fold in Unilateral Recurrent Laryngeal Nerve Paralysis.* Vol 51993.

64. Yumoto E, Oyamada Y, Nakano K, Nakayama Y, Yamashita Y. Three-dimensional characteristics of the larynx with immobile vocal fold. *Archives of otolaryngology--head & neck surgery.* 2004;130(8):967-974.

65. Tsujimura T, Suzuki T, Yoshihara M, et al. Involvement of hypoglossal and recurrent laryngeal nerves on swallowing pressure. *Journal of applied physiology (Bethesda, Md : 1985).* 2018;124(5):1148-1154.

66. Fukushima S, Shingai T, Takahashi Y, Taguchi Y, Noda T, Yamada Y. Genesis of the decrement of intraluminal pressure in the UES during swallowing in rabbits. *Brain Res.* 2005;1044(1):122-126.

67. Wilson JA, Pryde A, White A, Maher L, Maran AG. Swallowing performance in patients with vocal fold motion impairment. *Dysphagia.* 1995;10(3):149-154.

68. Aneas GCG, Ricz HMA, Mello-Filho FV, Dantas RO. Swallowing Evaluation in Patients With Unilateral Vocal Fold Immobility. *Gastroenterology research.* 2010;3(6):245-252.

69. Thomas DA, Talalas L, Barfield RJ. Effect of devocalization of the male on mating behavior in rats. *Journal of Comparative and Physiological Psychology.* 1981;95(4):630-637.

70. Xue Q, Mittal R, Zheng X, Bielamowicz S. A computational study of the effect of vocal-fold asymmetry on phonation. *The Journal of the Acoustical Society of America.* 2010;128(2):818-827.

71. Sridhara SR, Ashok KG, Raghunathan M, Mann SB. To study voice quality before and after thyroplasty type 1 in patients with symptomatic unilateral vocal cord paralysis. *American journal of otolaryngology.* 2003;24(6):361-365.

72. Junuzovic-Zunic L, Ibrahimagic A, Altumbabic S, Umihanic S, Izic B. *Improving Voice Outcomes After Injury to the Recurrent Laryngeal Nerve.* Vol 152017.

73. Francis DO, McKiever ME, Garrett CG, Jacobson B, Penson DF. Assessment of patient experience with unilateral vocal fold immobility: a preliminary study. *Journal of voice : official journal of the Voice Foundation.* 2014;28(5):636-643.

74. Lowrie MB, Lavalette D, Davies CE. Time Course of Motoneurone Death after Neonatal Sciatic Nerve Crush in the Rat. *Developmental Neuroscience.* 1994;16(5-6):279-284.

75. Snider WD, Elliott JL, Yan Q. Axotomy-induced neuronal death during development. *Journal of Neurobiology.* 1992;23(9):1231-1246.

76. Mattsson P, Hydman J, Svensson M. Recovery of laryngeal function after intraoperative injury to the recurrent laryngeal nerve. *Gland Surg.* 2015;4(1):27-35.

77. Haney MM, Allen J, Deninger I, Ohlhausen D, Ballenger B, Robbins K, Lever T. Dysphagia Research Society Annual Meeting March 2-4, 2017 : The Hilton Portland and Executive Tower, Portland, Oregon. *Dysphagia.* 2017;32(6):799-858.

Chapter Five

EFFECTS OF INTRAOPERATIVE VAGAL NERVE STIMULATION ON THE GASTROINTESTINAL MICROBIOME IN A MOUSE MODEL OF AMYOTROPHIC LATERAL SCLEROSIS

This chapter has been accepted for publication in the

Journal of Comparative Medicine

and has been reprinted with permission.

Megan M Haney[1], Aaron C Ericsson[1], and Teresa E Lever[2]

[1]Metagenomics Center, University of Missouri, Columbia, Missouri

[2]Department of Otolaryngology–Head and Neck Surgery, University of Missouri, Columbia, Missouri

5.1 Abstract

Objectives: The gastrointestinal microbiota (GM) plays a fundamental role in health and disease and contributes to the bidirectional signaling between the gastrointestinal system and brain. The direct line of communication between these organ systems is through the vagus nerve. Therefore, vagal nerve stimulation (VNS), a commonly used technique for multiple disorders, has potential to modulate the enteric microbiota, enabling investigation and possibly treatment of numerous neurologic disorders in which the microbiota has been linked with disease. Here we investigate the effect of VNS in a mouse model of amyotrophic lateral sclerosis (ALS).

Methods: B6SJL-Tg(SOD1*G93A)$^{\mathbf{dl}}$1Gur (SOD1^{dl}) and wildtype mice underwent ventral neck surgery to access the vagus nerve. During surgery, the experimental group received 1 h of VNS, whereas the sham group underwent 1 h of sham treatment. The third (control) group did not undergo any surgical manipulation. Fecal samples were collected before surgery and at 8 d after the initial collection. Microbial DNA was sequenced to determine the GM profiles at both time points.

Results: GM profiles did not differ between genotypes at either the initial or end point. In addition, VNS did not alter GM populations, according to the parameters chosen in this study.

Conclusions: Results indicated that this short intraoperative treatment is safe and has no lasting effects on the GM. Future studies are warranted to determine whether different stimulation parameters or chronic use of VNS affect GM profiles.

5.2 Introduction

The vagus nerve, the tenth and longest cranial nerve in the body, innervates numerous structures including the larynx, pharynx, heart, lungs, and gastrointestinal tract. The vagus nerve is composed of thousands of axons that work to provide a vast majority of the autonomic innervation in the body.[39,70] This nerve plays a large role in interoceptive awareness and is often regarded as the body's 'sixth sense'.[12,61,73] Although the function of the vagus nerve is largely parasympathetic, it also provides somatic innervation, mainly to the muscles responsible for swallowing and upper airway function.[6] The vagus nerve comprises A, B, and C fiber types, all of which are characterized by different conduction velocities and stimulation thresholds.[14,39,55,60] This nerve consists of both afferent (80%) and efferent (20%) fibers that provide sensory and motor information to maintain homeostasis in nearly every organ system in mammals.[12,39,43,54,65,70]

Given the vagus nerve's wide-ranging anatomic targets and neuromodulatory effects, targeted manipulation of this nerve has a broad range of potential experimental and therapeutic applications. In fact, vagal nerve stimulation (VNS) has been used experimentally to establish the contribution of the vagus nerve to numerous behaviors, including immune function, mood, pain, and memory.[70] Furthermore, there is immense interest in using implantable and noninvasive VNS devices to modulate essential functions within the body.[39] VNS has been shown as an effective therapeutic strategy for diverse disorders, and various forms of VNS are currently FDA-approved for treating refractory epilepsy, depression, migraines, cluster headaches, and obesity.[12,30,51,55,60,70-72] In addition,

this technology is currently being explored in a multitude of other disorders, including arthritis, asthma, heart failure, gastroparesis, and inflammatory bowel disease, among many others.[30,54,70] Despite the effectiveness of VNS as a treatment strategy, the richness and complexity of the information transmitted along the vagus nerve raises serious challenges that must be considered before widespread use of VNS.[39] Because the vagus nerve innervates multiple organ systems, it is imperative to examine how using VNS to treat a disorder of one organ system might affect healthy function in another.

Numerous studies have been conducted on the safety of VNS in regard to cardiovascular and respiratory function.[6,8,10,30] However, although studies have examined the effects of VNS on gastrointestinal function,[45,46,50] no published study has investigated how VNS might influence gastrointestinal microbial populations.[12] This dearth is surprising, given that the vagus nerve is the direct link between the CNS and gastrointestinal tract, serving as a complex bidirectional line of communication between these 2 organ systems.[9,12,16,38] This brain–gut axis is essential for maintaining homeostasis and is greatly influenced by the gastrointestinal microbiota in both health and disease states, thus yielding its label as the 'brain–gut–microbiota axis'.[9,15,16,38,67]

As part of this 3-component axis, the gastrointestinal microbiome (GM) consists of more than 10^{13} microorganisms, predominantly bacterial species.[28,33] These commensal enteric bacteria are crucial for preventing invasion of pathogens and for maintaining gastrointestinal morphology, intestinal barrier function, normal digestion, mucosal immune function, and host metabolism.[38] The bacteria in this

population have a substantial capacity for secretory and metabolic activity that influence the signals sent and received by the gastrointestinal tract to and from the brain. Through this complex system, the brain controls motor, antiinflammatory, and secretory functions of the gastrointestinal tract, and the gastrointestinal viscera can return sensory messages to modulate nervous system function.[9,12,13,16,38] Miscommunication between the 2 organ systems can elicit stress responses, influence mood and behavior, and has been linked to chronic diseases throughout the body, including obesity, inflammatory bowel disease, colorectal cancer, among many others.[16,22,38,62,69] Therefore, alteration of the enteric microbiota has tremendous effects on both health and pathologic conditions.[57]

Moreover, the GM, through the vagus nerve, has been suggested as a contributor to the development of neurodevelopmental and neurodegenerative disorders, including Autism Spectrum Disorder, Alzheimer disease, and Parkinson disease.[21,27,53,63] Amyotrophic lateral sclerosis (ALS) is another neurodegenerative disease with potential involvement of the GM. ALS is a fatal disease characterized by progressive loss of motor neurons. Typical clinical signs include limb paralysis, aspiration pneumonia due to swallowing impairment, and asphyxiation.[32] Although the role of the gastrointestinal tract in ALS is largely unexplored, patients with ALS have exhibited delayed gastric emptying and extended colonic transit times,[7,64] signifying abnormal gastrointestinal function. Perhaps most promising, a previous study demonstrated alterations in the GM and gastrointestinal morphology in a mouse model of ALS.[69,75] Because many human patients with ALS have mutations in the superoxide dismutase 1 (*SOD1*) gene, the most common mouse models

used to study ALS carry a mutated human *SOD1* transgene.[40] Recent studies using an SOD1 mouse model demonstrate that GM changes occur in young mice before the onset of disease and show that disease onset can be delayed by restoring the GM.[69,75] These findings indicate that altered microbial populations and gastrointestinal pathology may contribute to the pathogenesis of ALS. Consequently, perhaps VNS could play a role in manipulating the gastrointestinal microbes that contribute to ALS and other neurologic diseases.

Whether VNS will have beneficial or detrimental effects on the microbial populations in the gastrointestinal tract is unclear currently. It is concerning that patients undergoing VNS for treatment of disease conditions may experience changes in their GM profiles, potentially contributing to other chronic diseases or negatively modulating the treatment effect. Alternatively, VNS might produce a favorable effect, positively influencing the treatment efficacy and proving useful as an entirely separate therapeutic strategy for disorders with a known gastrointestinal dysbiosis. Therefore, as the use of VNS becomes more prevalent for a multitude of disorders, it is essential to understand the potential off-target effects of this treatment on GM composition. Therefore, the primary objective of this study was to examine the effects of intraoperative VNS on GM profiles in healthy and neurologically diseased mice.

In this study, we used an SOD1^{dl} mouse model of ALS,[1,5] which has fewer copies of the mutated transgene, corresponding to a delayed onset of disease compared with the high transgene copy number SOD1 model used in the aforementioned studies.[40,69,75] Primarily, we sought confirmation that commonly

used experimental stimulation parameters for promoting swallowing and upper airway function did not alter the GM profiles of the mouse models used in our studies. Our secondary objective was to classify the GM composition of mice from our transgenic SOD1^{dl} colony compared with age-matched WT controls to explore whether altered GM populations were present prior to disease onset, analogous to recent findings in the similar high-copy-number SOD1 model.[69,75]

5.3 Materials and Methods

5.3.1 Animals

All experimental procedures performed in this study were reviewed and approved by the University of Missouri Animal Care and Use Committee (protocol no. 8980). The University of Missouri is USDA-licensed and AAALAC-accredited. The line of mice used in this study, B6SJL-Tg(SOD1*G93A)^{dl}1Gur (SOD1^{dl}), originally was purchased from Jackson Laboratories (Bar Harbor, ME), but a breeding colony has been maintained at the University of Missouri for 3 to 4 y. Mice undergo tail snips at weaning for genotyping purposes to discriminate transgenic from WT animals and confirm the copy number of the transgene. The animals for this study were moved from the barrier breeding room to a conventional room at least 1 mo (age, approximately 4 mo) prior to data collection and were housed in IVC (Tecniplast, West Chester, PA) with aspen chip bedding. Mice were group-housed by sex whenever possible. Mice had free access to food (Laboratory Rodent Diet 5001, Purina, St Louis, MO) and water. Room temperature was maintained between 20.0 °C and 26.0 °C, relative humidity was between 30% and

70%, and the photoperiod was a 12:12-h light:dark cycle. Standard enrichment (cotton squares) was provided to all cages.

All mice were of the same health status and were housed in the same room during the experiment; surgery was performed in a separate room in the laboratory, outside of the vivarium. At the time of the study, colony sentinels were tested quarterly and were considered free of the following agents: mouse hepatitis virus, minute virus of mice, mouse parvovirus, Sendai virus, Theiler murine encephalomyelitis virus, mouse rotavirus, *Mycoplasma pulmonis, Pasteurella pneumotropica, Salmonella* spp., mouse pneumonia virus, reovirus 3, lymphocytic choriomeningitis virus, Ectromelia, mouse adenovirus types 1 and 2, K virus, and polyoma virus. Fecal PCR analysis was used to detect pinworms in sentinel mice, whereas cage PCR assays (pooled swabs by room) were used to detect fur mites. According to the standard procedures for the room, mice were not tested for *Helicobacter* spp.

5.3.2 Experimental Design

A total of 30 B6SJL-Tg(SOD1*G93A)^{dl}1Gur (SOD1^{dl}) mice and 30 age-matched WT controls were used for this study. Mice (age, 5 mo) were randomly selected from our SOD1^{dl} colony. This time point is approximately 1 mo prior to disease onset, which typically is observed around 6 mo of age in our colony.[17,56] Experimental procedures were performed over the course of 3 mo by using 7 cohorts of mice, depending on the availability of mice at the correct age. Mice were divided into 3 groups, each with 10 SOD1^{dl} and 10 WT mice (equal sexes). The experimental group underwent surgery for 1 h of unilateral VNS. A second group

underwent surgery for 1 h of sham stimulation. The control group did not undergo surgery and remained in the animal housing room throughout the study. As such, control animals were not housed with mice from other groups, but animals from the experimental and sham treatment groups were housed together randomly. Fecal samples were collected from individual mice 1 d prior to surgery (day 0) and 8 d later (that is, 1 wk after surgery). Fecal samples were stored at –80.0 °C until the end of the study, when microbial DNA was extracted and sequenced to characterize the GM at both time points. **Figure 5.1** shows a timeline of experimental procedures.

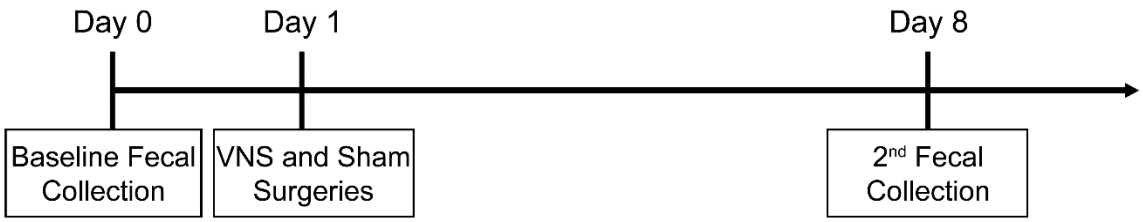

Figure 5.1. Timeline of fecal sample collections. All mice underwent baseline fecal collection at 5 mo of age (day 0). Mice in the experimental and sham groups underwent either vagal nerve stimulation (VNS) or sham stimulation surgeries on day 1. Mice in the control group remained in the vivarium, with no surgical manipulation. Feces were collected again from all mice at 8 d after the initial collection.

5.3.3 Surgical Procedure

Mice in the experimental and sham groups underwent surgery with a ventral neck approach to access the right cervical vagus nerve. Mice were anesthetized by using a ketamine (90 mg/kg SC; Henry Schein, Melville, NY)–xylazine (11.25 mg/kg SC; Akorn, Lake Forest, IL) cocktail. Half doses of ketamine were given subcutaneously as needed to maintain the surgical plane of anesthesia throughout the procedure. We chose injectable anesthesia because our lab has anecdotally

experienced decreased efficacy of electrical stimulation in isoflurane-anesthetized mice. The eyes were lubricated to prevent drying, and the ventral neck was shaved and prepared aseptically for surgery. Mice were positioned in dorsal recumbency on a custom platform beneath a surgical microscope (model M125, Leica Microsystems, Buffalo Grove, IL). Core body temperature was maintained at 37 °C by using a homeothermic heating system (DC Temperature Controller; FHC, Bowdoin, ME), and reflexes were checked every 10 to 15 min. Supplemental oxygen (100%) was delivered through a nose cone at a flow rate of 1 L/min during stimulation or sham treatment.

A midline neck incision was made from the suprasternal notch to the mandible. The salivary glands were gently retracted laterally, and the right vagus nerve was identified in its cervical location. After careful isolation from the carotid artery and jugular vein, the vagus nerve was placed on bipolar electrodes (FHC, Bowdoin, ME). Mice in the experimental group received VNS for 1 h while maintained at surgical depth of anesthesia. For mice in the sham group, the vagus nerve was placed on the electrodes for 1 h while they remained under surgical anesthesia.

For both groups, the vagus nerve was removed from the electrodes after 1 h of stimulation or sham treatment, and the neck incision was closed by using absorbable sutures (6-0 Monocryl, Ethicon, Somerville, NJ) and surgical glue (Tissumend II, Veterinary Products Laboratories, Phoenix, AZ). After suturing was complete, 0.3 mL of warm, sterile saline was administered subcutaneously; sustained-release buprenorphine (1 mg/kg SC; Zoopharm, Windsor, CO) and

flunixin meglumine (2.2 mg/kg SC; Merck, Kenilworth, NJ) were given as separate injections for pain control. Mice were transferred to a clean, heated cage for recovery; mice were monitored at least every 10 to 15 min and were returned to their home cage once fully ambulatory. The home cages were placed half on, half off of a heated water blanket overnight and returned to the vivarium the following morning. All mice were monitored daily after surgery for any signs of pain, distress, or surgical complications. Control mice had no experimental manipulation beyond fecal collection at days 0 and 8.

5.3.4 Vagal Nerve Stimulation

Mice in the experimental group received VNS for 1 h during surgery. The right vagus nerve was placed on the electrodes, with the anode positioned distally (**Figure 5.2**). Once positioned, the nerve was stimulated by using a constant current stimulator connected to a laptop equipped with LabChart software (ADInstruments, Colorado Springs, CO). Stimulation was verified by using a digital oscilloscope (Tektronix, Beaverton, OR) coupled to a current probe (Tektronix, Beaverton, OR) attached to the electrode leads. The nerve was stimulated according to the following parameters: biphasic 0.5-ms square-wave pulses (interstimulus interval, 0.1 ms) delivered at 20 Hz (stimulus intensity, 0.2 mA). We chose these parameters because of their effectiveness in peripheral nerve regeneration after injury[2-4,34-37,68] and are commonly used parameters in our lab for various other projects to promote swallow and upper airway function in neurologic disorders.

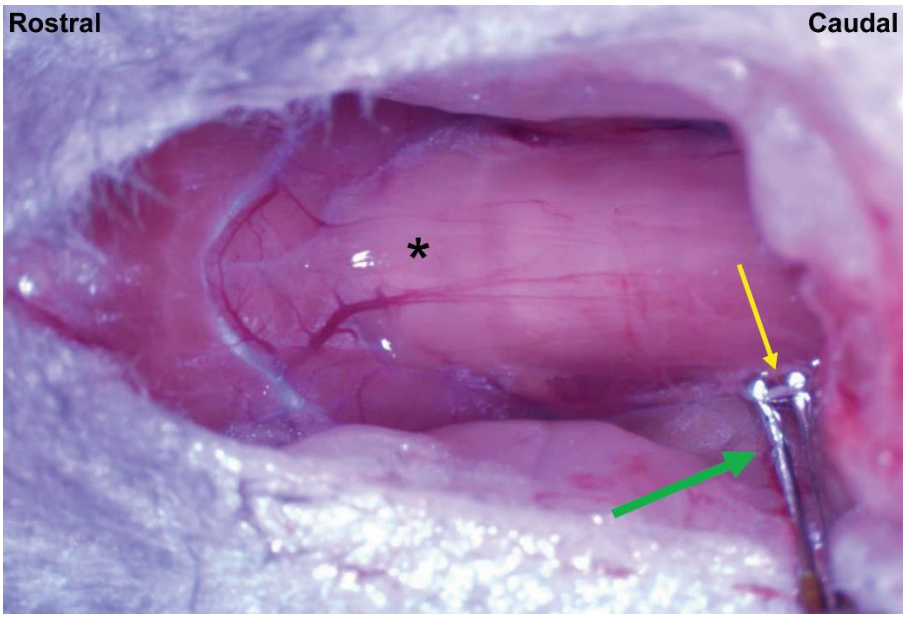

Figure 5.2. Vagal nerve stimulation. The right vagus nerve (yellow arrow) was isolated in its cervical location and placed on bipolar electrodes (green arrow) for electrical stimulation delivered at 20 Hz with a 0.2-mA stimulus intensity. *, larynx.

5.3.5 Fecal Collection

Fecal collection took place early in the morning (0700 to 0800) after the lights were turned on in the housing facility. Mice temporarily were placed individually into empty autoclaved cages and allowed to defecate. Approximately 2 fecal pellets were collected aseptically from each mouse and placed into a sterile 2-mL tube containing a stainless steel bead (diameter, 0.5 cm; Penn Ball Bearing, Delran, NJ).[24] Fecal samples were collected the day prior to surgery (day 0) and 1 wk after surgery (day 8). Fecal samples were stored at –80.0 °C prior to DNA extraction.

5.3.6 DNA Extraction

DNA was extracted from all samples within 3 consecutive days, by using previously described methods.[24,26] Briefly, lysis buffer was placed in all tubes

containing fecal samples. The samples were homogenized, followed by incubation at 70.0 °C for 20 min. After incubation, samples were centrifuged; the entire supernatant was transferred to a fresh tube, supplemented with 200 μL of 10 M ammonium acetate, and allowed to incubate on ice for 5 min. After centrifugation at 5000 × *g* for 5 min at room temperature, the supernatant was removed, mixed with an equivalent volume of isopropanol, and allowed to incubate on ice for 30 min. Precipitated nucleic acids were pelleted by centrifuging at 16,000 × *g* for 15 min at 4 °C, rinsed twice with 70% ethanol, resuspended in 10 mM Tris–1 mM EDTA, and then purified (DNeasy Blood and Tissue kit, Qiagen, Hilden, Germany) according to the manufacturer's instructions. DNA yields were determined through fluorometry (Qubit, Life Technologies, Carlsbad, CA) by using a reagent kit (Quant-iT BR dsDNA Kit, Invitrogen, Carlsbad, CA) according to the manufacturer's instructions.

5.3.7 Preparation of 16S rRNA Library and Sequencing

Extracted fecal DNA was sent to the University of Missouri DNA Core Facility for bacterial 16S rRNA amplification and sequencing according to a previously described protocol.[24,26,42] Briefly, amplification of the V4 hypervariable region of the 16S rDNA gene with previously developed universal primers was used to create bacterial 16S rDNA amplicons. Amplicons were purified and evaluated by using an automated electrophoresis system (Fragment Analyzer, Advanced Analytical, Ankeny, IA). A fluorometer (Qubit, Life Technologies) was

used for quantification purposes, and samples were sequenced by using a desktop sequencer (MiSeq, Illumina, San Diego, CA).

5.3.8 Informatics Analysis

Assembly, filtering, binning, and annotation of DNA sequences was performed at the University of Missouri Informatics Research Core Facility (Columbia, MO). Operational taxonomic units (OTU) were identified and given taxonomic assignments by using BLAST against the SILVA database of 16S rRNA sequences and taxonomy.[24,26,42] Principal coordinate analysis of 1/4 root-transformed sequence data and α-diversity indices were performed at the University of Missouri Metagenomics Center by using open-access Past 3.18 software (https://folk.uio.no/ohammer/past/).

5.3.9 Statistics

Differences in α-diversity and richness between genotypes on day 0 were evaluated by using *t* tests or Mann– Whitney rank–sum tests, depending on the results from Shapiro–Wilk normality tests. Differences in α-diversity and richness between treatment groups and genotypes on day 8 were tested by using 2-way ANOVA. Changes in α-diversity and richness among treatment groups and genotypes between days 0 and 8 were assessed by using 2-way ANOVA. All statistical analyses were performed by using SigmaPlot 12.5 (Systat Software, San Jose, CA). Differences between genotype GM compositions at day 0 were tested by using one-way permutational multivariate ANOVA (PERMANOVA) of ranked

Bray–Curtis and unranked Jaccard distances by using PAST 3.18 software. Two-way PERMANOVA of ranked Bray–Curtis and unranked Jaccard distances were used to assess genotype and treatment effects on the GM profiles on day 8. Uncorrected *P* values less than 0.05 were considered significant.

5.4 Results

5.4.1 Surgical Procedures

Overall the SOD1^{dl} and WT mice tolerated the surgical procedure well. Three mice (2 SOD1^{dl}, 1 WT) in the experimental group received only 42 to 44 min of VNS treatment because they showed increased respiratory effort; in these mice, the treatment was stopped prematurely, and they recovered uneventfully. In addition, 2 WT mice in the experimental group stopped breathing during recovery. Although resuscitation with atipamezole (0.22 mg/kg; SQ) and chest compressions was attempted, the mice did not recover. Consequently, these mice were replaced with 2 additional age-matched WT mice to complete the study. Another 7 mice (4 SOD1^{dl}, 3 WT; 2 VNS, 5 sham) developed bradypnea and mild respiratory distress after surgery. During recovery, these mice were given atipamezole (0.22 mg/kg SC) to reverse anesthesia, which restored respiration and facilitated recovery.

5.4.2 Fecal Collection and DNA Extraction

Fecal samples were collected from all mice in the study at day 0, except for one SOD1^{dl} mouse that did not defecate in a timely manner and therefore was replaced in the study. Fecal samples were obtained from all surviving mice (*n* =

60) on day 8. DNA was extracted from all samples; all but one day 0 sample (WT mouse) and 2 day 8 samples (1 WT and 1 SOD1^{dl}) generated sufficient high-quality reads to be interpreted.

5.4.3 GM Richness, Diversity, and Composition Profiles

Prior to determining the GM composition, the number of OTUs (a measure of the richness of the sample) was quantified, and the relative abundance of those OTUs (that is, the diversity of the sample) was calculated for each fecal sample. Richness and diversity were compared between SOD1^{dl} mice and age-matched WT controls at day 0 (before surgery) to determine whether differences between genotypes exist prior to disease onset in this model.[69] According to Chao1 and Simpson indices, richness and diversity did not differ significantly between transgenic and WT mice at 5 mo of age (**Figure 5.3A**). Similarly, richness and diversity were compared between the 3 treatment groups (VNS treated, sham, and control) and 2 genotypes at day 8, and no significant differences were found (**Figure 5.3B**). Furthermore, changes in richness and diversity between days 0 and 8 were not significantly influenced by genotype or treatment group (**Figure 5.3C**). Therefore, the overall number of OTUs and their relative abundance in each sample was not affected by genotype or treatment.

Next, we sought to determine whether the bacterial composition of the GM was unique to each genotype at day 0 and to each genotype and treatment group at day 8. In all mice, the most abundant bacteria included those in the Bacteroidales S24-7 group and the bacterial families of Rikenellaceae and

Lachnospiraceae. Taking into account all detected OTUs, samples at each time point were compared by using principal coordinate analysis. Unexpectedly, there was no separation between genotypes at day 0 (**Figure 5.4A**) or day 8 (**Figure 5.4B**). Furthermore, there was no separation between treatment groups on day 8. At both time points, samples showed marked overlap, regardless of treatment group or genotype. Statistical analysis through PERMANOVA using Bray–Curtis and Jaccard indices confirmed no significant differences between the independent variables of this study. This finding suggests that GM profiles are not altered in presymptomatic SOD1^{dl} mice compared with age-matched WT controls. In addition, the GM composition remained relatively stable over an 8-d time period, despite surgical procedures and electrical stimulation of the vagus nerve. We also confirmed that administration of antisedan after surgery to reverse anesthesia in 7 mice did not significantly influence the GM composition (data not shown).

Interestingly but unsurprisingly, the GM composition varied depending on which breeding group from the SOD1^{dl} colony produced the experimental animal, given that GM profiles are typically passed to offspring from the dam.[38,41,52] The mice in the current study were born from 5 different breeder pairs within the SOD1^{dl} colony. Breeder groups consisted of one affected SOD1^{dl} male mated with a B6SJLF1/J female. Principal coordinate analysis showed distinct clustering of offspring produced from different breeding groups, regardless of genotype, treatment group, or time point (day 0 or 8; **Figure 5.5**). Results from 2-way PERMANOVA comparing mice from the different breeder groups and each time point of the study showed the GM composition differed significantly (P = 0.0001)

between mice from the different breeding groups but not between time points. In addition, analyses were performed separately for the offspring from each breeder group to determine whether genotype or treatment effects differed significantly between mice from each breeding group; however, no significant results were found. These findings further support that neither genotype nor treatment affected the GM composition of the mice used in this study.

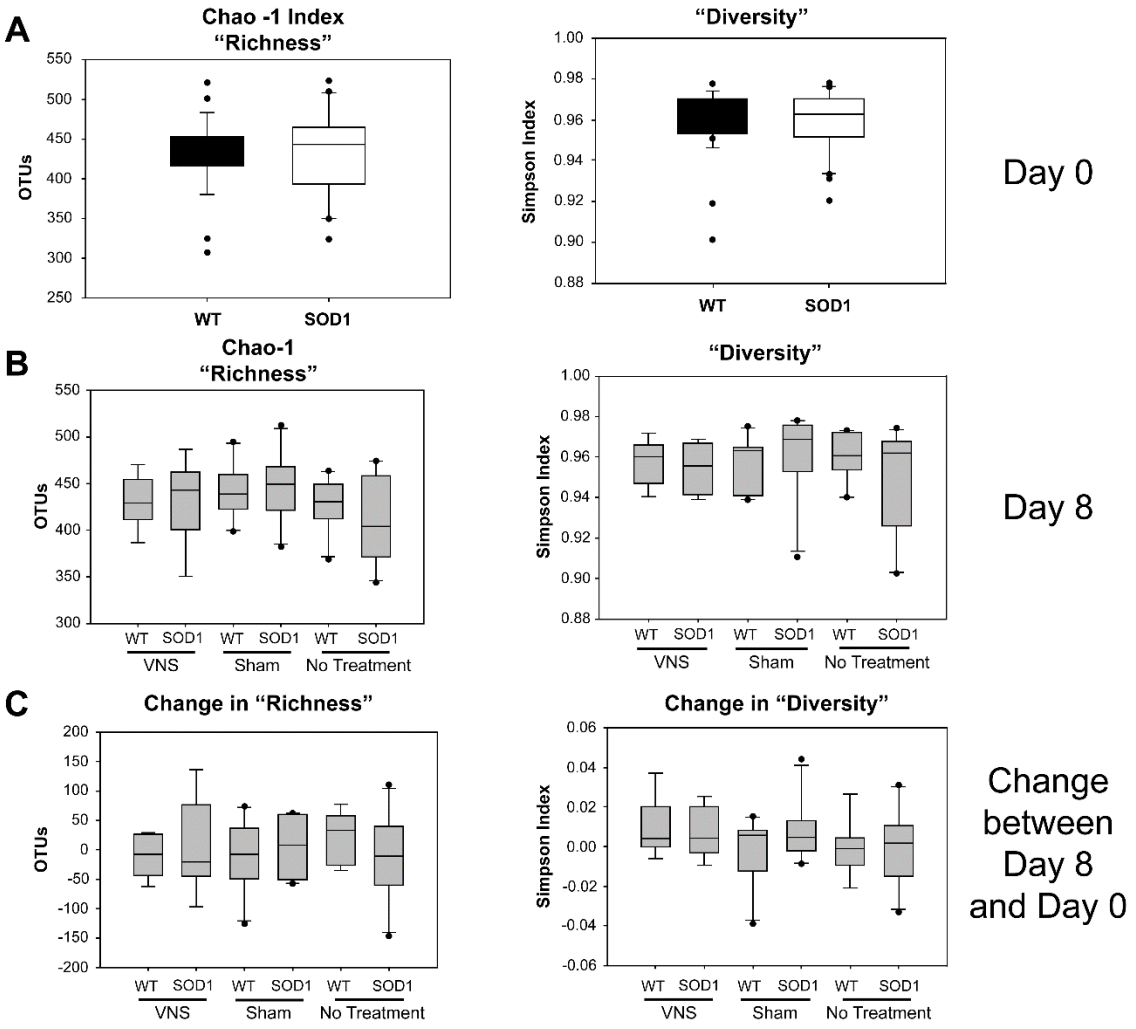

Figure 5.3. Richness and α-diversity of fecal samples. Richness (left panels) was quantified according to the Chao1 index, whereas α-diversity (right panels) was characterized by using the Simpson index. (A) Neither richness nor α-diversity differed significantly between genotypes at day 0. (B) Neither richness nor α-diversity differed significantly between genotypes or treatment groups at day 8. (C) Neither richness nor α-diversity differed between day 0 and day 8 samples across genotypes or treatment groups. OTU, operational taxonomic unit; VNS, vagal nerve stimulation.

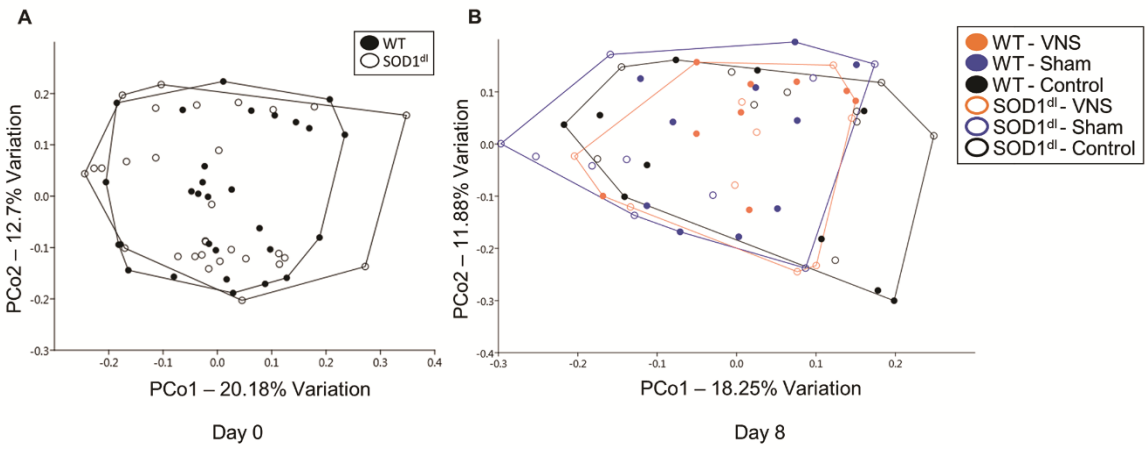

Figure 5.4. Principal coordinate analyses of the samples at (A) day 0 and (B) day 8. Operational taxonomic unit-level data were normalized through 1/4 root transformation. No distinct clustering or separation of samples between genotypes or treatment groups was evident at either time point. VNS, vagal nerve stimulation.

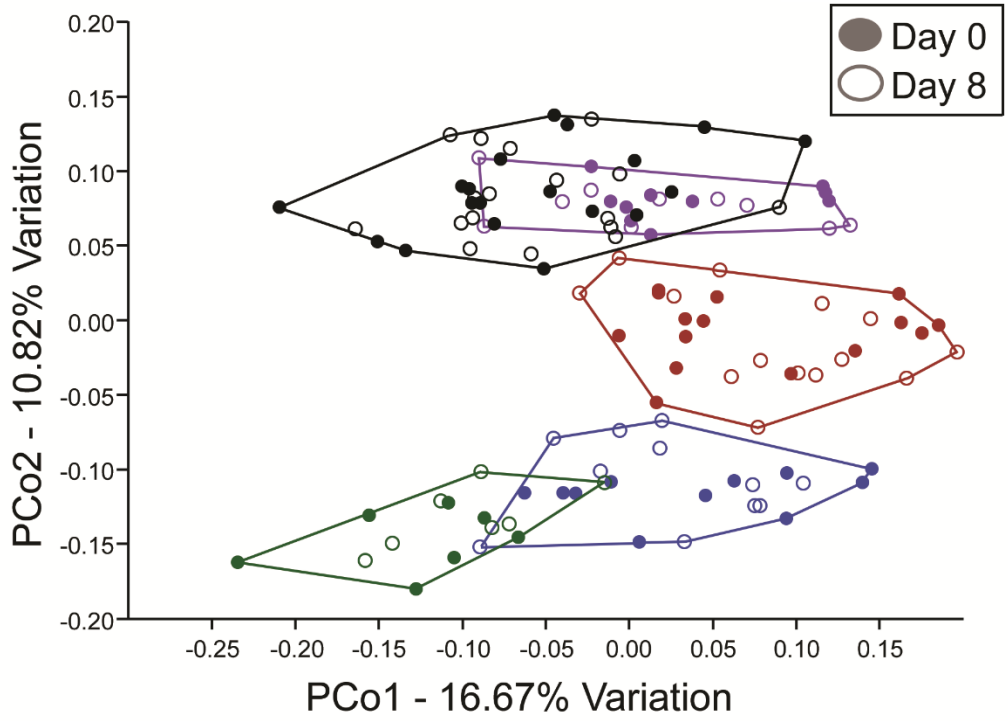

Figure 5.5. Principal coordinate analyses of samples from both time points (days 0 and 8). Different colors represent the offspring from different breeding groups at both time points (n = 7 to 18 per group of offspring); filled symbols represent day 0 data; open symbols indicate day 8 data. GM profiles cluster among offspring born from the same breeder pairs. Samples cluster significantly between breeder groups ($P < 0.0001$, PERMANOVA). No separation according to genotype occurred when each breeder group was analyzed separately (data not shown).

5.5 Discussion

In summary, the results obtained from this study suggest that brief periods of intraoperative VNS, using the described stimulation parameters, do not have long-term effects on the GM composition in mice. In addition, GM profiles were similar between presymptomatic SOD1^{dl} mice and their age-matched WT controls. Although GM profiles differed among offspring from different breeder pairs, the GM was consistent across both time points, regardless of genotype or treatment group. Given that this study is the first to investigate how VNS may modulate the GM, the lack of changes between treated and untreated mice does not automatically warrant dismissal of this experimental and potential therapeutic modality. Several explanations might account for the observed lack of GM modification due to treatment or genotype, and various study limitations must be discussed.

The first caveat of this study was that VNS was applied for a short duration (1 h) during a surgical procedure. Not only may surgery itself be a confounding variable, the short duration of VNS is minimally translatable to human patients, who receive implantable devices for VNS therapy.[39,58,66] In the current study, the surgery variable was controlled by using a sham surgery group and a control group that did not receive either treatment or surgery. The surgical procedure and experimental protocol for this study were chosen to ensure that the VNS procedure does not alter the GM in the experimental mice undergoing the same procedures for different studies in our lab. It is reassuring to know that our experimental paradigm does not have lasting effects on the GM in our mouse models. However, for many human patients, VNS is often delivered through an implantable device

enabling long-term therapy,[39,58,66] which operates when patients are awake and freely living their lives. Chronic application of VNS likely would have a greater effect on GM populations than a brief exposure to VNS during surgery.[12] Therefore, additional studies using implantable VNS devices that can deliver chronic VNS therapy outside of a surgical procedure are warranted.

A second limitation of this study was that only one set of stimulation parameters was used. Again, we selected these stimulation parameters because they are commonly used in our laboratory to promote normal swallowing[49] and upper airway function. We are currently examining laryngeal nerve stimulation in the SOD1^{dl} mouse model and intraoperative VNS stimulation in a mouse model of recurrent laryngeal nerve injury. The parameters used in our studies are based on numerous other published works indicating these parameters are useful in peripheral nerve regeneration.[2-4,34-37,68] Although it is reassuring to confirm that the stimulation parameters used in our studies do not significantly alter the GM in our mouse models, how other stimulation parameters might affect the GM is unknown. Stimulation parameters consist of variables including the frequency, pulse width, waveform, amplitude, and continuity of the pulses delivered to the nerve.[11] Furthermore, electrode design itself adds additional variables, which include the geometry, materials used, impedance, and the location of the electrode on the nerve.[39] Finally, it is essential to consider the characteristics of the target neurons themselves. Given that the vagus nerve is composed of both afferent and efferent neurons, consisting of A, B, and C fiber types,[14,39,55,60] different parameters and electrode designs might target some fiber types over others. Therefore, factors

such as axonal diameter, conduction velocity, and threshold potential[60] of the target axons directly influence the stimulation parameters that should be used for the intended function.[55] Consequently, all variables must be optimized for the effective use of VNS in its proposed function, whether that is inhibiting seizures, promoting vocal function, or manipulating the GM.

Identifying the optimal VNS parameters for a given function is challenging. Even when VNS is applied in an approved manner, such as for refractory epilepsy, the optimal VNS parameters for each individual patient are unknown.[39,55,71] The stimulation parameters used in the current study were designed to target degenerating motor neurons by sending signals to the cell bodies in the brainstem to trigger upregulation of neurotrophic factors and regeneration-associated genes to promote nerve regeneration.[2,4,31,36,59] Therefore, it remains likely that the GM could be modulated by using different stimulus parameters and electrode orientations that specifically target the gastrointestinal tract. For instance, in a swine model of obesity, bilateral thoracic VNS was delivered as bipolar pulse trains consisting of 30-Hz, 500-μs pulses for 30 s every 5 min at a maximum intensity of 2 mA for 14 wk.[66] In this swine model, there was a delay between the onset of simulation and the appearance of beneficial effects (that is, decreased weight gain, food consumption, and sweet cravings). Although VNS causes changes in the brain regions involved in the regulation of food intake, the underlying mechanisms of action for the observed beneficial effects of VNS in obesity are largely unknown.[39,66] Given that the GM has been implicated in contributing to obesity,[53] perhaps part of the equation of VNS efficacy in this obesity model is its GM

modulation potential. In other words, VNS may be modulating the GM in experimental models where the gastrointestinal tract is targeted, thus contributing to the efficacy of treatment. However, this possibility has not been explored at this time.

Unexpectedly, we could not replicate the results of a recent study.[69] This outcome likely was due to slight variations in experimental and statistical design, making comparisons between the 2 studies difficult. The previous study[69] used the most common ALS mouse model, G93A-SOD1, which harbors high copy numbers of a transgene construct carrying a human *SOD1* gene with a glycine-to-alanine transition at position 93.[40,69] Fecal samples were collected from 2-mo-old mice to determine GM compositions prior to ALS symptom onset around 3 mo of age.[69] The authors used qPCR analysis to show that transgenic mice had reduced levels of *Butyrivibrio fibrisolvens*, *Escherichia coli*, and *Peptostreptococcus*, which may have contributed to an observed shift in the GM profiles between affected and WT mice.[69] In our present study, we used mice with the same transgenic construct, although it is present at lower copy numbers, corresponding to a delayed phenotypic onset of disease.[1,18] We, too, explored GM profiles in transgenic and age-matched WT controls approximately 1 mo prior to disease onset in our colony (6 mo of age). However, we found no significant differences in GM compositions between genotypes in our study.

One explanation for why we were unable to replicate the previous results[69] might be due to differences in the background strain. Our mice are maintained as a B6SJL hybrid strain. The background strain of mice in the aforementioned study

was not specifically stated.[40] However, background strain significantly influences disease phenotype in SOD1 mouse models of ALS.[1,44] Age at onset of disease symptoms, such as tremor, loss of limb tone, and decreased grip strength, as well as duration of survival differ significantly by genetic background. Different background strains of mice harbor distinct GM profiles, which vary by institutional vendor[24] and various husbandry and environmental factors.[25,29] Therefore, background strain likely influences the potential differences observed in GM profiles between transgenic and age-matched WT mice.

In addition, it is worth noting that our present study had large sample sizes (30 SOD1^{dl} and 30 WT mice) and equal distribution according to sex between genotypes, because ALS phenotype can vary markedly depending on sex.[44] Due to our large sample size, mice used in this study comprised offspring from 5 different breeder pairs in our colony. For feasibility purposes, the study was performed by using 7 cohorts of mice. The mice in the previous study[40] likely were offspring from a single litter, with the entire study conducted as a single run. Therefore, the question arises regarding whether genotype-dependent differences in GM profiles might have emerged between offspring from the same breeder pair. Therefore, we confirmed our negative results by investigating the GM profiles between offspring from each breeder pair. Again we found no significant differences between genotypes in this second analysis.

Diet and caloric intake are 2 additional factors that might alter the GM composition in the high-copy-number SOD1 strain used in the previous study[69] but not the low-copy-number SOD1^{dl} strain used in our study. These factors have been

shown to greatly influence the GM.[19,20,22,23,74] In our lab, we have demonstrated that the high-copy SOD1 strain develops dysphagia at weaning (approximately 3 to 4 wk of age).[17] High-copy SOD1 mice have decreased swallowing,[47] licking, and mastication rates[48] that can be identified prior to the onset of limb paralysis. Therefore, the high-copy strain develops dysphagia during the developmental and maturation life stages. The low-copy SOD1^{dl} strain develops similar symptoms of dysphagia; however, they do not develop swallowing impairment until fully mature (that is, near 6 mo of age), consistent with the onset of other ALS symptoms in this model. Therefore, potential variations in diet and total caloric intake between transgenic and WT mice during developmental stages might affect the GM more strongly in the high-copy *SOD1* strain than in the low-copy model, which already has established and maintained a GM profile prior to disease onset.

In conclusion, this study assessed the GM modulatory potential of VNS in healthy and neurologically diseased mice. Although the GM profiles did not differ significantly between transgenic and WT controls or with VNS treatment, numerous possibilities remain regarding future explorations in this continuously expanding neuromodulatory technology. Some of our mice undergoing surgery experienced respiratory difficulty, but this side effect likely was due to the prolonged anesthesia produced through an injectable anesthetic regimen rather than to genotype or treatment factors. Therefore, short-term intraoperative VNS is a relatively safe procedure to perform and, under specific stimulation parameters, does not alter GM populations. Additional studies examining VNS with stimulation parameters that better target the gastrointestinal tract and using chronic VNS are

warranted. Despite the neutral results from this study, VNS remains a promising experimental and therapeutic modality for manipulating gastrointestinal microbial communities.

5.6 Acknowledgments

We thank Kate Osman for the management of the SOD1^{dl} mouse colony at the University of Missouri and for all of her assistance in the lab. In addition, we thank Giedre Turner for providing training to MH on fecal DNA extraction and for assisting with sample preparation for sequencing. Furthermore, MH acknowledges financial support from the NIH (T32 training grant 5T32OD011126-39) and Mu Phi Zeta for this project.

5.7 References

1. Acevedo-Arozena A, Kalmar B, Essa S, Ricketts T, Joyce P, Kent R, Rowe C, Parker A, Gray A, Hafezparast M, Thorpe JR, Greensmith L, Fisher EM. 2011. A comprehensive assessment of the SOD1G93A low-copy transgenic mouse, which models human amyotrophic lateral sclerosis. Dis Model Mech 4:686–700. https://doi.org/10.1242/dmm.007237.

2. Al-Majed AA, Brushart TM, Gordon T. 2000. Electrical stimulation accelerates and increases expression of *BDNF* and *trkB* mRNA in regenerating rat femoral motoneurons. Eur J Neurosci 12:4381–4390.

3. Al-Majed AA, Neumann CM, Brushart TM, Gordon T. 2000. Brief electrical stimulation promotes the speed and accuracy of motor axonal regeneration. J Neurosci 20:2602–2608. https://doi. org/10.1523/JNEUROSCI.20-07-02602.2000.

4. Al-Majed AA, Tam SL, Gordon T. 2004. Electrical stimulation accelerates and enhances expression of regeneration-associated genes in regenerating rat femoral motoneurons. Cell Mol Neurobiol 24:379–402. https://doi.org/10.1023/B:CEMN.0000022770.66463.f7.

5. Alexander GM, Erwin KL, Byers N, Deitch JS, Augelli BJ, Blankenhorn EP, Heiman-Patterson TD. 2004. Effect of transgene copy number on survival in the G93A SOD1 transgenic mouse model of ALS. Brain Res Mol Brain Res 130:7–15. https://doi. org/10.1016/j.molbrainres.2004.07.002.

6. Ardesch JJ, Sikken JR, Veltink PH, van der Aa HE, Hageman G, Buschman HP. 2010. Vagus nerve stimulation for epilepsy activates the vocal folds maximally at therapeutic levels. Epilepsy Res 89:227–231. https://doi.org/10.1016/j.eplepsyres.2010.01.005.

7. Baltadzhieva R, Gurevich T, Korczyn AD. 2005. Autonomic impairment in amyotrophic lateral sclerosis. Curr Opin Neurol 18:487–493. https://doi.org/10.1097/01.wco.0000183114.76056.0e.

8. Banzett RB, Guz A, Paydarfar D, Shea SA, Schachter SC, Lansing RW. 1999. Cardiorespiratory variables and sensation during stimulation of the left vagus in patients with epilepsy. Epilepsy Res 35:1–11. https://doi.org/10.1016/S0920-1211(98)00126-0.

9. Bauer KC, Huus KE, Finlay BB. 2016. Microbes and the mind: emerging hallmarks of the gut microbiota-brain axis. Cell Microbiol 18:632–644. https://doi.org/10.1111/cmi.12585.

10. Binks AP, Paydarfar D, Schachter SC, Guz A, Banzett RB. 2001. High-strength stimulation of the vagus nerve in awake humans: a lack of cardiorespiratory effects. Respir Physiol 127:125–133. https://doi.org/10.1016/ S0034-5687(01)00252-3.

11. Bollini CA, Cacheiro F. 2006. Peripheral nerve stimulation. Tech Reg Anesth Pain Manag 10:79–88. https://doi.org/10.1053/j. trap.2006.07.007.

12. Bonaz B, Bazin T, Pellissier S. 2018. The vagus nerve at the interface of the microbiota–gut–brain axis. Front Neurosci 12:1–9. https://doi.org/10.3389/ fnins.2018.00049.

13. Borovikova LV, Ivanova S, Zhang M, Yang H, Botchkina GI, Watkins LR, Wang H, Abumrad N, Eaton JW, Tracey KJ. 2000. Vagus nerve stimulation attenuates the systemic inflammatory response to endotoxin. Nature 405:458–462. https://doi. org/10.1038/35013070.

14. Castoro MA, Yoo PB, Hincapie JG, Hamann JJ, Ruble SB, Wolf PD, Grill WM. 2011. Excitation properties of the right cervical vagus nerve in adult dogs. Exp Neurol 227:62–68. https://doi. org/10.1016/j.expneurol.2010.09.011.

15. Cryan JF, Dinan TG. 2012. Mind-altering microorganisms: the impact of the gut microbiota on brain and behaviour. Nat Rev Neurosci 13:701–712. https://doi.org/10.1038/nrn3346.

16. Cryan JF, O'Mahony SM. 2011. The microbiome–gut–brain axis: from bowel to behavior. Neurogastroenterol Motil 23:187–192. https://doi.org/10.1111/j.1365-2982.2010.01664.x.

17. Daghlas I MH, Kadosh M, Goding G, Mancini S, Dougherty D, Harris K, Robbins KA, Lever TE. 2015. Effect of gene copy number on dysphagia onset in SOD1-G93A transgenic mice. Amyotroph Lateral Scler Frontotemporal Degener 16 Sup 1:225. https://www. tandfonline.com/doi/abs/10.3109/21678421.2015. 1098818

18. Dal Canto MC, Gurney ME. 1997. A low expressor line of transgenic mice carrying a mutant human Cu–Zn superoxide dismutase (SOD1) gene develops pathological changes that most closely resemble those in human amyotrophic lateral sclerosis. Acta Neuropathol 93:537–550. https://doi.org/10.1007/ s004010050650.

19. David LA, Maurice CF, Carmody RN, Gootenberg DB, Button JE, Wolfe BE, Ling AV, Devlin AS, Varma Y, Fischbach MA, Biddinger SB, Dutton RJ, Turnbaugh PJ. 2013. Diet rapidly and reproducibly alters the human gut microbiome. Nature 505:559–563. https://doi.org/10.1038/nature12820.

20. de Lartigue G, de La Serre CB, Raybould HE. 2011. Vagal afferent neurons in high-fat diet-induced obesity: intestinal microflora, gut inflammation, and cholecystokinin. Physiol Behav 105:100–105. https://doi.org/10.1016/j. physbeh.2011.02.040.

21. Doenyas C. 2018. Gut microbiota, inflammation, and probiotics on neural development in autism spectrum disorder. Neuroscience 374:271–286. https://doi.org/10.1016/j.neuroscience.2018.01.060.

22. DuPont AW, DuPont HL. 2011. The intestinal microbiota and chronic disorders of the gut. Nat Rev Gastroenterol Hepatol 8:523–531. https://doi.org/10.1038/nrgastro.2011.133.

23. Eisenstein M. 2016. Microbiome: bacterial broadband. Nature 533:S104–S106. https://doi.org/10.1038/533S104a.

24. Ericsson AC, Davis JW, Spollen W, Bivens N, Givan S, Hagan CE, McIntosh M, Franklin CL. 2015. Effects of vendor and genetic background on the composition of the fecal microbiota of inbred mice. PLoS One 10:1–19. https://doi.org/10.1371/journal. pone.0116704.

25. Ericsson AC, Gagliardi J, Bouhan D, Spollen WG, Givan SA, Franklin CL. 2018. The influence of caging, bedding, and diet on the composition of the microbiota in different regions of the mouse gut. Sci Rep 8:4065. https://doi.org/10.1038/s41598-018-21986-7.

26. Ericsson AC, Personett AR, Turner G, Dorfmeyer RA, Franklin CL. 2017. Variable colonization after reciprocal fecal microbiota transfer between mice with low and high richness microbiota. Front Microbiol 8:1–13. https://doi.org/10.3389/fmicb.2017.00196.

27. Fang X. 2015. Potential role of gut microbiota and tissue barriers in Parkinson's disease and amyotrophic lateral sclerosis. Int J Neurosci 126:771–776.

28. Forsythe P, Sudo N, Dinan T, Taylor VH, Bienenstock J. 2010. Mood and gut feelings. Brain Behav Immun 24:9–16. https://doi. org/10.1016/j.bbi. 2009.05.058.

29. Franklin CL, Ericsson AC. 2017. Microbiota and reproducibility of rodent models. Lab Anim (NY) 46:114–122. https://doi. org/10.1038/laban.1222.

30. Garamendi-Ruiz I, Gomez-Esteban JC. 2017. Cardiovascular autonomic effects of vagus nerve stimulation. Clin Auton Res 1–12. https://doi.org/10.1007/s10286-017-0477-8. [Epub ahead of print].

31. Geremia NM, Gordon T, Brushart TM, Al-Majed AA, Verge VMK. 2007. Electrical stimulation promotes sensory neuron regeneration and growth-associated gene expression. Exp Neurol 205:347–359. https://doi.org/10.1016/j.expneurol.2007.01.040.

32. Gil J, Funalot B, Verschueren A, Danel-Brunaud V, Camu W, Vandenberghe N, Desnuelle C, Guy N, Camdessanche JP, Cintas P, Carluer L, Pittion S, Nicolas G, Corcia P, Fleury MC, Maugras C, Besson G, Le Masson G, Couratier P. 2008. Causes of death amongst French patients with amyotrophic lateral sclerosis: a

prospective study. Eur J Neurol 15:1245–1251. https://doi.org/10.1111/j.1468-1331.2008.02307.x.

33. Gill SR, Pop M, Deboy RT, Eckburg PB, Turnbaugh PJ, Samuel BS, Gordon JI, Relman DA, Fraser-Liggett CM, Nelson KE. 2006. Metagenomic analysis of the human distal gut microbiome. Science 312:1355–1359. https://doi.org/10.1126 /science.1124234.

34. Gordon T. 2016. Electrical stimulation to enhance axon regeneration after peripheral nerve injuries in animal models and humans. Neurotherapeutics 13:295–310. https://doi.org/10.1007/s13311- 015-0415-1.

35. Gordon T, Amirjani N, Edwards DC, Chan KM. 2010. Brief postsurgical electrical stimulation accelerates axon regeneration and muscle reinnervation without affecting the functional measures in carpal tunnel syndrome patients. Exp Neurol 223:192–202. https:// doi.org/10.1016/j.expneurol.2009.09.020.

36. Gordon T, Brushart TM, Chan KM. 2008. Augmenting nerve regeneration with electrical stimulation. Neurol Res 30:1012–1022. https://doi.org/10.1179/ 174313208X362488.

37. Gordon T, Udina E, Verge VM, de Chaves EI. 2009. Brief electrical stimulation accelerates axon regeneration in the peripheral nervous system and promotes sensory axon regeneration in the central nervous system. Motor Control 13:412–441. https://doi. org/10.1123/mcj.13.4.412.

38. Grenham S, Clarke G, Cryan JF, Dinan TG. 2011. Brain–gut– microbe communication in health and disease. Front Physiol 2:1–15. https://doi.org/ 10.3389/fphys.2011.00094.

39. Guiraud D, Andreu D, Bonnet S, Carrault G, Couderc P, Hagege A, Henry C, Hernandez A, Karam N, Le Rolle V, Mabo P, Maciejasz P, Malbert CH, Marijon E, Maubert S, Picq C, Rossel O, Bonnet JL. 2016. Vagus nerve stimulation: state-of-the-art of stimulation and recording strategies to address autonomic function neuromodulation. J Neural Eng 13:041002. https://doi. org/10.1088/1741-2560/13/4/041002.

40. Gurney ME, Pu H, Chiu AY, Dal Canto MC, Polchow CY, Alexander DD, Caliendo J, Hentati A, Kwon YW, Deng HX, Chen W, Zhai P, Sufit RL, Siddique T. 1994. Motor neuron degeneration in mice that express a human Cu–Zn superoxide dismutase mutation. Science 264:1772–1775. https://doi.org/10.1126/ science.8209258.

41. Hart ML, Ericsson AC, Franklin CL. 2017. Differing complex microbiota alter disease severity of the IL10–/– mouse model of inflammatory bowel disease. Front Microbiol 8:1–15. https://doi.org/10.3389/fmicb.2017.00792.

42. Hart ML, Meyer A, Johnson PJ, Ericsson AC. 2015. Comparative evaluation of DNA extraction methods from feces of multiple host species for downstream next-generation sequencing. PLoS One 10:1–16. https://doi.org/10.1371/journal.pone.0143334.

43. Hatton KW, McLarney JT, Pittman T, Fahy BG. 2006. Vagal nerve stimulation: overview and implications for anesthesiologists. Anesth Analg 103:1241–1249. https://doi.org/10.1213/01.ane.0000244532.71743.c6.

44. Heiman-Patterson TD, Deitch JS, Blankenhorn EP, Erwin KL, Perreault MJ, Alexander BK, Byers N, Toman I, Alexander GM. 2005. Background and gender effects on survival in the TgN(SOD1-G93A)1Gur mouse model of ALS. J Neurol Sci 236:1–7. https://doi.org/10.1016/j.jns.2005.02.006.

45. Królczyk G, Zurowski D, Dobrek L, Laskiewicz J, Thor PJ. 2001. The role of vagal efferents in regulation of gastric emptying and motility in rats. Folia Med Cracov 42:141–148.

46. Krolczyk G, Zurowski D, Sobocki J, Slowiaczek MP, Laskiewicz J, Matyja A, Zaraska K, Zaraska W, Thor PJ. 2001. Effects of continuous microchip (MC) vagal neuromodulation on gastrointestinal function in rat JPhysiolPharmacol 52:705–715

47. Lever TE, Braun SM, Brooks RT, Harris RA, Littrell LL, Neff RM, Hinkel CJ, Allen MJ, Ulsas MA. 2015. Adapting human videofluoroscopic swallow study methods to detect and characterize dysphagia in murine disease models. J Vis Exp 97:1–16. https://doi.org/10.3791/52319.

48. Lever TE, Gorsek A, Cox KT, O'Brien KF, Capra NF, Hough MS, Murashov AK. 2009. An animal model of oral dysphagia in amyotrophic lateral sclerosis. Dysphagia 24:180–195. https://doi.org/10.1007/s00455-008-9190-z.

49. Lever TE, Simon E, Cox KT, Capra NF, O'Brien KF, Hough MS, Murashov AK. 2010. A mouse model of pharyngeal dysphagia in amyotrophic lateral sclerosis. Dysphagia 25:112–126. https://doi.org/10.1007/s00455-009-9232-1.

50. Matyja A, Thor PJ, Sobocki J, Laskiewicz J, Kekus J, Tuz R, Koczanowski J, Zaraska W. 2004. Effects of vagal pacing on food intake and body mass in pigs. Folia Med Cracov 45:55–62.

51. McGregor A, Wheless J, Baumgartner J, Bettis D. 2005. Right-sided vagus nerve stimulation as a treatment for refractory epilepsy in humans. Epilepsia 46:91–96. https://doi.org/10.1111/j.0013-9580.2005.16404.x.

52. Mueller NT, Bakacs E, Combellick J, Grigoryan Z, Dominguez-Bello MG. 2015. The infant microbiome development: mom matters. Trends Mol Med 21:109–117. https://doi.org/10.1016/j.molmed.2014.12.002.

53. Naseer MI, Bibi F, Alqahtani MH, Chaudhary AG, Azhar EI, Kamal MA, Yasir M. 2014. Role of gut microbiota in obesity, type 2 diabetes, and Alzheimer's

disease. CNS Neurol Disord Drug Targets 13:305–311. https://doi.org/10.2174/18715273113126660147.

54. Paulon E, Nastou D, Jaboli F, Marin J, Liebler E, Epstein O. 2017. Proof of concept: short-term noninvasive cervical vagus nerve stimulation in patients with drug-refractory gastroparesis. Frontline Gastroenterol 8:325–330. https://doi.org/10.1136/flgastro-2017-100809.

55. Pelot NA, Grill WM. 2018. Effects of vagal neuromodulation on feeding behavior. Brain Res 1693:180–187.https://doi.org/10.1016/j.brainres.2018.02.003.

56. Robbins K, Allen M, Lever TE. 2015. Low copy number SOD1-G93A mice are better suited for dysphagia research compared to the high copy-number model. Amyotroph Lateral Scler Frontotemporal Degener 16 sup1:225–226. DOI: 10.3109/21678421.2015.1098818/0017

57. Rodrigues Hoffmann A, Proctor LM, Surette MG, Suchodolski JS. 2015. The microbiome: the trillions of microorganisms that maintain health and cause disease in humans and companion animals. Vet Pathol 53:10–21. https://doi.org/10.1177/0300985815595517.

58. Ryvlin P, Gilliam FG, Nguyen DK, Colicchio G, Iudice A, Tinuper P, Zamponi N, Aguglia U, Wagner L, Minotti L, Stefan H, Boon P, Sadler M, Benna P, Raman P, Perucca E. 2014. The long-term effect of vagus nerve stimulation on quality of life in patients with pharmacoresistant focal epilepsy: the PuLsE (Open Prospective Randomized Long-term Effectiveness) trial. Epilepsia 55:893–900. https://doi.org/10.1111/epi.12611. Erratum. Epilepsia 2014. 55:1476.

59. Sharma N, Marzo SJ, Jones KJ, Foecking EM. 2010. Electrical stimulation and testosterone differentially enhance expression of regeneration-associated genes. Exp Neurol 223:183–191. https://doi.org/10.1016/j.expneurol.2009.04.031.

60. Simon B, Blake J. 2017. Mechanism of action of noninvasive cervical vagus nerve stimulation for the treatment of primary headaches. Am J Manag Care 23:S312–S316.

61. Strigo IA, Craig AD. 2016. Interoception, homeostatic emotions, and sympathovagal balance. Philos Trans R Soc Lond B Biol Sci 371:1–9.

62. Sun J, Chang EB. 2014. Exploring gut microbes in human health and disease: pushing the envelope. Genes Dis 1:132–139. https://doi.org/10.1016/j.gendis.2014.08.001.

63. Svensson E, Horvath-Puho E, Thomsen RW, Djurhuus JC, Pedersen L, Borghammer P, Sorensen HT. 2015. Vagotomy and subsequent risk of Parkinson’s disease. Ann Neurol 78:522–529. https://doi.org/10.1002/ana.24448.

64. Toepfer M, Folwaczny C, Klauser A, Riepl RL, Muller-Felber W, Pongratz D. 1999. Gastrointestinal dysfunction in amyotrophic lateral sclerosis. Amyotroph Lateral Scler Other Motor Neuron Disord 1:15–19. https://doi.org/10.1080/146608299300079484.

65. Ueda H, Suga M, Yagi T, Kusumoto-Yoshida I, Kashiwadani H, Kuwaki T, Miyawaki S. 2016. Vagal afferent activation induces salivation and swallowing-like events in anesthetized rats. Am J Physiol Regul Integr Comp Physiol 311:R964–R970. https://doi.org/10.1152/ajpregu.00292.2016

66. Val-Laillet D, Biraben A, Randuineau G, Malbert CH. 2010. Chronic vagus nerve stimulation decreased weight gain, food consumption, and sweet craving in adult obese minipigs. Appetite 55:245–252. https://doi.org/10.1016/j.appet.2010.06.008.

67. Wang HX, Wang YP. 2016. Gut–microbiota–brain axis. Chin Med J (Engl) 129:2373–2380. https://doi.org/10.4103/0366-6999.190667.

68. Wong JN, Olson JL, Morhart MJ, Chan KM. 2015. Electrical stimulation enhances sensory recovery: a randomized controlled trial. Ann Neurol 77:996–1006. https://doi.org/10.1002/ana.24397.

69. Wu S, Yi J, Zhang YG, Zhou J, Sun J. 2015. Leaky intestine and impaired microbiome in an amyotrophic lateral sclerosis mouse model. Physiol Rep 3:1–10.

70. Yuan H, Silberstein SD. 2015. Vagus nerve and vagus nerve stimulation, a comprehensive review: part I. Headache 56:71–78. https://doi.org/10.1111/head.12647.

71. Yuan H, Silberstein SD. 2015. Vagus nerve and vagus nerve stimulation, a comprehensive review: part II. Headache 56:259–266. https://doi.org/10.1111/head.12650.

72. Yuan H, Silberstein SD. 2015. Vagus nerve and vagus nerve stimulation, a comprehensive review: part III. Headache 56:479–490. https://doi.org/10.1111/head.12649.

73. Zagon A. 2001. Does the vagus nerve mediate the sixth sense? Trends Neurosci 24:671–673. https://doi.org/10.1016/S0166-2236(00)01929-9.

74. Zhang C, Li S, Yang L, Huang P, Li W, Wang S, Zhao G, Zhang M, Pang X, Yan Z, Liu Y, Zhao L. 2013. Structural modulation of gut microbiota in life-long calorie-restricted mice. Nat Commun 4:1–10. https://doi.org/10.1038/ncomms3163.

75. Zhang YG, Wu S, Yi J, Xia Y, Jin D, Zhou J, Sun J. 2017. Target intestinal microbiota to alleviate disease progression in amyotrophic lateral sclerosis. Clin Ther 39:322–336. https://doi.org/10.1016/j.clinthera.2016.12.014.

Chapter Six

SUMMARY AND FUTURE DIRECTIONS

6.1 Summary

The goal of this work was to develop and refine a mouse model to investigate recurrent laryngeal nerve (RLN) injury and potential therapeutic interventions. As highlighted in the introduction of this dissertation, RLN injury and subsequent vocal fold (VF) paralysis often result in diminished health and poor quality of life for the patient due to airway complications associated with swallowing, respiration, and vocalization. Current studies that investigate these somatic manifestations of VF paralysis, especially in a single model, are lacking. Thus, this work sought to increase the translational potential in a mouse model of RLN injury. By developing a comprehensive behavioral regimen and refining methodology, we have added to the collective knowledge of RLN injury and have created a model that will aid researchers to better assess RLN injury and recovery in their studies.

In Chapter 2, we started our model development journey by differentiating the effects of superior laryngeal nerve (SLN) versus RLN injury on VF mobility and swallowing behavior. As both nerves branch from the vagus and supply sensory and motor information to intrinsic laryngeal muscles, it was essential to confirm the fidelity of the laryngeal innervation pattern and functional outcomes between mice

and humans. In this study, we confirmed chronic VF immobility after RLN transection with small changes in swallowing behavior. In contrast, the SLN had no visible effect on VF mobility and only affected swallow function if the nerve was injured bilaterally. In this study, we also performed preliminary work to investigate a more clinically prevalent injury, a crush injury, and a potential treatment strategy, intraoperative Vagal Nerve Stimulation (iVNS). Though the results of this pilot iVNS study are promising, additional work is necessary to refine the crush injury model and optimize iVNS treatment parameters in a larger sample size.

While it was relatively simple to determine if the VFs were mobile versus immobile after laryngeal nerve injury, quantification of mobility during functional recovery was quite challenging and inconsistent due to subjectivity between reviewers. Furthermore, objective methods were time consuming and did not capture the true motion of the VFs during dynamic movement. Thus, we sought to create a method for objective quantification of dynamic VF movement that could be automated for increased efficiency and high throughput analysis. By collaborating with students and faculty in the Department of Electrical Engineering and Computer Science at the University of Missouri, we have developed a novel software to track and quantify VF motion. As discussed in Chapters 3 and 4, with this software, we can now automatically and objectively quantify the range, frequency, and directionality of VF motion, as well as determine if paradoxical VF motion is present and characterize its activity.

In addition to enhancing the methods for VF motion quantification, in Chapter 4, we further refined available behavioral analyses to investigate the

sequela of RLN injury over time in a single animal model. With this study, we identified novel outcome metrics to identify voice and respiratory dysfunction in the mouse after RLN transection. Multiple ultrasonic acoustic parameters analogous to human vocal outcomes were affected by RLN injury. The mice also showed evidence of dyspnea during increased respiratory effort similar to humans with unilateral VF paralysis. Though dysphagia was not noted in this work, other methods such as manometry or automated video tracking with a higher speed camera may be useful in future studies to assess swallow dysfunction that cannot be captured with manual videofluoroscopic swallow study analysis.

Lastly, before moving forward with therapeutic investigations using iVNS in this model, it was necessary to ensure our chosen stimulation parameters did not have any off-target effects in the many other organ systems innervated by the vagus nerve. While numerous studies have been conducted on the safety of vagal nerve stimulation in regard to cardiorespiratory function,[1-4] no published study has examined how iVNS may influence the gastrointestinal microbiome. As the brain-gut-microbiome axis is critical for maintaining homeostasis,[5-7] it is necessary to determine if iVNS alters the microbial population living within the mammalian gastrointestinal system. Thus, we performed iVNS in a mouse model of amyotrophic lateral sclerosis (ALS), a neurologic disorder affecting motor neurons. This model of neurologic disease (maintained on a hybrid B6-SJL background) was chosen over the standard B6 model used in our previous studies for several reasons. First, previous literature had noted altered gastrointestinal microbiota populations in a similar ALS model,[8] and we sought to determine if the ALS model

in use in our lab had related changes. Second, nerve stimulation has therapeutic potential for multiple neurodegenerative diseases, and the lab plans to utilize implantable VNS devices in this model in future experiments. Therefore, this work laid the groundwork for multiple investigations in various models in the lab. Importantly, we have shown that our chosen stimulation parameters do not affect the gastrointestinal microbiome when applied for a short duration. However, it remains critical to examine long-term stimulation with different parameters to ensure chronic treatment will not influence gastrointestinal microbial populations.

6.2 Future Directions

6.2.1 Recurrent Laryngeal Nerve Crush Injury

Work in our lab has already began to extrapolate the RLN transection model for use in more clinically relevant injury types, such as a crush (i.e., compression) injury, and for therapeutic investigations using iVNS. Multiple methods of inducing an RLN crush injury were attempted, yet many of these resulted in variable or inadequate severity of injury, making recovery analysis difficult. Thus, a custom designed “crush tool” (**Figure 6.1**) was developed to overcome the limitation of previously used compression methods. This tool is micromanipulator-controlled to relieve traction forces and utilizes positioning hooks on the compression surface to ensure each nerve is placed in the same location on the tool. The crush tool also features a remote activation of the crush to enhance ergonomics and avoid inadvertent movement of the crush tool. This tool provides adequate compression forces (~30 N) to fully disrupt all axons within the crush site, as seen on

transmission electron microscopy in **Figure 6.2**. The lab aims to utilize this tool in future RLN and facial nerve crush experiments. Plans to automate the crush action of the tool are in progress to further reduce human error in pressure on the remote activation lever and timing of the crush injury.

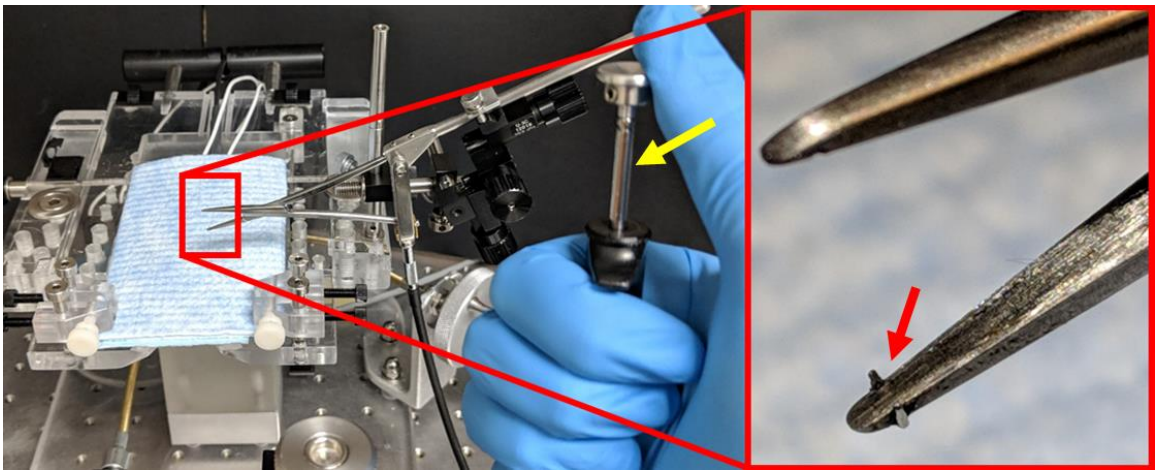

Figure 6.1. Novel Nerve Crush Tool. A micromanipulator-controlled crush tool was developed to ensure reproducible compression forces across mice and studies. Features include positioning hooks (red arrow) and a remote activation device (yellow arrow). Automation of the crush tool is currently in progress.

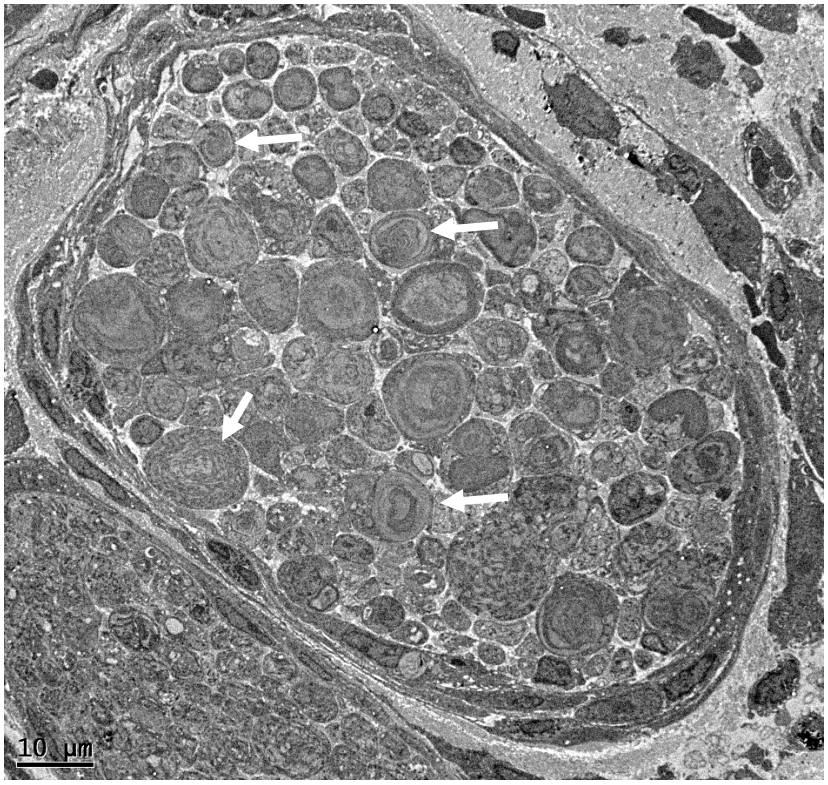

Figure 6.2. Transmission Electron Microscopy of the RLN three days post-crush injury. The newly developed crush tool was utilized to crush the RLN in B6 mice, resulting in complete destruction of all axons (i.e., lack of myelin sheath and evidence of myelin debris (arrows)) within the nerve distal to the injury site. Functionally, the mice had complete ipsilateral vocal fold immobility at three days post-injury.

6.2.2 Intraoperative Vagal Nerve Stimulation (iVNS)

Because a crush injury is more prevalent in human patients with RLN injury, it is essential to perform therapeutic investigations using a crush technique to further increase the translational potential of this model. As such, we have started to perform additional studies using an RLN crush injury to investigate iVNS as a potential therapy. In these studies, we have begun to utilize the behavioral regimen outlined in this dissertation work to evaluate functional recovery in mice with and without iVNS treatment.

Without iVNS treatment, our preliminary results have indicated that mice with an RLN crush injury exhibit similar functional outcomes as mice with RLN

transection injuries (i.e., ipsilateral, VF immobility and decreased apnea formation). However, as the nerve remains intact, spontaneous functional recovery is observed in the weeks following injury. The goal of iVNS treatment would be to hasten this recovery time, as human patients with RLN injury can take weeks to years to recover completely, if at all. This recovery period in mice is extremely quick due to their relatively short length of the RLN; thus, the most opportune time points for functional analysis to evaluate treatment outcomes remain to be elucidated in the crush injury model.

Once identified, further work to investigate iVNS treatment can begin, including identifying the most optimal stimulation parameters specific for RLN regeneration and functional recovery. If effective, iVNS could be used during anterior neck and thoracic surgeries to prevent post-operative complications associated with RLN injury. This technology would be particularly advantageous in procedures in which intraoperative monitoring equipment is utilized. If an RLN injury is detected during surgery, therapy could be applied, perhaps through the monitoring equipment itself, with modifications incorporated to permit changes in current flow direction and stimulus parameters (e.g., frequency and duration).

In conclusion, the RLN is a complex nerve that can dramatically impact quality of life if injured. This work has provided the foundations for an animal model to thoroughly investigate functional outcomes after RLN injury. With this model, we can better understand RLN injury and begin to explore treatments to regenerate RLN neurons in hopes to improve patient health outcomes.

6.3 References

1. Ardesch JJ, Sikken JR, Veltink PH, van der Aa HE, Hageman G, Buschman HP. Vagus nerve stimulation for epilepsy activates the vocal folds maximally at therapeutic levels. *Epilepsy research.* 2010;89(2-3):227-231.

2. Banzett RB, Guz A, Paydarfar D, Shea SA, Schachter SC, Lansing RW. Cardiorespiratory variables and sensation during stimulation of the left vagus in patients with epilepsy. *Epilepsy research.* 1999;35(1):1-11.

3. Binks AP, Paydarfar D, Schachter SC, Guz A, Banzett RB. High strength stimulation of the vagus nerve in awake humans: a lack of cardiorespiratory effects. *Respiration physiology.* 2001;127(2-3):125-133.

4. Garamendi-Ruiz I, Gomez-Esteban JC. Cardiovascular autonomic effects of vagus nerve stimulation. *Clinical autonomic research : official journal of the Clinical Autonomic Research Society.* 2017.

5. Bauer KC, Huus KE, Finlay BB. Microbes and the mind: emerging hallmarks of the gut microbiota-brain axis. *Cellular microbiology.* 2016;18(5):632-644.

6. Cryan JF, Dinan TG. Mind-altering microorganisms: the impact of the gut microbiota on brain and behaviour. *Nature reviews Neuroscience.* 2012;13(10):701-712.

7. Cryan JF, O'Mahony SM. The microbiome-gut-brain axis: from bowel to behavior. *Neurogastroenterology and motility : the official journal of the European Gastrointestinal Motility Society.* 2011;23(3):187-192.

8. Wu S, Yi J, Zhang YG, Zhou J, Sun J. Leaky intestine and impaired microbiome in an amyotrophic lateral sclerosis mouse model. *Physiol Rep.* 2015;3(4).

Appendix

TRANSMISSION ELECTRON MICROSCOPY PROTOCOL

Recurrent Laryngeal Nerve Sample Collection

1) Euthanize mouse with an overdose of pentobarbital (0.2 ml)
2) Perfuse mouse
    a) Approximately 30 ml saline
    b) Followed by approximately 30 ml 4% paraformaldehyde (PFA)
3) Incise ventral neck and reflect or transect skin from chin down to sternum
4) Remove salivary glands and caudal portion of rib cage
5) Prepare trachea, esophagus and RLNs for removal *en block*
    a) Use gentle blunt dissection to loosen connective tissue under trachea, esophagus, and RLNs
    b) Use microscissors to cut connective tissue and muscle at rib cage
    c) Transect *en bloc* section at level of the first rib, proximal to heart and lungs
    d) Make a midline cut through mandible
    e) Use microscissors to loosen larynx from oral cavity and transect at caudal portion of the tongue
6) Remove *en bloc* section from mouse and transfer to a glass cutting dish
7) Using a razor and scalpel blade transect entire section immediately proximal to carbon powder that is marking the crush site (if present).

8) Fix desired section (usually the rostral half) in 4% PFA + 2% Glutaraldehyde prior to resin embedding

Follow standard TEM embedding and staining procedures

Divide *en bloc* section into left and right sides prior to imaging

1) Stain a thin section with Toluidine blue and confirm visualization of the left and right RLN
2) Using a diamond knife, cut the block into left and right sides to image separately

VITA

Megan M. Haney was born in Lincoln, Nebraska to Robert and Margie Haney. She was raised in Lincoln, where she attended Saint Pius X High School and grew a passion for animals and science. After high school, she attended Kansas State University for her undergraduate education. As a freshman, she was admitted into the Kansas State University College of Veterinary Medicine Early Admission Program. This program allowed her to start her veterinary career a year early. Thus, she graduated *Summa Cum Laude* with a BS in Animal Sciences and Industry in 2010, followed by graduation *Magna Cum Laude* with her veterinary medicine degree (DVM) in 2014.

Immediately following veterinary school, she entered the University of Missouri Comparative Medicine Program. Through this program she completed a residency in laboratory animal medicine while working towards a doctoral degree (PhD) in Veterinary Pathobiology, partly supported by NIH T32 grant funding. She has conducted her dissertation work in the lab of Dr. Teresa E. Lever developing and characterizing a translational mouse model of recurrent laryngeal nerve injury for use in future therapeutic investigations.